Order Number 9419756

Studies of gravity-wave filtering and tidal interaction in the middle atmosphere

Lu, Wentong, Ph.D.

University of Alaska Fairbanks, 1993

U·M·I
300 N. Zeeb Rd.
Ann Arbor, MI 48106

STUDIES OF GRAVITY-WAVE FILTERING AND TIDAL INTERACTION IN THE MIDDLE ATMOSPHERE

A

THESIS

Presented to the Faculty

of the University of Alaska Fairbanks

in Partial Fulfillment of the Requirements

for the Degree of

DOCTOR OF PHILOSOPHY

By

Wentong Lu, B.S., M.S.

Fairbanks, Alaska

December 1993

Studies of Gravity-Wave Filtering and Tidal Interaction in the Middle Atmosphere

By

Wentong Lu

RECOMMENDED BY:

Dr. Roger W. Smith, Advisory Committee Chair

Dr. David C. Fritts , Advisory Committee Co-chair

Dr. Glen E. Shaw

Dr. Lou-Chuang Lee

Dr. David L. Musgrave

Dr. Brenton J. Watkins

Dr. John L. Morack, Department Head

APPROVED BY:

Dr.John L. Morack, Interim Dean, College of Natural Sciences

Dr. Edward C. Murphy, Acting Dean, Graduate School

16 November 1993

Date

Abstract

Based on the spectral character of the observed gravity wave field, a parameterization scheme for gravity wave propagation and effects in the lower and middle atmosphere has been proposed. This effort begins with spectral expressions for gravity wave energy and momentum fluxes and prescribes the manner in which such idealized spectra respond to variations in the gravity wave environment. Means of specifying spectral amplitudes in response to specific wave sources at lower levels and the spread of wave influences horizontally as the spectrum propagates vertically through the lower and middle atmosphere are suggested. The parameterization scheme relies on a separable and invariant spectral form that is consistent with observations throughout the atmosphere. By choosing representative gravity wave parameters, the scheme yields predictions of mean fluxes of momentum for winter and summer CIRA 1986 model atmosphere profiles that agree well with mean flux observation in the lower and middle atmosphere. In the troposphere and lower stratosphere, both winter and summer profiles imply a negative zonal mean flux of $\sim 0.2 m^2 s^{-2}$, consistent with airborne and radar measurements and the needs of large-scale GCM models. In the mesosphere, mean fluxes tend to oppose the zonal mean wind with flux maxima above the wind maxima and vertical profiles in general agreement with radar estimates at these heights.

To assess the importance of gravity wave-tidal interactions in the middle atmosphere, the parameterization scheme is further applied to a static mean wind plus a typical tidal wind structure. The results suggest that the gravity wave-tidal interaction is likely to be strong where tidal amplitudes become large, yielding a significant modulation in the anisotropy of the gravity wave field due to differential filtering and saturation processes. Consistent with observations, this filtering leads to wave momentum fluxes that are approximately anti-correlated with the tidal wind field and which may far exceed mean values in magnitude.

Contents

List of Figures

Acknowledgements

I would like to express my greatest thanks to my advisor, Dr. David C. Fritts. Without his long time constant support and encouragement , it is impossible for me to finish this thesis. I would also like to express my great appreciation to the chairman of my thesis committee, Dr. Roger W. Smith. It is he who offered me constant help in completing my graduate studies here at the University of Alaska when Dr. David C. Fritts is in Colorado.

Thanks also to my other committee members, Dr. Glen E. Shaw, Dr. Lou-Chuang Lee, Dr. David L. Musgrave, Dr. Brenton J. Watkins, and my thesis defence committee member Dr. Sue Ann Bowling.

Of many of my friends and colleagues who offered me constant help and assistance in the last few years, I would like to express my appreciation to: Yongxiang Hu, Tingjun Zhang, Xiaohong Zhao, Zhangai Luo , Qilong Min and Josph Isler.

This thesis is dedicated to my beloved parents, Xiangheng Lu and Jilan Xiang, without their unflagging love and spiritual encouragement this task would have been impossible.

Chapter 1

Introduction

Internal gravity waves refer to harmonic oscillating motions occurring in a stably stratified atmosphere with frequencies ranging from the buoyancy frequency, N, to the inertial frequency, f. Internal gravity waves are more and more believed to play a very important role in the middle atmosphere during the last few decades. Hines (1960) first recognized that internal gravity waves play a key role in middle atmosphere dynamics. Since that time, numerous studies have investigated the significance of gravity waves in establishing the large-scale circulation and structure of the lower and middle atmosphere. Both theoretical and observational studies have revealed the importance of internal gravity waves in the transports of energy and momentum, their forcing of the large scale circulation and structure of the lower and middle atmosphere, and the modulation of these processes by variable sources, filtering, or interactions with other components of atmospheric motions (Fritts and VanZandt, 1993).

The main effects are commonly believed to include a reduction of the mean zonal wind in the lower stratosphere leading to mean poleward motions at these heights (Palmer at al., 1986; Tanaka, 1986), the reversal of the vertical shear of the mean zonal wind in the mesosphere and a corresponding reversal of the meridional temperature gradient near the mesopause (Lindzen, 1981; Fritts and Vincent , 1987), the turbulent diffusion of heat and constituents throughout regions of wave dissipation (Fritts and Dunkerton, 1985), and the vertical transport of horizontal momentum and the complex wave and turbulence interactions by which gravity waves are saturated (Fritts, 1989). Another significant effect in terms of their middle atmosphere effects is the observed temporal and geographic variability of the wave spectrum (Fritts, 1989).

As gravity waves propagate upward, their amplitudes increase with height owing to the decrease of atmospheric density. Gravity wave saturation refers to processes that act to limit or reduce wave amplitudes due to instabilities or interactions arising from large-amplitude motions. On the other hand, dissipation processes such as molecular diffusion and radiative cooling, are more or less independent of wave amplitudes. The mechanism of gravity wave saturation thought to be most important in the middle atmosphere is the turbulent breakdown of convectively unstable regions caused by the differential advection of more dense over less dense air by internal gravity wave motions. The

turbulent diffusion resulting from these convective instabilities acts to reduce the wave amplitude to that value that just permits the continued generation of turbulence. Other mechanisms which may contribute to gravity wave saturation under certain circumstances are dynamical instabilities due to large vertical wind shear within the wave field and nonlinear interactions among the spectrum of large-amplitude waves (Fritts, 1984).

Gravity wave saturation processes are thought to be very important since they act in concert with wave sources and filtering to determine the spectrum of middle atmosphere motions and their influences on small and meso scale motions (Fritts, 1989). At the beginning, attempts intending to understand these processes were mainly focused on the conditions necessary for the local instabilities of an essentially linear wave field (Hodges, 1967; Hines, 1971) and were successful in explaining the observed limit on wave amplitudes. The success of linear theory has prompted its use in the parameterization of gravity wave effects on large scale motions (Holton, 1982, 1983; Holton and Zhu, 1984; Garcia and Solomon, 1985; Palmer et al., 1986; Rind et al., 1988), the development of more complete spectral descriptions of the saturated wave field and its effects (Dewan and Good, 1986; Smith et al., 1987; Fritts et al., 1988a; VanZandt and Fritts, 1989), and further studies of the time scales and likely modes of linear instabilities (Hines, 1988). Other theoretical studies have addressed the effects of nonlinear interactions within the atmospheric inter-

nal wave field (Mied, 1976; Klostermeyer, 1982; Weinstock, 1982, 1985; Yeh and Liu, 1981, 1985; Fritts 1985; Inhester, 1987; Dunkerton, 1987; Dong and Yeh, 1988) and the implications of wave dissipation and turbulence generation for heat and constituent transports (Walterscheid, 1981; Weinstock, 1983; Schoeberl et al., 1983; Chao and Schoeberl, 1984; Fritts and Dunkerton, 1985; Strobel et al., 1985, 1987; Coy and Fritts, 1988). Parallel to the above theoretical efforts, observational studies have attempted to identify the processes responsible for wave field saturation and to provide evidence of their effects. Recent observational and theoretical studies have revealed considerable temporal and geographic variability of the gravity wave spectrum and its effects in the lower and middle atmosphere, such as variations in wave energy densities (Meek et al., 1985a; Vincent and Fritts, 1987; Fritts and Nastrom, 1992), momentum fluxes (Vincent and Reid, 1983; Fritts and Vincent, 1987; Reid and Vincent, 1987a; Reid et al., 1988; Fritts et al., 1989; Fritts and Yuan, 1989; Thrane et al., 1985; Blix et al., 1990) , turbulence intensities (Hocking, 1987; Watkins et al., 1988), and concentrations (Thomas et al., 1984) on time scales ranging from minutes or hours to one year. Theoretical studies suggest that such variability may arise in response to variable sources and filtering by mean or low frequency planetary, tidal, or gravity wave motions (Dunkerton and Butchart, 1984; Miyahara et al., 1986).

Observational studies of gravity wave forcing and the mean circulation

in the lower and middle atmosphere have both reinforced the theoretical view of wave forcing of the mean structure and provided evidence of a surprising degree of variability of this forcing on small temporal and spatial scales. The mean forcing is now known to vary seasonally fashion at middle and high latitudes in the middle atmosphere due to filtering of the gravity wave spectrum by the intervening wind field (Vincent and Reid, 1983; Reid and Vincent, 1987; Fritts and Vincent, 1987; Fritts and Yuan, 1989; Reid et al., 1988; Tsuda et al., 1990; Wang and Fritts, 1990). Likewise, observations of a large mean meridional circulation and temperature far below radiative equilibrium values provide additional indirect evidence of local gravity wave forcing near the mesopause (Nastrom et al., 1982; von Zahn and Meyer, 1989; Garcia, 1989; McIntyre, 1989). Significant momentum fluxes have also been noted in the equatorial middle atmosphere (Hitchman et al., 1992), while other observations have displayed large modulations of the momentum flux (much larger than mean values) by tidal or other low-frequency motions (Fritts and Vincent, 1987; Wang and Fritts, 1991; Fritts et al., 1992). Recent reviews of gravity wave saturation, the processes influencing their spectral characteristics and their middle atmosphere effects were provided by Fritts (1989) and Dunkerton (1989). At lower levels, significant momentum fluxes have been measured only over mountainous terrain (Lilly and Kennedy, 1973; Lilly, 1978; Smith, 1978; Lilly et al., 1982; Brown, 1983; Hoinka, 1984, 1985; Fritts et al., 1990b; Nas-

trom and Fritts, 1992), but modeling studies and observations of statistically enhanced variances over various other wave sources, including fronts, convection, and wind shear, suggest that these may contribute significant fluxes in the lower and middle atmosphere (Peltier and Clark, 1979; Lu et al., 1984; Clark et al., 1986; Nastrom et al., 1987; Jasperson et al., 1990; Fritts and Nastrom, 1992; Fovel et al., 1992).

In this thesis, some basic mechanisms of internal gravity wave generation and some properties of wave propagations are presented in Chapter 1. Chapter 2 gives a brief review of gravity wave saturation theories introduced during the past few decades. Previous studies of the gravity wave spectrum are reviewed in detail in Chapter 3 which provides the up-to-date model gravity wave spectrum. Chapter 4 is the main work of this thesis in which a one-dimensional spectral gravity wave parameterization scheme is proposed and developed. In Chapter 5, the proposed scheme is applied to the CIRA (Cooperative Institute for Research of the Atmosphere) model atmosphere and the predicted results of momentum fluxes and the associated vertical divergences are in very good agreement with observations. Gravity wave-tidal interactions are investigated in Chapter 6. Gravity wave-tidal interactions are likely to be strong where tidal amplitudes are large, consistent with observations. Summary and conclusions are included in Chapter 7.

1.1 Basic Mechanism of Internal Gravity Waves

As mentioned in the beginning, internal gravity waves are oscillations occurring in a stratified atmosphere. In other words, internal gravity waves are oscillatory motions in the presence of a buoyancy force. Assuming that the basic state of the atmosphere is hydrostatic with a mean density profile of $\overline{\rho}(z)$, the so-called Brunt-Väisälä frequency or buoyant frequency is defined as

$$N^2 = -g(\frac{1}{\overline{\rho}}\frac{\partial \overline{\rho}}{\partial z} + \frac{g}{c_s^2}), \tag{1.1}$$

where g is the gravitational constant, $c_s^2 = \gamma RT$ is the phase speed of sound waves with $\gamma = C_p/C_v$, or using the definition of potential temperature

$$\theta = T(\frac{p_s}{p})^{R/C_p}, \tag{1.2}$$

where p_s is the pressure at some reference level, we have

$$N^2 = \frac{g}{\overline{\theta}}\frac{\partial \overline{\theta}}{\partial z} = \frac{g}{\overline{T}}(\frac{\partial \overline{T}}{\partial z} + \frac{g}{C_p}), \tag{1.3}$$

where $\overline{T}$ and $\overline{\theta}$ are temperature and potential temperature of the basic state of the atmosphere, respectively. For an atmosphere in which the potential temperature is constant with height, the dry adiabatic lapse rate is

$$\Gamma_d \equiv \frac{g}{C_p}, \tag{1.4}$$

Under normal conditions, the atmosphere is not dry. The potential temperature is a function of height. Thus the atmospheric lapse rate

$$\Gamma \equiv -\frac{\partial \overline{T}}{\partial z}, \tag{1.5}$$

will differ from the adiabatic lapse rate and we have

$$N^2 = \frac{g}{\overline{T}}(\Gamma_d - \Gamma), \tag{1.6}$$

The adiabatic lapse rate of dry air is $\sim 9.8^0 C/km$, and the typical atmospheric lapse rate in the troposphere is $\sim 6.5^0 C/km$. If $\Gamma < \Gamma_d$ (θ increases with height), an air parcel that undergoes an adiabatic displacement from its equilibrium level will be positively (negatively) buoyant when displaced vertically downward (upward) so that it will tend to return to its equilibrium level and the atmosphere is said to be statically stable or stably stratified.

Now imagine that an air parcel initially located at height $z = 0$ has the same pressure, temperature and density as its surrounding atmosphere. Under the influence of certain kinds of pulse force due to instabilities, such as convective instability, the air parcel undergoes some small vertical displacement, ζ, without disturbing its environment and arrives at a new height $z = \zeta$. If the

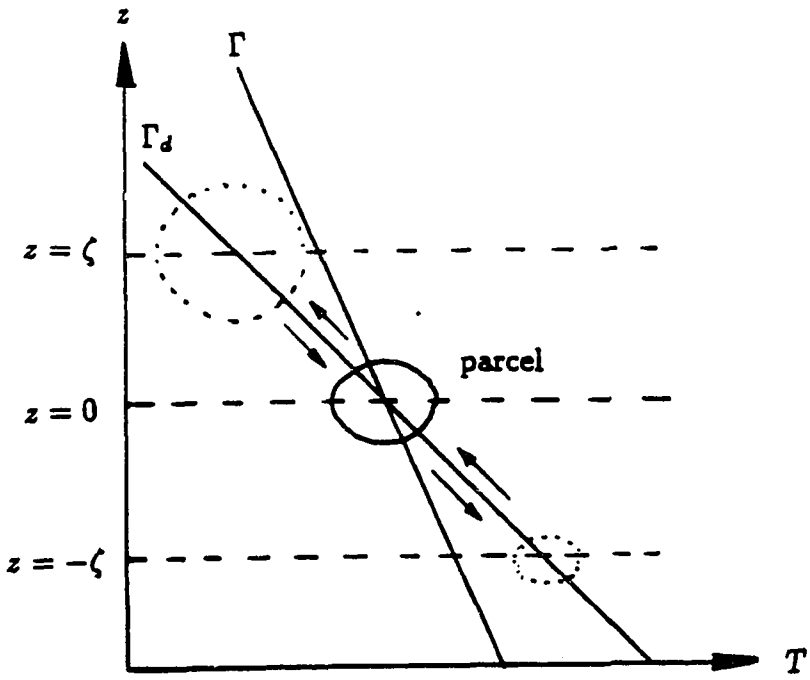

Figure 1.1: Schematic illustration of gravity wave motion. A fluid parcel will oscillate around $z = 0$ due to the buoyancy force after the disturbance. Assuming this is an adiabatic process, arrows indicate the motion of the parcel, where Γ is a typical lapse rate, Γ_d is the adiabatic lapse rate, and T is the temperature.

process is adiabatic, at height $z = \zeta$, the temperature of the air parcel is lower than that of its surrounding atmosphere and the density is larger than that of the surrounding atmosphere due to the difference between the adiabatic lapse rate Γ_d of the air parcel and the atmospheric lapse rate Γ of the surrounding atmosphere. Thus the air parcel will move downward and tend to return to its original position. When it reaches height $z = 0$ it will keep going downward due to the inertial effects. After it reaches height $z = -\zeta$, its temperature is higher than the surrounding air and its density is lower than the surrounding air. The air parcel will tend to go upward to it equilibrium position. During the above process the air parcel will oscillate around its equilibrium level (see Fig. 1.1). Such an oscillation occurs in a stratified atmosphere and is caused by buoyant forces, and the oscillatory motion is called gravity wave. The vertical momentum equation of the air parcel can be derived by using the parcel method (Holton, 1992). Considering a parcel that is displaced vertically small distance ζ without disturbing its environment, the vertical acceleration of the parcel is

$$\frac{d^2\zeta}{dt^2} = -g - \frac{1}{\rho}\frac{\partial p}{\partial z}, \tag{1.7}$$

where p and ρ are the pressure and density of the parcel. In the parcel method it is assumed that the pressure of the parcel instantaneously adjusts to the environmental pressure during the displacement, i.e., $p = \overline{p}$. This condition must

be true if the parcel is to leave the environment undisturbed. Furthermore, it is assumed that the environmental atmosphere is in hydrostatic balance,

$$\frac{d\overline{p}}{dz} = -\overline{\rho}g, \tag{1.8}$$

where $\overline{p}$ and $\overline{\rho}$ are the pressure and density of the environment. So that eq.(1.7) can be expressed

$$\frac{d^2\zeta}{dt^2} = g(\frac{\overline{\rho} - \rho}{\rho}), \tag{1.9}$$

The righthand side term is the buoyancy force which causes the oscillation of the parcel. It can further be expressed in terms of potential temperature. Using the ideal gas law, $p = \rho RT$, and eq.(1.2), the above equation maybe written as

$$\frac{d^2\zeta}{dt^2} = g\frac{\theta(\zeta) - \overline{\theta}(\zeta)}{\overline{\theta}(\zeta)}, \tag{1.10}$$

If the parcel is initially at height level $z = 0$ where the potential temperature is the same as its environment, $\theta(0) = \overline{\theta}(0)$, then for a small displacement ζ the environmental potential temperature at height $z = \zeta$ can be represented as

$$\overline{\theta}(\zeta) \simeq \overline{\theta}(0) + \frac{d\overline{\theta}}{dz}\zeta, \tag{1.11}$$

The process of the parcel displacement is adiabatic, so that the potential temperature of the parcel is conserved, $\theta(\zeta) = \theta(0)$. Thus

$$\theta(\zeta) - \overline{\theta}(\zeta) = \overline{\theta}(0) - \overline{\theta}(\zeta) = -\frac{d\overline{\theta}}{dz}\zeta, \tag{1.12}$$

and eq.(1.10) becomes

$$\frac{d^2\zeta}{dt^2} = -\frac{g}{\overline{\theta}}\frac{d\overline{\theta}}{dz}\zeta = -N^2\zeta, \tag{1.13}$$

So that the vertical momentum equation of the parcel maybe written as

$$\frac{d^2\zeta}{dt^2} + N^2\zeta = 0. \tag{1.14}$$

The above equation has a general solution of the form

$$\zeta = Ae^{iNt}, \tag{1.15}$$

which describes a simple harmonic motion, and the oscillating frequency is the buoyant frequency N. Therefore, if $N^2 > 0$ the parcel will oscillate about its initial level with a period $\tau = 2\pi/N$. For average tropospheric conditions $N \simeq 1.2 \times 10^{-2}s^{-1}$, thus the period of a buoyancy oscillation is about $8min$. From eq. (1.14), we can see that if $N^2 = 0$, i.e., $\overline{\theta}_z = 0$, the atmosphere is neutral, there will be no periodic oscillation, internal gravity waves become impossible. Also as noted, if $N^2 < 0$, or $\overline{\theta}$ decreases with height, the amplitude

of the motion will increase with time (the motion is unstable), and there will also be no internal gravity wave. So we know that internal gravity waves only occur in a stably stratified atmosphere.

Internal gravity waves appear to be common in the lower and middle atmosphere. Figure 1.2 shows some radar observations of internal gravity waves in this region. The periods of waves of this type are typically a few minutes to an hour or so, horizontal wavelengths are about tens to hundreds of kilometers, and vertical wavelengths range from 5 to 15 *km* (Andrews et al., 1987).

1.2 Properties of Gravity Wave Propagation

Another important issue is that after an internal gravity wave is generated, how does it propagate in a stratified atmosphere? This can be discussed through the dispersion relations. The basic equations for three-dimensional motion of an incompressible atmosphere may be written as follows:

$$\frac{\partial u}{\partial t} + u\frac{\partial u}{\partial x} + v\frac{\partial u}{\partial y} + w\frac{\partial u}{\partial z} - fv + \frac{1}{\rho}\frac{\partial p}{\partial x} = 0, \tag{1.16}$$

$$\frac{\partial v}{\partial t} + u\frac{\partial v}{\partial x} + v\frac{\partial v}{\partial y} + w\frac{\partial v}{\partial z} + fu + \frac{1}{\rho}\frac{\partial p}{\partial y} = 0, \tag{1.17}$$

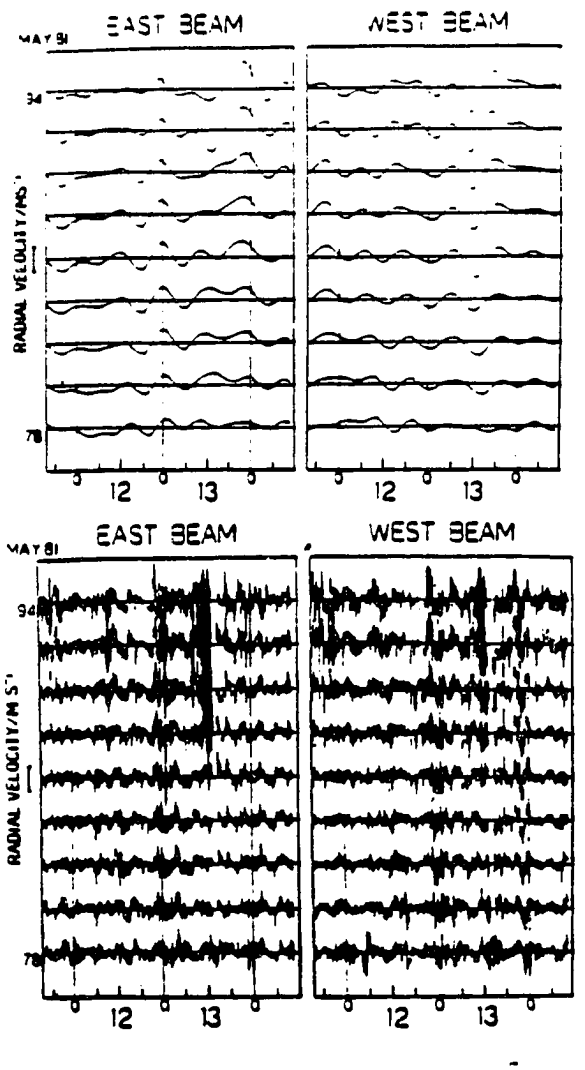

Figure 1.2: Radar measurements of gravity waves. High-frequency radar measurements of line-of-sight velocities at heights between 78 and 94km in the upper mesosphere measured in two directions, equally inclined at small angles to the vertical. Top panels show data filtered to include only periods longer than 8hr and bottom panels show data filtered to include only periods from 8 min to 8hr. The data were collected during May 11-14, 1981 (After Vincent and Reid, 1983).

$$\frac{\partial w}{\partial t} + u\frac{\partial w}{\partial x} + v\frac{\partial w}{\partial y} + w\frac{\partial w}{\partial z} + \frac{1}{\rho}\frac{\partial p}{\partial z} + g = 0, \tag{1.18}$$

$$\frac{\partial u}{\partial x} + \frac{\partial v}{\partial y} + \frac{\partial w}{\partial z} = 0, \tag{1.19}$$

$$\frac{\partial \theta}{\partial t} + u\frac{\partial \theta}{\partial x} + v\frac{\partial \theta}{\partial y} + w\frac{\partial \theta}{\partial z} = 0, \tag{1.20}$$

where u,v and w are velocity components in x,y and z directions respectively, p is the pressure, θ is the potential temperature, $f = 2\Omega sin\varphi$ is the Coriolis parameter. Linearizing (1.16) - (1.20) by letting

$$u = \overline{u} + u', \qquad v = v',$$

$$w = w', \qquad \rho = \rho_0 + \rho',$$

$$p = \overline{p}(z) + p', \qquad \theta = \overline{\theta}(z) + \theta',$$

where the mean zonal wind $\overline{u}$ of the basic state and the density ρ_0 are both assumed to be constant, results in the linearized version of the set (1.16) - (1.20)

$$(\frac{\partial}{\partial t} + \overline{u}\frac{\partial}{\partial x})u' - fv' + \frac{1}{\rho_0}\frac{\partial p'}{\partial x} = 0, \tag{1.21}$$

$$(\frac{\partial}{\partial t} + \overline{u}\frac{\partial}{\partial x})v' + fu' + \frac{1}{\rho_0}\frac{\partial p'}{\partial y} = 0, \tag{1.22}$$

$$(\frac{\partial}{\partial t}+\overline{u}\frac{\partial}{\partial x})w^{'}+\frac{1}{\rho_0}\frac{\partial p^{'}}{\partial z}-\frac{\theta^{'}}{\overline{\theta}}g=0, \tag{1.23}$$

$$\frac{\partial u^{'}}{\partial x}+\frac{\partial v^{'}}{\partial y}+\frac{\partial w^{'}}{\partial z}=0, \tag{1.24}$$

$$(\frac{\partial}{\partial t}+\overline{u}\frac{\partial}{\partial x})\theta^{'}+w^{'}\frac{d\overline{\theta}}{dz}=0, \tag{1.25}$$

Assuming a constant N, the above equations have harmonic wave solutions of the form

$$(u^{'},v^{'},w^{'},\theta^{'})=Re[(\hat{u},\hat{v},\hat{w},\hat{\theta})exp(i\phi)], \tag{1.26}$$

where all quantities with a ' ^ ' are complex amplitudes, and $\phi = kx + ly + mz - \nu t$ is the phase, which is assumed to depend linearly on x, y, z and t, and ν is the intrinsic frequency which is the frequency relative to the mean flow. Here the horizontal wave numbers k and l are real since the solutions are always sinusoidal in x and y. However, the vertical wave number $m = m_r + m_i$ may be complex, in which case m_r describes sinusoidal variation in z and m_i describes exponential decay or growth in z depending on whether m_i is positive or negative. When m is real the total wave number may be regarded as a vector

$$\vec{\kappa} \equiv (k, l, m), \tag{1.27}$$

directed perpendicular to constant phase lines, and in the direction of phase increase, whose components, $k = 2\pi/L_x$, $l = 2\pi/L_y$ and $m = 2\pi/L_z$, are inversely proportional to the horizontal and vertical wavelengths, respectively. Substitution of the assumed solution (1.26) into (1.21) - (1.25) yields the dispersion relation

$$\nu^2 = f^2 + \frac{(N^2 - f^2)(k^2 + l^2)}{k^2 + l^2 + m^2} = N^2 - \frac{(N^2 - f^2)m^2}{k^2 + l^2 + m^2}, \tag{1.28}$$

Note that in middle latitudes f is $\sim 10^{-4}s^{-1}$ and in the troposphere and lower stratosphere N is $\sim 10^{-2}s^{-1}$, thus all propagating waves with real k, l, m requires that

$$f^2 < \nu^2 < N^2, \tag{1.29}$$

For those waves with a frequency close to f, the rotational effects of the earth are important. What we are most interested here are 2-D gravity waves with horizontal wavelengths less than $500km$ and vertical wavelengths less than $50km$ and with $\nu^2 \gg f^2$. Thus the rotation effects of the earth can be neglected. If we assume that the motion occurs only in (x, z) plane, equation (1.28) reduces to

$$\nu^2 = \frac{N^2 k^2}{k^2 + m^2}, \tag{1.30}$$

or

$$\nu = \omega - \overline{u}k = \pm \frac{Nk}{(k^2 + m^2)^{1/2}}, \tag{1.31}$$

where the plus (minus) sign is to be taken for eastward (westward) phase propagation relative to the mean wind.

If we let $k > 0$ and $m < 0$, then lines of constant phase tilt eastward with respect to height as shown in Fig. 1.3 (i.e., for $\phi = kx + mz$ to remain constant as x increases, z must also increase when $k > 0$ and $m < 0$). The choice of the positive root in (1.31) then corresponds to eastward and downward phase propagation relative to the mean flow with horizontal and vertical phase speeds (relative to the mean wind) given by

$$c_x = \frac{\nu}{k} = \pm \frac{N}{(k^2 + m^2)^{1/2}}, \tag{1.32}$$

and

$$c_z = \frac{\nu}{m} = \pm \frac{N}{(k^2 + m^2)^{1/2}}. \tag{1.33}$$

The components of the group velocity, c_{gx} and c_{gz}, on the other hand, are given by

$$c_{gx} = \frac{\partial \nu}{\partial k} = \overline{u} \pm \frac{Nm^2}{(k^2 + m^2)^{3/2}}, \tag{1.34}$$

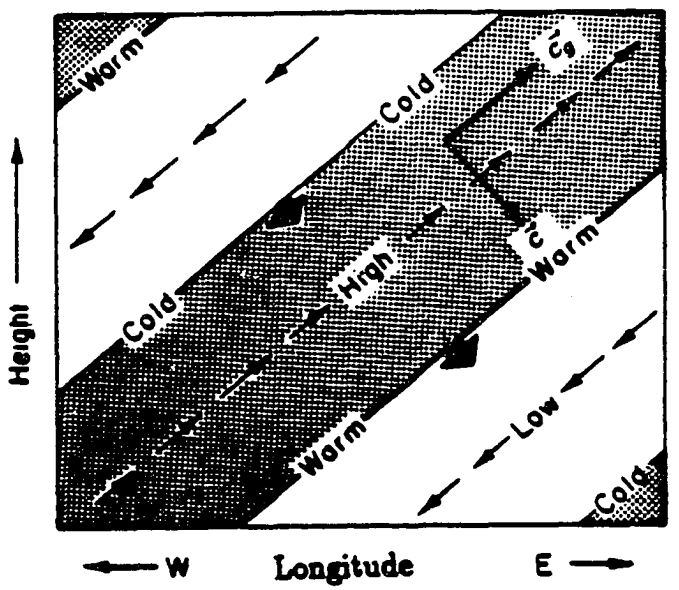

Figure 1.3: Cross section of gravity phases and group velocity. Idealized cross section showing phases of the pressure , temperature, and velocity perturbations for an internal gravity wave. Thin arrows indicate the perturbation velocity filed, blunt arrows the phase velocity($\vec{c}$). $\vec{c}_g$ is the group velocity. Shading shows regions of upward motion. (After Holton, 1992.)

$$c_{gz} = \frac{\partial \nu}{\partial m} = \pm \frac{-Nkm}{(k^2 + m^2)^{3/2}}. \tag{1.35}$$

Thus the vertical component of group velocity has a sign opposite to that of the vertical phase speed relative to the mean wind (downward phase propagation implies upward energy propagation). Furthermore, it is easily shown from (1.34) and (1.35) that the group velocity vector is parallel to lines of constant phase. Thus internal gravity waves have the remarkable property that the group velocity is perpendicular to the direction of phase propagation. Since energy propagates at the group velocity, this implies that the energy propagates parallel to the wave crests and troughs. In the atmosphere, internal gravity waves generated in the troposphere by cumulus convection, by flow over topography, and by other processes may propagate energy upward many scale heights into the upper atmosphere, even though individual fluid parcel oscillations may be confined to vertical distances of the order of a kilometer or less (Holton 1992).

Chapter 2

Gravity Wave Saturation Theories

There have been a number of theoretical studies that have addressed various aspects of the gravity wave saturation problem. Observations of wind and temperature fluctuations in the middle atmosphere have shown both the amplitudes and the vertical wavelengths of gravity waves to increase with height, but more slowly than that implied by the decrease in density in the absence of dissipation (Fritts, 1984). There is a tendency for the velocity shears and the temperature gradients to be bounded, with representative values being near that required to achieve local convective instability. A number of theories have been advanced to explain either the apparent amplitude limits or the evolution of and interactions within the motion spectrum. They range from linear studies of the gravity wave amplitudes and time scales required for convective or dynamical instability to nonlinear studies of the resonant and nonresonant

interactions among gravity waves or between gravity waves and other modes of motion. Some studies indicate that the motion spectrum may be largely a manifestation of quasi-geostrophic (quasi-two-dimensional) turbulence. But this interpretation is contradicted by some observational data (Fritts, 1989). Linear studies rely on convective or dynamical instabilities within the wave field to dissipate wave energy and thus limit the primary wave amplitudes. Nonlinear theory assumes that the wave amplitudes are limited not by instabilities within the wave field, but by nonlinear interactions among the components of the gravity wave spectrum. In this chapter, all the above mentioned studies will be reviewed briefly.

2.1 Linear Saturation Theory

Linear theory assuming a vertical convective instability of the wave field was first used by Hodges (1967) to explain the occurrence of turbulence in the middle atmosphere. Subsequently, Hodges (1969) and Hines (1970) calculated the level of turbulent diffusion needed to balance wave growth with height in an unsheared environment. Lindzen (1981) extended these ideas and attempted to describe, in a quantitative manner, the principal effects of gravity wave saturation thought to be important in the middle atmosphere. This theory provides the basis of our review of linear theories.

Assuming adiabatic inviscid gravity wave motions with intrinsic frequen-

cies ω such that $f \ll \omega \ll N$, an atmosphere in hydrostatic balance, and that motions occur in an $x - z$ plane with a mean velocity $\overline{u}(z)$ in the x direction, then the x and z momentum equations, the continuity equation, and the adiabatic equation are as follows

$$\frac{\partial u}{\partial t} + u\frac{\partial u}{\partial x} + w\frac{\partial u}{\partial z} + \frac{1}{\rho}\frac{\partial p}{\partial x} = 0, \tag{2.1}$$

$$\frac{\partial w}{\partial t} + u\frac{\partial w}{\partial x} + w\frac{\partial w}{\partial z} + \frac{1}{\rho}\frac{\partial p}{\partial z} + g = 0, \tag{2.2}$$

$$\frac{\partial u}{\partial x} + \frac{\partial w}{\partial z} = 0, \tag{2.3}$$

and

$$\frac{\partial \theta}{\partial t} + u\frac{\partial \theta}{\partial x} + w\frac{\partial \theta}{\partial z} = 0. \tag{2.4}$$

where u, and w are the horizontal (x-direction) and vertical velocities, respectively, p is the pressure, θ is the potential temperature, and g is the gravitational constant. In accordance with the theory of linearization, all field variables can be expressed as the sum of a horizontal mean and a perturbation about the mean,

$$\phi(x, z, t) = \overline{\phi}(z) + \phi'(x, z, t), \tag{2.5}$$

with

$$\overline{\phi}(z) = \frac{1}{\lambda_x}\int_0^{\lambda_x} \phi \, dx. \tag{2.6}$$

For hydrostatic motions, $\theta'/\overline{\theta} = -\rho'/\overline{\rho}$ (Holton, 1979), yielding the linearized equations

$$\frac{\partial u'}{\partial t} + \overline{u}\frac{\partial u'}{\partial x} + w'\frac{d\overline{u}}{dz} + \frac{1}{\overline{\rho}}\frac{\partial p'}{\partial x} = 0, \tag{2.7}$$

$$\frac{\partial w'}{\partial t} + \overline{u}\frac{\partial w'}{\partial x} - \frac{\theta'}{\overline{\theta}}g + \frac{1}{\overline{\rho}}\frac{\partial p'}{\partial z} = 0, \tag{2.8}$$

$$\frac{\partial u'}{\partial x} + \frac{\partial w'}{\partial z} = 0, \tag{2.9}$$

and

$$\frac{\partial \theta'}{\partial t} + \overline{u}\frac{\partial \theta'}{\partial x} + w'\frac{d\overline{\theta}}{dz} = 0. \tag{2.10}$$

The perturbation quantities can be represented as single Fourier components,

$$\phi'(x,z,t) = \phi'(z)e^{z/2H}e^{ik(x-ct)}, \tag{2.11}$$

where k and m are the horizontal and vertical wavenumbers of the perturbation, respectively, and $H = R\overline{T}/g$ is the scale height of the atmosphere. The factor $e^{z/2H}$ is just that required to offset the density decay with height and insure that energy is conserved until saturation occurs. Combining the

momentum equations, the adiabatic equation and the continuity equation, we obtain

$$w'_{zz} + [\frac{N^2}{(\overline{u}-c)^2} - \frac{\overline{u}_{zz}}{(\overline{u}-c)} - k^2 - \frac{\overline{u}_z}{(\overline{u}-c)H} - \frac{1}{4H^2}]w' = 0. \qquad (2.12)$$

where N^2 is the Brunt-Väisälä frequency, and c is the horizontal phase velocity of the wave motion. This equation, known as the Taylor-Goldstein equation, describes the amplitude and vertical structure of the vertical perturbation velocity of atmospheric gravity waves in an environment with variable $N > 0$ and $\overline{u}$. For our purposes, it is reasonable to assume that N^2 is constant, that $\overline{u}_{zz}$ is small, and that H is large. Also, since $\omega = k(c-\overline{u}) \ll N$, k^2 itself is small compared with $N^2/(c-\overline{u})^2$. Then the above equation may be reduced to

$$w'_{zz} + [\frac{N^2}{(\overline{u}-c)^2}]w' = 0. \qquad (2.13)$$

This equation has the approximate WKB solution (Bender and Orszag, 1978)

$$w'(z) = Am^{-1/2}e^{i\int m\,dz'}. \qquad (2.14)$$

where $m = N/(\overline{u}-c)$ is the vertical wavenumber. Provided that m is slowly varying, the vertical perturbation velocity has the form

$$w'(x,z,t) = Am^{-1/2}e^{z/2H}e^{i(kx+mz-kct)}. \qquad (2.15)$$

Other quantities are obtained in terms of w' from the linearized equations of motion. From the continuity equation we see that for m slowly varying,

$$u' = -\frac{mw'}{k}, \tag{2.16}$$

and from the adiabatic energy equation we find that

$$\theta' = -\frac{\overline{\theta}_z}{ik(\overline{u}-c)}w'. \tag{2.17}$$

Differentiating equation (2.17) with respect to z and assuming that perturbation quantities contribute most to the vertical variations, we get

$$\theta'_z = -\frac{\overline{\theta}_z}{(\overline{u}-c)}\frac{mw'}{k} = \frac{\overline{\theta}_z u'}{(\overline{u}-c)}. \tag{2.18}$$

The atmosphere is statically unstable whenever

$$(\overline{\theta}+\theta')_z < 0, \tag{2.19}$$

or from the definition of N^2

$$N^2(z) = \frac{g}{\overline{T}}[\frac{\partial \overline{T}}{\partial z} + \frac{g}{c_p}] = \frac{g}{\overline{\theta}}\frac{\partial \overline{\theta}}{\partial z} \tag{2.20}$$

we have

$$(\overline{T}+T')_z < -\frac{g}{c_p}. \tag{2.21}$$

But with equation (2.18) we see that these conditions correspond, in the case of monochromatic wave motions, to a simple condition on the horizontal perturbation velocity,

$$u' > c - \overline{u}. \tag{2.22}$$

Thus for monochromatic wave motions, occurrences of convectively unstable regions within the wave field correspond to regions in which the total parcel velocity, $\overline{u}+u'$, exceeds the horizontal phase speed c of the wave. This means that any wave amplitude in excess of the threshold value will lead to instability and the production of turbulence that acts to prevent further growth of the wave amplitude.

The basic premise of the linear saturation theory advanced by Hodges (1967, 1969), and Lindzen (1967, 1968a, 1981) is that convectively unstable regions appearing within the wave field result in the production of turbulence and just that level eddy diffusion necessary to restrain wave amplitudes to values near neutral static stability. If we assume that the effects of turbulent diffusion are immediate and complete, the saturation conditions become

$$\theta_z' \geq -\overline{\theta}_z \qquad or \qquad T_z' \geq -\overline{T}_z - \frac{g}{c_p}, \tag{2.23}$$

and for monochromatic wave motions,

$$| u' | \leq | c-u | . \tag{2.24}$$

The saturation conditions place no constraints on small amplitude wave motions. However, wave motions with fluctuations that exceed saturation values are subjected to turbulent dissipation that limits wave amplitudes and produces a vertical divergence of the gravity wave momentum flux, which is

nondivergent for steady, conservative wave motions. These effects are illustrated in Figure 2.1. The turbulent dissipation of saturating gravity waves was suggested by Hodges (1969) to account for the observed level of turbulent diffusion in the middle atmosphere. Momentum deposition accompanying gravity wave dissipation was suggested by Houghton (1978) and Lindzen (1981) to provide the momentum source needed to satisfy the thermal and momentum budgets of the middle atmosphere.

The gravity wave motions can be dynamically unstable at substantially smaller wave amplitudes for intrinsic frequencies, $\omega \sim f$, due to the transverse shear in the velocity field of such motions (Fritts, 1984; Dunkerton, 1984; Fritts and Rastogi, 1985). The threshold amplitude assuming a minimum Richardson number of 1/4 is given by (Fritts, 1988a)

$$\frac{u'}{(c-\overline{u})} = \frac{\theta'_z}{\overline{\theta}_z} = \frac{2(1-f^2/\omega^2)^{1/2}}{1+(1-f^2/\omega^2)^{1/2}}. \tag{2.25}$$

While the amplitude required for instability(scaled by the intrinsic phase speed) falls to zero at f, the vertical shear of the velocity field at the threshold amplitude actually increases to a value of $u'_z = 2N$ due to the increase in the vertical wavenumber as ω approaches f (Fritts, et al., 1988a). The linear theory was generalized by Hines (1971, 1987) for the case of convective instability, to account for possible slantwise instability along a path of arbitrary orientation. Hines examined both the threshold for instability for various growth rates

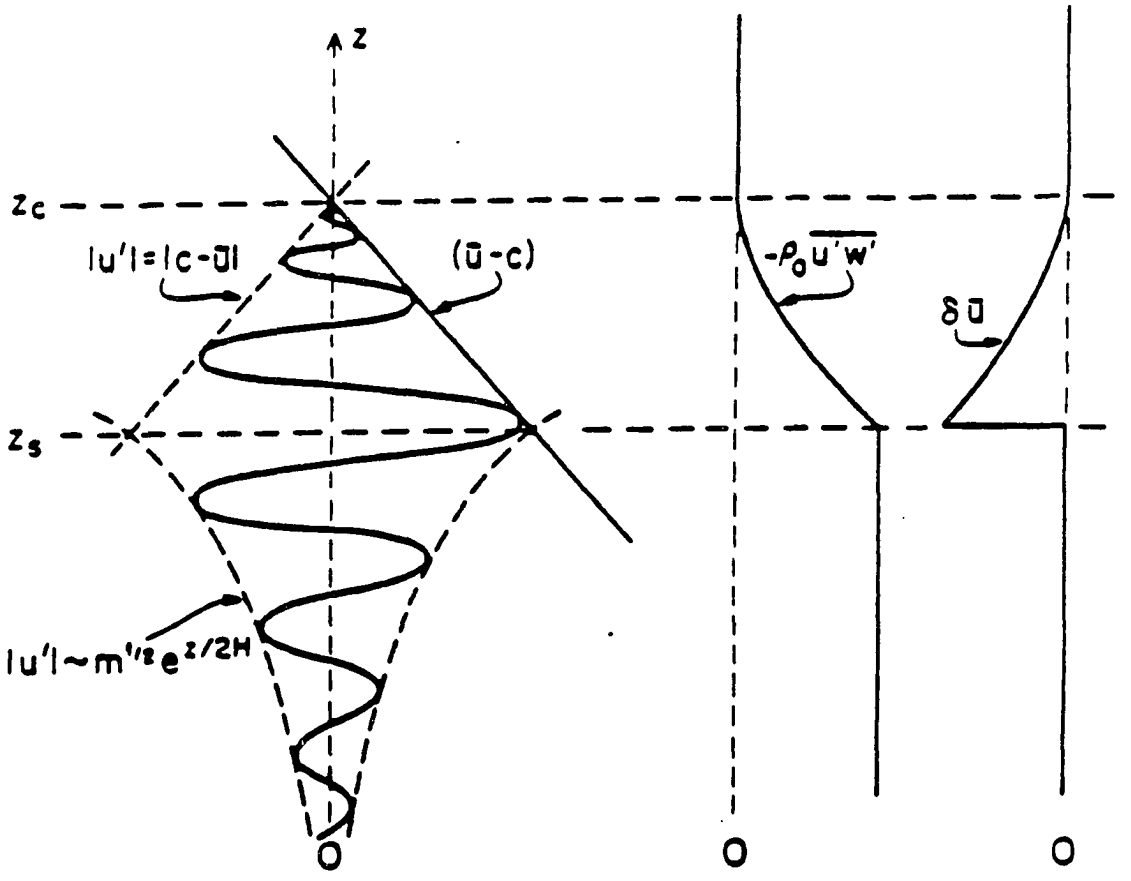

Figure 2.1: Schematic illustration of the growth with height and saturation of a gravity wave due to convective instability. Wave damping produces both a divergence of the vertical flux of horizontal momentum and an acceleration of the mean flow toward the phase speed of the wave. Deceleration and diffusion cease above the critical level ($z = z_c$) in the linear theory(Fritts,1984).

and the axis of maximum instability and concluded that slantwise static instability(SSI), of which the vertical convective instability considered by Hodges (1967) is a special case, is the more likely mode of instability. It was suggested that the slantwise instability is always dominant, with the axis of maximum instability more nearly horizontal than vertical for reasonable growth rates or turbulence lifetimes. These results imply a more anisotropic turbulence spectrum than anticipated in the classical linear theory and may provide a ready means of excitation at small scales of the vortical mode(quasi-two-dimensional turbulence with essentially vertical vorticity) in the atmosphere.

Gravity wave momentum fluxes act to accelerate or decelerate the large-scale flow at levels where the waves are transient or dissipating (Bretherton, 1969; Hines, 1972; Lilly, 1972). This has significant consequences for the mean circulation and the thermal and constituent structures in the mesosphere and lower thermosphere, where gravity wave drag is the major contributor to the reversal of the vertical shear of the mean zonal wind and to the resulting mean meridional circulation and the reversal of the meridional temperature gradient near the mesopause (Houghton, 1978; Lindzen, 1981; Holton, 1982; Dunkerton, 1982). These results are consistent with the observational studies in the mesosphere that revealed the strength of the mean meridional circulation and the magnitude of the gravity wave momentum flux divergence (Nastrom et al., 1982; Vincent and Reid, 1983; Smith and Lyjak, 1987).

Following Lindzen (1981), we assume that gravity waves propagate upward from source regions in the troposphere or lower stratosphere in a conservative fashion until they achieve saturation amplitudes. Therefore we assume that wave amplitudes are limited by saturation conditions (2.23) and (2.24). The phase velocity spectra and the regions of saturation envisaged by Lindzen for winter and summer at mid-latitudes are illustrated in Figure 2.2. Below the level at which waves saturate, denoted z_s, the mean flow acceleration,

$$\frac{\partial \overline{u}}{\partial t} = -\frac{1}{\rho}\frac{\partial}{\partial z}(\rho_0 \overline{u'w'}), \tag{2.26}$$

is zero since the gravity wave momentum flux is constant away from critical levels (Eliassen and Palm, 1960). The saturation level z_s maybe inferred from the wave and mean flow parameters specified in the lower atmosphere by using the saturation conditions [Holton, 1982; Lindzen, 1984]. Above z_s the saturated horizontal perturbation velocity (assuming that $c - \overline{u}$ does not increase faster than $e^{z/2H}$) is

$$| u_s' | = | c - \overline{u} |, \tag{2.27}$$

and from (2.15) the saturated vertical perturbation velocity is

$$w_s' = -\frac{k}{m}u_s' = \frac{k}{N}(\overline{u} - c)^2, \tag{2.28}$$

The momentum flux associated with the saturated gravity wave is then

$$\rho_0 \overline{u_s' w_s'} = -\frac{\rho_0}{2}u_s' w_s' = -\frac{\rho_0}{2}\frac{k}{N}(\overline{u} - c)^3. \tag{2.29}$$

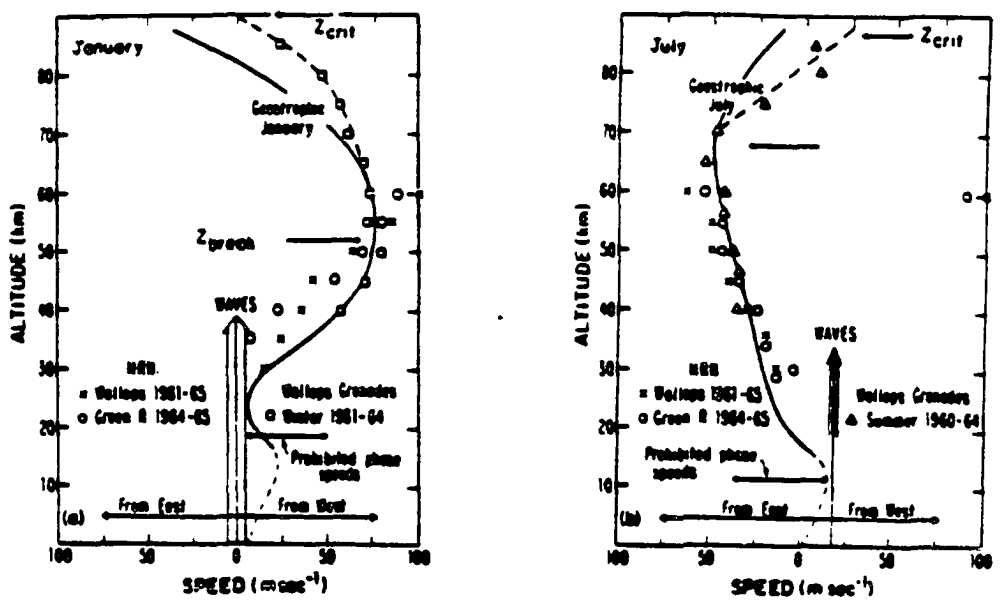

Figure 2.2: Schematic illustration of the allowed and prohibited phase speeds for gravity waves at Wallops Island for winter and summer(Lindzen, 1981). Note that the summer wind profile prevents stationary waves from entering the middle atmosphere.

The momentum flux above z_s reflects variations in vertical direction z both of the density, $\rho_0(z)$, and of the mean velocity in the direction of wave motion, $\overline{u}(z)$ and, in general, N. Assuming N is constant, the induced mean flow acceleration given by (2.26) above z_s is the sum of two terms,

$$\frac{\partial \overline{u}}{\partial t} = -\frac{k(\overline{u}-c)^2}{2N}\left[\frac{(\overline{u}-c)}{H} - 3\overline{u}_z\right]. \tag{2.30}$$

The form and direction of the mean flow acceleration are shown in Figure 2.1 with the dashed mean velocity profile. The tendency is always to accelerate the mean flow toward the phase speed of the gravity wave. Thus the saturation of gravity waves with positive and negative zonal phase speeds, respectively, provides a mechanism by which the summer and winter mean zonal flows in the upper mesosphere may be reversed, consistent with observations. The induced acceleration is not limited to the zonal direction but is applied in whatever direction the wave is propagating in relation to the local mean flow.

2.2 Nonlinear Saturation Theory

In contrast to the linear saturation theories, nonlinear interactions do not rely on a threshold wave amplitude for energy exchange, but simply operate more efficiently for waves of large amplitudes(Fritts, 1989). These interactions are of two types, resonant and nonresonant interactions. Resonant interactions require an (approximate) quantization of total wavenumber and intrinsic

frequency such that the sum or difference for an interacting pair must equal that of the third wave, $k_1 \pm k_2 = k_3$ and $\omega_1 \pm \omega_2 = \omega_3$. Resonant interaction theory is also most appropriate for waves of small amplitudes, a condition that is of dubious relevance to middle atmosphere gravity waves. Nonresonant or off-resonant interactions become more significant at large wave amplitudes, may involve other wave components, and are poorly approximated by weak (resonant) interaction theory.

As in the oceans, much of our knowledge of nonlinear interactions among gravity waves in the atmosphere has come from application of weak, or resonant, interaction theory. This followed closely the early work of Hasselmann (1967) and McComas and Bretherton (1977), who first identified the three dominant resonant interaction triads: induced diffusion, elastic scattering, and the parametric subharmonic instability. These are the interactions that permit an efficient energy exchange while simultaneously satisfying the resonance conditions and the gravity wave dispersion relation. Of these, induced diffusion amounts to a random walk of the wavenumber in response to a small, near-vertically oriented, wavenumber with low intrinsic frequency. Elastic scattering involves an interaction between a high-frequency wave motion and a low-frequency wave motion with approximately half the vertical scale and drives this component of the wave spectrum towards equilibration of upward and downward propagating waves. Of the three interactions, the parametric sub-

harmonic instability(PSI) is almost certain to be the most relevant in terms of effecting a transfer of energy in the atmosphere to small scales of motion. The PSI involves the decay of a large-scale motion of low frequency via excitation of upward and downward propagating motions at primarily smaller vertical scales and approximately half the parent wave frequency (Fritts, 1989).

These interactions have been considered in an atmospheric context by Yeh and Liu (1981, 1985) and found to be of potential significance in the decay of wave motions under various circumstances. Elastic scattering was found to operate efficiently for motions with small scales and relatively high frequencies, whereas induced diffusion was found to have small interaction times for either very small horizontal or vertical scales. The PSI, on the other hand, operates most efficiently on waves with relatively low intrinsic frequencies and small scales. These results imply that such interactions should be important for motions with small vertical wavelengths but relatively less significant for the more energetic wave motions with large vertical wavelengths (Fritts, 1989).

Further implications of nonlinear interactions were investigated by Inhester (1987), Dunkerton(1987), Dong and Yeh(1988), Yeh and Dong(1989), and Fritts et al.(1992). Wave packet localization and nonuniform stratification were found to lead to threshold PSI amplitudes and smaller interaction rates (Inhester, 1987). Dunkerton(1987) addressed the effects of the PSI on the momentum flux of the wave field and concluded that nonlinearity serves

to reduce the momentum flux through excitation of other wave motions but fails to prevent the attainment of linearly unstable wave amplitudes, in accordance with the study by Fritts(1985). Dong and Yeh(1988) considered both resonant and nonresonant interactions among gravity waves and between gravity waves and acoustic and vortical modes of motion, and found that gravity wave-acoustic wave interactions are unlikely to be significant, but that the nonresonant interaction of a gravity wave and two vortical modes would occur above a threshold wave amplitude of $u' = \sqrt{2}(c-\overline{u})$. This threshold was found to disappear in the present of mean shear or rotation(Yeh and Dong, 1989; Fritts et al., 1992). This could prove to be an efficient means of transferring energy from the gravity wave field to vortical modes.

Other studies have attempted to address the relative importance of competing amplitude-limiting mechanisms within the gravity wave field. Weinstock (1985) suggested that the buoyancy subrange theory of Lumley (1964) can be used as an appropriate framework within which to understand the high wavenumber portion of atmospheric vertical wavenumber spectra, which are seen to have a near universal amplitude and a slope near -3 (Dewan et al., 1984; Smith et al., 1987; Fritts et al., 1988a). If appropriate, this would imply a range of vertical wavenumbers over which gravity wave interactions are strong and rapid. Fritts (1985) performed numerical simulations of gravity wave propagation and saturation under the influence of convective adjustment

and full nonlinearity. The results suggest that while nonlinear interactions are able to restrain wave amplitudes to some degree, they are unable to prevent the occurrence of wave amplitudes sufficient to induce linear convective or dynamical instabilities within the wave field. Therefore, nonlinear wave-wave interactions were not the principal mechanism for limiting wave amplitudes at large vertical scales, but rather that gravity wave saturation at these scales must involve a rapid cascade of energy into turbulence. This does not imply that the saturation mechanism is linear but only that linear theory provides a reasonable guide to the wave amplitudes at which such processes become significant.

Chapter 3

Gravity Wave Spectrum

It has been known for many years that in the lower and middle atmosphere the shapes of the observed spectra of atmospheric mesoscale velocities and temperatures as functions of horizontal wavenumber, k, vertical wavenumber, m, and intrinsic frequency, ω , are insensitive to the geographical parameters obtained when the data were taken (VanZandt and Fritts,1989). Observational studies have revealed a high degree of universality in the mean atmospheric motion spectrum (VanZandt, 1982, 1985). Mean frequency spectra of horizontal motions typically exhibit only slight amplitude variations with a slope near $-5/3$ (Balsley and Carter, 1982; Carter and Balsley, 1982; Vincent, 1984; Balsley and Garello, 1985), while vertical wavenumber spectra suggest a saturated gravity wave spectrum with a high-wavenumber slope near -3 (Dewan et al., 1984; Smith et al., 1987; Fritts and Chou, 1987; Fritts et al., 1988; Wu and Widdel, 1990). Similar spectral features are seen in temper-

ature and density fields, although vertical wavenumber spectra obtained using lidar data suggest wave amplitudes smaller than saturated values in the upper stratosphere (Fritts, 1988; Kwon et al., 1990; Wilson et al., 1990). At smaller vertical wavenumbers, wave amplitudes depart from apparent saturated values with the characteristic vertical scale of the motion spectrum increasing with height (Smith et al., 1987; Fritts and Chou, 1987; Sidi et al., 1988). The form of the vertical wavenumber spectrum appears generally to be consistent with models proposed originally by Garrett and Munk (1975) and Desaubies (1976) for oceanic waves and adopted by VanZandt (1982) for atmospheric gravity waves. VanZandt and Fritts (1989) noted that it is necessary to have a positive slope at low wavenumbers in order to ensure that the vertical flux of wave action remains finite. To account for this additional constraint, they proposed modified Garrett-Munk and Desaubies spectra. In this chapter, a brief review of all these spectral models will be provided.

3.1 Garrett-Munk and Desaubies Models

Following a suggestion by Dewan (1979), VanZandt (1982) showed that the spectra are consistent with the gravity wave dispersion relation by fitting the Garrett and Munk (1972, 1975) oceanic gravity wave spectral model to the atmospheric spectra. The Garrett and Munk (1975) model for the total

energy is

$$E(m,\omega) = E_0 \frac{A(\mu)}{m_*} B(\omega), \tag{3.1}$$

where E_0 is the total (kinetic plus potential) energy, $A(\mu)$ is the model vertical wavenumber spectrum as a function of $\mu = m/m_*$, m_* is the characteristic vertical wavenumber, and $B(\omega)$ is the model frequency spectrum. This model assumes, as a first approximation, that the dependence of the spectrum on vertical wavenumber, m, and intrinsic frequency, ω, is separable. Garrett and Munk expressed the frequency spectra $B(\omega)$ as a negative power of ω

$$B(\omega) = (p - 1) f^{p-1} \omega^{-p}, \tag{3.2}$$

normalized so that

$$\int_f^N B(\omega)\, d\omega = 1. \tag{3.3}$$

Garrett and Munk fitted the oceanic frequency spectra with $p = 2$, and VanZandt fitted the atmospheric spectra with $p = 5/3$, a nominal, long-term average value. Recently, Fritts and Wang [1991] in their observational study of gravity wave spectra near the summer mesopause using MST radar data from Poker Flat revealed a value near $p = 4/3$, consistent with the observations reported by Vincent (1984). Thus, p appears not to be constant, but varies within a small range near 5/3.

The observed vertical wavenumber spectra at large m can be described by negative powers of m, so $A(\mu)$ was expressed by Garrett and Munk (1975)

and Desaubies, respectively as

$$A_G(\mu) = \frac{C_G}{(1+\mu)^t}, \qquad C_G = t - 1, \tag{3.4}$$

and

$$A_D(\mu) = \frac{C_D}{1+\mu^t}, \qquad C_D = \frac{t}{\pi} sin\frac{\pi}{t}, \tag{3.5}$$

where the constants, C_G and C_D, normalize $A(\mu)$ to unity,

$$\int_0^\infty A(\mu)\, d\mu = 1. \tag{3.6}$$

With a positive value of t the models $A(\mu)$ approach a constant value at small μ and are asymptotic to C/μ^t at large μ. Garrett and Munk (1975) found that the observed oceanic spectra could be fitted with $t = 2.5$. VanZandt (1982) fitted the observed lower atmospheric spectra with $t = 2.4$, and later observations of atmospheric vertical wavenumber spectra show that t is closer to 3 (Dewan et al., 1984; Smith et al., 1987; Fritts and Chou, 1987).

3.2 VanZandt and Fritts Models

The Garrett and Munk models cited above lead to unrealistic vertical fluxes of wave action or energy at small μ. The energy flux is given by

$$S_E = \int_0^\infty dm \int_f^N \rho_0 c_{gz} E(m,\omega)\, d\omega, \tag{3.7}$$

where ρ_0 is the atmospheric density c_{gz} is the vertical group velocity of the gravity wave. Using the gravity wave dispersion relation and (3.1), we have

$$S_E = \rho_0 \frac{E_0}{m_*} \int_0^\infty \frac{A(\mu)}{\mu} d\mu \int_f^N \omega B(\omega) d\omega. \tag{3.8}$$

Then with $t = 3$, for example, the μ integral of $A_D(\mu)$ is

$$-\frac{1}{3} ln(1 + \frac{1}{\mu^3}) \mid_{\mu_L}^{\infty} = \frac{1}{3} ln(1 + \frac{1}{\mu^3}).$$

As μ_L decreases toward 0, the integral increases toward ∞. In order to avoid this, VanZandt and Fritts (1989) proposed the modified spectral models. The modified vertical wavenumber spectra were obtained by multiplying $A_G(\mu)$ and $A_D(\mu)$ by μ^s with $s > 0$, so that

$$A_{MG}(\mu) = \frac{C_{MG}\mu^s}{(1+\mu)^{s+t}}, \qquad C_{MG} = \frac{\Gamma(s+t)}{\Gamma(s+1)\Gamma(t-1)}, \tag{3.9}$$

and

$$A_{MD}(\mu) = \frac{C_{MD}\mu^s}{1+\mu^{s+t}}, \qquad C_{MD} = \frac{s+t}{\pi} sin(\frac{s+1}{s+t})\pi. \tag{3.10}$$

Again here the constants C_{MG} and C_{MD} are introduced to normalize $A_{MG}(\mu)$ and $A_{MD}(\mu)$ to unity. Since $A_{MG}(\mu)$ and $A_{MD}(\mu)$ are functions varying as μ^s when $\mu \ll 0$, they permit the convenience of setting μ_L to 0.

The value of s is uncertain, but some recent observed spectra increase at small μ with a slope between 1/2 and 1 (Maekawa et al., 1987; Fritts 1988). VanZandt and Fritts showed that $s = 1$ and $t = 3$ are representative and

convenient descriptions of the observed gravity wave spectra. Thus, $A_{MG}(\mu)$ and $A_{MD}(\mu)$ become

$$A_{MG}(\mu) = 6\frac{\mu}{(1+\mu)^4}, \tag{3.11}$$

and

$$A_{MD}(\mu) = \frac{4}{\pi}\frac{\mu}{1+\mu^4}. \tag{3.12}$$

Recent studies indicate that the MD model spectrum is the best model spectrum in fitting the observed vertical wavenumber spectra (Fritts and Wang, 1991).

Fritts and VanZandt (1993) further updated the VF89 model to the following form

$$E(\mu,\omega,\phi) = E_0 A(\mu)B(\omega)\Phi(\phi), \tag{3.13}$$

where the frequency spectrum $B(\omega)$ and the vertical wave number spectrum $A(\mu)$ are the same as that described earlier. But a new horizontal spectrum $\Phi(\phi)$ is introduced to describe the horizontal anisotropy in the azimuthal directions of propagation with

$$\int_0^{2\pi} \Phi(\phi)d\phi = 1. \tag{3.14}$$

and ϕ is measured counterclockwise from east. The spectrum $\Phi(\phi)$ expresses the orientation and isotropy or anisotropy of the wave field. In the real at-

mosphere, wave energy spectra are more likely to anisotropic, especially in regions where orography plays an important role in the generation and propagation of gravity waves. Thus the newly-proposed spectrum, $\Phi(\phi)$, is expected to provide a more representative and more convenient way of describing the anisotropy within gravity wave energy spectra.

3.3 A Saturated Vertical Wavenumber Spectrum

Another result of gravity wave saturation that has potentially significant implications in the lower and middle atmosphere is the attainment of a near-universal spectral amplitude at large vertical wavenumbers due to wave superposition and wave field instability (Fritts, 1989). Dewan and Good (1986) have shown that for hydrostatic gravity wave motions, dynamical or convective instabilities of the wave field cause the saturated power spectral density of horizontal velocity at large m to vary as

$$E_u(m) \simeq b\frac{N^2}{m^3}, \tag{3.15}$$

where b is a constant, and N and m are the Brunt-Väisälä frequency and the vertical wavenumber. By integrating the contributions to the variance of potential temperature gradient over all wavenumbers, Smith et al. (1987) inferred a coefficient of $b \sim 1/6$ for a spectrum of waves at marginal saturated amplitudes. The resulting saturated power spectral densities for velocity and

normalized temperature (T'/T) due to hydrostatic motions, assuming a frequency spectrum for total energy of the form ω^{-p} with $p = 5/3$, are

$$E_u^s(m) \simeq \frac{1}{6}\frac{N^2}{m^3}, \tag{3.16}$$

and

$$E_T^S(m) \simeq \frac{1}{10}\frac{N^4}{g^2 m^3}. \tag{3.17}$$

These saturated spectral amplitudes are in excellent agreement with observations (Endlich et al., 1969; Dewan et al., 1984; Smith et al., 1987; Fritts et al., 1988a; Sidi et al., 1988). The average velocity and normalized temperature spectra obtained by Fritts et al. (1988a) are shown in Figure 3.1 and reveal a close correspondence between the observed and predicted amplitudes and slopes at large vertical wavenumbers.

Despite the apparent utility of the saturated spectrum concept, there are reasons to believe that the gravity wave spectrum may undergo systematic changes in response to variations in the environment that depart from normal growth with height at small m (Fritts, 1989). This can be seen by noting that the saturated momentum flux for individual wave motions given by eq. (2.29) depends on both $\overline{u}(z)$ and $N(z)$. As a result, wave motions that experience a reduction in the intrinsic phase speed $(c - \overline{u})$ will dissipate preferentially while those that experience an increase in $(c - \overline{u})$ will grow with height. This results in a filtering of the gravity wave spectrum (Lindzen, 1981, 1985) and may

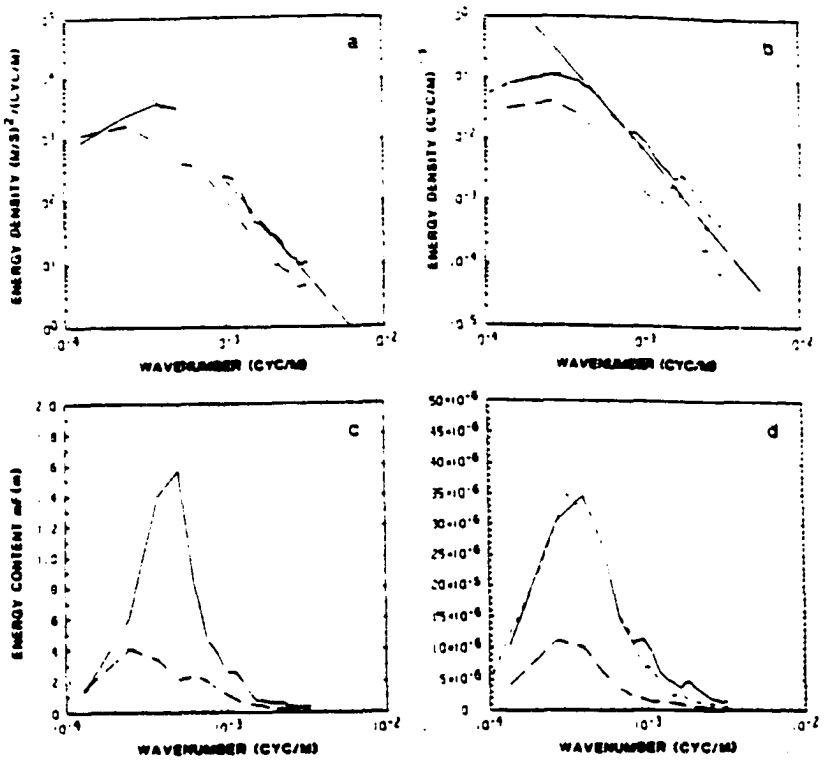

Figure 3.1: An example of observed and modified gravity wave spectrum. Mean power spectral densities a) of eastward plus northward radial velocity and b) of normalized temperature at 5-12.5(long-dashed), 12.5-20.5(solid), and 20.5-30(short-dashed) km heights measured at the MU observatory. The long-dashed straight lines show the predicted saturated spectral amplitudes for the 12.5-20.5 km height range. Shown in c) and d) are the corresponding area-preserving spectra. Note the excellent agreement with the predicted amplitudes at high wavenumbers in the stratosphere(Fritts, et al., 1988).

also account for much of the geographic, seasonal, and short-term variability seen in a variety of observational and numerical studies (Meek et al., 1985a; Miyahara et al., 1986; Fritts and Vincent, 1987; Vincent and Fritts, 1987; Reid and Vincent, 1987a). Likewise, wave motions that encounter an increase in N should experience enhanced saturation and a reduction in the vertical energy and momentum fluxes. These arguments were quantified by VanZandt and Fritts (1989) and appear to account for the needed wave drag and enhanced radar echoes near the tropopause (Larsen and Rottger, 1982; Palmer et al., 1986; Tanaka, 1986) and the high-latitude summer mesopause (Balsley et al., 1983; Fritts et al., 1988b). Therefore, the saturated gravity wave spectrum and its variation with height and environment may provide a convenient framework within which to develop a useful parameterization of gravity wave drag and dissipation in the lower and middle atmosphere (Fritts, 1989).

3.4 Integrated Energy and Momentum Fluxes

With the above expressions of the spectral form, the spectra of energy flux and the component momentum fluxes (per unit mass) can be calculated as (Fritts and VanZandt, 1993)

$$F_E(\mu,\omega) = c_{gz}E(\mu,\omega) = \frac{\omega}{m}\delta_{-\gamma}E(\mu,\omega), \tag{3.18}$$

$$F_{P_x}(\mu,\omega) = \frac{\omega}{N} b_x E(\mu,\omega)(\delta_+\delta_-\gamma)^{1/2}, \tag{3.19}$$

and

$$F_{P_y}(\mu,\omega) = \frac{\omega}{N} b_y E(\mu,\omega)(\delta_+\delta_-\gamma)^{1/2}, \tag{3.20}$$

where

$$b_{x,y} \equiv (b_x, b_y) = \int_0^{2\pi} \Phi(\phi)(cos\phi, sin\phi)d\phi. \tag{3.21}$$

and $\mid b_{x,y} \mid \leq 1$ is a measure of the anisotropy in the east-west and north-south directions. The quantities δ_+, δ_-, and γ are defined as follows

$$\delta_\pm = 1 \pm (\frac{f}{\omega})^2,$$

and

$$\gamma = 1 - (\frac{\omega}{N})^2.$$

Integrating over all μ and ω , to a good approximation, the corresponding integrated energy flux (per unit mass) may be expressed as

$$F_E \simeq C\frac{NE_0}{m_*}, \tag{3.22}$$

Similarly, the integrated component momentum fluxes (per unit mass) can be written as

$$F_{P_x,P_y} = (F_{P_x}, F_{P_y}) \simeq D(b_x, b_y)E_0, \tag{3.23}$$

with

$$C \simeq \frac{1}{18}, \tag{3.24}$$

and

$$D \simeq \frac{1}{22}. \tag{3.25}$$

Note here that both C and D are non-dimensional constants.

Likewise, energy flux and momentum flux divergences are calculated following Fritts and VanZandt (1993). Equating the energy dissipation rate with the vertical divergence of wave energy flux normalized by N per unit mass, we have

$$\epsilon = -\frac{N}{\rho}\frac{\partial}{\partial z}(\frac{\rho}{N}F_E), \tag{3.26}$$

The corresponding momentum flux divergences are given by

$$D_{F_x} = -\frac{1}{\rho}\frac{\partial}{\partial z}(\rho F_{P_x}) = -\frac{1}{\rho}\frac{\partial}{\partial z}(\rho D b_x E_0), \tag{3.27}$$

and

$$D_{F_y} = -\frac{1}{\rho}\frac{\partial}{\partial z}(\rho F_{P_y}) = -\frac{1}{\rho}\frac{\partial}{\partial z}(\rho D b_y E_0). \tag{3.28}$$

Apart from the sensitivity to variations in N discussed by VanZandt and Fritts (1989), these expressions display a dependence on both the background variations of wave energy at large and small vertical wavenumbers and, in the case of momentum fluxes, the anisotropy and its variations with height. The wave energy flux and energy dissipation rate are not influenced by wave field anisotropy, of course. Observed momentum fluxes, however, suggest that wave field anisotropy is highly variable and dependent on both the mean and low-frequency components of the motion field through which the higher-frequency motions accounting for the majority of momentum and energy fluxes must propagate.

Chapter 4

A Spectral Gravity Wave Parameterization Scheme

As mentioned in previous chapters, it is widely accepted that gravity waves play an essential role in the evolution of the large-scale circulation and structure of the lower and middle atmosphere. Theoretical and modeling studies have revealed that without considering the gravity wave drag and its energy and momentum transports, it is impossible to get a wind and thermal structure as observed in the lower and middle atmosphere. It is widely believed that gravity wave drag is necessary to close the tropospheric jet in the lower atmosphere and the mesospheric jet near the mesopause. Recent efforts have revealed that gravity waves are also necessary to properly describe the evolution of the QBO (quasi-biennial oscillation) and SAO (semiannual oscillation) in the tropical atmosphere (Hamilton and Mahlman, 1988; Takahashi and Boville, 1992; Sassi et al., 1992) and are also likely to account in part for the

thermal structure of the polar stratosphere (Hitchman et al., 1989).

During the last few decades a number of efforts have attempted the parameterization of gravity wave forcing in large scale general circulation models, and great progress has been made in understanding the transports of energy and momentum fluxes caused by gravity waves. But up until now, all parameterization methods were based on artificial and/or simplistic assumptions of monochromatic wave propagation, and the results are not so satisfactory in parameterizing gravity wave forcing effects. Fortunately the achievements made by previous investigators in the successful description of gravity wave spectrum, which properly describes the main characteristics of gravity wave energy and momentum transport and their forcing effects as they propagate from the lower atmosphere to higher altitudes, make it possible for us to construct a more sophisticated parameterization scheme in the manner of spectral analysis. This development constitutes the major contribution of this thesis and has been reported by Fritts and Lu (1993).

The parameterization scheme developed in this chapter is based on the canonical model of the gravity spectrum described in the previous chapter. The model spectrum depends critically on the observed statistical structure of the motion field throughout the atmosphere. It is hoped that such a scheme will provide advantages relative to previous schemes based on the Lindzen-Holton representation of the wave spectrum as a collection of discrete and

noninteracting components (Holton, 1982; Garcia and Solomon, 1985). It will also permit an extension of the parameterization schemes for orographic wave stresses used in a number of general circulation models (Palmer et al., 1986; McFarlane, 1987; Reid et al., 1988) to other wave sources and their lower and middle atmospheric effects. In this chapter, we will give a detail description of our proposed parameterization scheme, including scheme developments, parameter specifications, and the necessary constraints.

4.1 Gravity Wave Spectra Evolution and Variations with Height

The parameterization scheme to be developed here is based on gravity wave saturation theories and the canonical vertical wavenumber spectrum model cited in Chapter 2 and Chapter 3. The idea here is try to find an easy and convenient way to describe the gravity wave energy and momentum flux variations with height as well as possible, as gravity waves propagate upward from their sources in the lower atmosphere. It is hoped that such a parameterization scheme can easily be implanted into large-scale general circulation models. A spectral analytic method is expected to provide an advantage in describing the gravity wave energy and momentum flux evolution with height relative to those using monochromatic and discrete wave approximations.

4.1.1 Energy Spectra and Variations with ρ and N

Following the previous chapter, assuming a separable gravity wave spectrum in vertical wave number, intrinsic frequency, and azimuthal direction of propagation for total wave energy, the vertical wave number spectrum can be expressed as

$$\hat{E}(\mu) = E_0 A(\mu) \int_f^N B(\omega)\, d\omega \int_0^{2\pi} \Phi(\phi)\, d\phi = E_0 A(\mu), \tag{4.1}$$

with

$$A(\mu) = \frac{4}{\pi} \frac{\mu}{1+\mu^4}, \tag{4.2}$$

or

$$E(m) = \frac{4}{\pi} \frac{E_0}{m_*} \frac{\mu}{1+\mu^4}. \tag{4.3}$$

where m is the vertical wavenumber, m_* is the characteristic vertical wavenumber, and $\mu = m/m_*$. Obviously, with the above expression, the total wave energy E_0 can be written as

$$E_0 = \int_0^\infty E(\mu)\, d\mu = \int_0^\infty E(m)\, dm. \tag{4.4}$$

The total gravity wave energy includes horizontal and vertical kinetic energy and potential energy. So that for a given gravity wave at a certain height, its

spectrum and wave energy will be influenced by atmospheric density, ρ, atmospheric stability, N, and the varying local mean wind as the wave propagates upward. Consistent with observations and theory (Dewan and Good, 1986; Smith et al., 1987), we assume a saturation of the spectrum at large vertical wavenumbers, with a horizontal velocity variance

$$\hat{E}_H(\mu) \propto e^{z/H_s} \simeq \frac{N^2}{6m_*^2\mu^3}, \tag{4.5}$$

for $H_s \rightarrow \infty$ at $\mu \gg 1$ and growth of wave energy for constant N as

$$\hat{E}(\mu) \propto e^{z/H_u},$$

with $H_u \geq H$ at $\mu \ll 1$. This implies a total energy and characteristic vertical wavenumber that vary as

$$E_0 \propto e^{z/H_E} \tag{4.6}$$

and

$$m_* \propto e^{-z/H_*}, \tag{4.7}$$

where $H_E = 2H_u$ and $H_* = 4H_u$. As noted by Fritts and VanZandt (1993), however, H_E and H_* appear not to be strictly constant with height. Instead, there is a tendency for less growth (larger scale heights) in the troposphere and

mesosphere, larger growth (smaller scale heights) in the stratosphere (Balsley and Garello, 1985), and a cessation of growth above $\sim 100km$ (Fritts et al., 1992). In Chapter 5, a special section will discuss a variable H_E in testing of our parameterization scheme.

It is also noted that an expectation of both the total wave energy and the characteristic vertical wavenumber will vary with atmospheric stability due to the dependence of μ and $\hat{E}(\mu)$ on N and the amplitude limits implied by saturation (VanZandt and Fritts, 1989). This results in dependencies on N given by

$$E_0 \propto N^{1/2}, \tag{4.8}$$

and

$$m_* \propto N^{3/4}, \tag{4.9}$$

in regions where N increases with altitude. The motivation here is to allow sensitivity to enhanced dissipation and the implied flux divergences in regions where N increases abruptly, such as the tropopause and the summer mesopause. We also assume, for simplicity, that the dependence is the same in regions where N decreases with altitude, though this represents a departure from saturated amplitudes and the approximately conservative wave propagation that may result at these heights. To simplify our parameterization as

much as possible while retaining sensitivity to both zonal and meridional variations in the local mean wind profiles, we assume that the full spectrum is composed of four components with discrete directions of propagation towards east, west, north, and south. With this assumption, the total energy may be written as

$$E_0 = E_e + E_w + E_n + E_s \tag{4.10}$$

with the fraction for each direction of propagation having the same spectral form and with the total spectrum having a saturated amplitude at $\mu \gg 1$.

4.1.2 Evolution of Energy Spectra with a Varying Mean Wind

Gravity wave energy spectra depend on variations in atmospheric density and atmospheric stability as they propagate vertically, as described in the previous section. They are also very sensitive to variations in the local mean wind in the plane of wave propagation as we can see from the following discussion. Variations in wave energy per unit mass with increasing altitude are due primarily to the changes in density and atmospheric stability, but changes in the anisotropy of the motion field are due largely to the variations of the mean wind. Our intent here is to anticipate the effects of mean wind variations on the component energy spectra and the corresponding variations in energy and

momentum fluxes in a manner as consistent as possible with both model and physical constraints.

The most significant approximation in the development of our parameterization scheme is the assumption that the shape of the vertical wavenumber spectrum is invariant with altitude, intrinsic frequency, and direction of propagation. This is suggested by numerous observations and simplifies our development substantially. However, it also includes implicit assumptions about the processes, the scales, and the effects of wave saturation at large and small vertical wave numbers.

For hydrostatic and two dimensional motions with k and $\omega > 0$ and m positive downward (for waves propagating upward and eastward), the WKB gravity wave dispersion relation may be expressed as

$$m = \frac{kN}{\omega} = \frac{N}{c}, \tag{4.11}$$

where k and m are the horizontal and vertical wavenumbers, $\omega = kc$ is the intrinsic frequency, and N is the buoyancy frequency. As defined by VanZandt and Fritts (1989), the gravity wave action flux is

$$S_A = c_{gz}\frac{\rho E(m)}{\omega} = \frac{\partial \omega}{\partial m}\frac{\rho E(m)}{\omega} = \frac{\rho E(m)}{m}, \tag{4.12}$$

where c_{gz} is the vertical group velocity and ρ is the background atmospheric density.

For a single component of the gravity wave spectrum propagating upward and eastward ($c > 0$) at some height z with initial intrinsic frequency

$$\omega_i = k(c_i - \overline{u}_i) > 0, \tag{4.13}$$

initial vertical wavenumber,

$$m_i \simeq \frac{kN}{\omega_i} = \frac{N}{c_i - \overline{u}_i}, \tag{4.14}$$

and an energy density, $E_i(m_i)$. If there is a steady mean zonal wind $\overline{u}$ that is increasing with height, this wave will encounter a critical level at height $z + \Delta z$ where $c = \overline{u}$, causing

$$\omega = k(c - \overline{u}) \rightarrow 0, \tag{4.15}$$

and

$$m = \frac{N}{c - \Delta\overline{u}} = \frac{m_i}{1 - m_i/m_c} \rightarrow \infty, \tag{4.16}$$

where m_c is the initial vertical wavenumber of the wave encountering the critical level at $z + \Delta z$ and is defined as

$$m_c = \frac{N}{\Delta\overline{u}}, \tag{4.17}$$

Likewise, the initial gravity wave energy occurring at $m_i > m_c$ will also experience critical level encounters (and dissipation) below $z + \Delta z$, while the

initial wave energy with $m_i < m_c$ will be shifted to those with larger, but finite, wavenumbers. Assuming that this spectral energy transfer at $m_i < m_c$ occurs subject to conservative wave propagation , the vertical gravity wave action flux will be conserved. Applying wave action flux conservation for spectral evolution between the initial height level z and the new level $z+\Delta z$, we obtain

$$\frac{\rho E(m)}{m} dm = \frac{\rho_i E_i(m_i)}{m_i} dm_i, \tag{4.18}$$

with

$$E_i(m_i) = \frac{4}{\pi} \frac{E_{ei}}{m_{*i}} \frac{\mu_i}{1+\mu_i^4}, \tag{4.19}$$

$$\mu_i = \frac{m_i}{m_{*i}}, \tag{4.20}$$

$$m_{*i} = \frac{N_i}{c_{*i} - \overline{u}}, \tag{4.21}$$

$$m = \frac{N}{c - \overline{u} - \Delta\overline{u}} = R_n \frac{m_i}{1 - \frac{m_i}{m_c}}, \tag{4.22}$$

where

$$R_n = \frac{N}{N_i}, \tag{4.23}$$

and E_e is the component energy at z in that direction.

Thus, at height $z + \Delta z$, the new spectrum can be obtained as

$$E(m) = \frac{\rho_i}{\rho} \frac{m}{m_i} \frac{dm_i}{dm} E_i(m_i), \tag{4.24}$$

From eq. (4.22), we have

$$\frac{dm_i}{dm} = R_n (\frac{m_i}{m})^2, \tag{4.25}$$

So that, the new spectrum may then be written as

$$E(m) = \frac{\rho_i}{\rho} R_n \frac{m_i}{m} E_i(m_i). = \eta A_i \frac{1}{m_{ei}} \frac{\mu (R_n + \beta\mu)^2}{(R_n + \beta\mu)^4 + \mu^4}, \tag{4.26}$$

where

$$\eta = \frac{\rho_i}{\rho} R_n = \frac{\rho_i}{\rho} \frac{N}{N_i},$$

$$\mu = \frac{m}{m_{ei}},$$

$$\beta = \frac{m_{ei}}{m_c} = \frac{\Delta \overline{u}}{c_{ei}},$$

$$A_i = \frac{4}{\pi} E_{ei}.$$

Hence, the transformed spectrum has a total energy

$$E_0 = \int_0^\infty E(m)\,dm = \eta A_i \int_0^\infty \frac{\mu(R_n + \beta\mu)^2}{(R_n + \beta\mu)^4 + \mu^4}\,d\mu. \qquad (4.27)$$

This implies that the gravity wave energy at height level $z + \Delta z$ depends on background density,ρ, atmospheric stability, N, and the vertical wind shear, $\Delta\overline{u}$, as we anticipated before. In order to focus on the energy change with the varying mean wind, for a moment, we neglect the changes in N and ρ with $R_n = 1$ and $\eta = 1$, yielding

$$E(m) = A_i \frac{1}{m_{*i}} \frac{(1 + \beta\mu)^2\mu}{(1 + \beta\mu)^4 + \mu^4}, \qquad (4.28)$$

At larger wavenumbers, $m \gg m_{*i}$ and m_c, the energy density $E(m)$ far exceeds the saturation limit, $E(m) \simeq N^2/30m^3$ (for each component spectrum), with a limiting amplitude and slope given by

$$E(m \gg m_{*i}) = \frac{E_{ei}}{\pi m_{*i}} \frac{\beta^2}{\beta^4 + 1} \mu^{-1}, \qquad (4.29)$$

implying an infinite integrated energy density. Alternatively, eq.(4.28) describes the evolution of a spectrum propagating against the mean flow with $\beta < 0$ for which conservative wave propagation demands a decreasing vertical wavenumber and an increasing wave energy density that decreases to zero at $m = m_c$. The initial and transformed spectra given by eq.(4.29) for

$$\beta = \frac{m_{*i}}{m_c} = \pm\frac{1}{2}$$

are shown for reference in Figure 4.1a. These reveal the difficulties in dealing in a simple parameterized manner with a complete description of the spectral evolution in the presence of mean wind shear.

Clearly, saturation processes must limit spectral amplitudes continuously, thus preventing such conservative amplitude growth at large m, as spectral amplitudes far in excess of saturated values are not observed. Conversely, at small vertical wavenumbers, $m_i \ll m_c$, only small changes in $E(m)$ and m occur and are more likely to take place in a conservative fashion. Of greater relevance to our parameterization are the spectral transfers implied near m_{*i}, as this is where the majority of wave energy resides. For cases where $m_{*i} < m_c$, the spectral transfers are small and approximately conservative, as discussed above. But for $m_{*i} \sim m_c$, these transfers may involve a large fraction of the wave energy in that spectral component. Thus, we assume that the full spectral energy transfers resulting from changes in the mean wind can be described in terms of the variations at m_{*i} given by eq. (4.21) for $m_{*i} < m_c$ and that the vertical wavenumber spectral shape is invariant to account for saturation processes at large m. This alternative representation of the vertical wavenumber spectral evolution is illustrated for $\beta = \pm 1/2$ in Figure 4.1b. Comparing the spectra in Figure 4.1a and 4.1b, we note obvious differences at large and small m. Spectral differences are minimized near m_{*i}, however, where the majority of wave energy resides. Together with energy changes dictated by variations

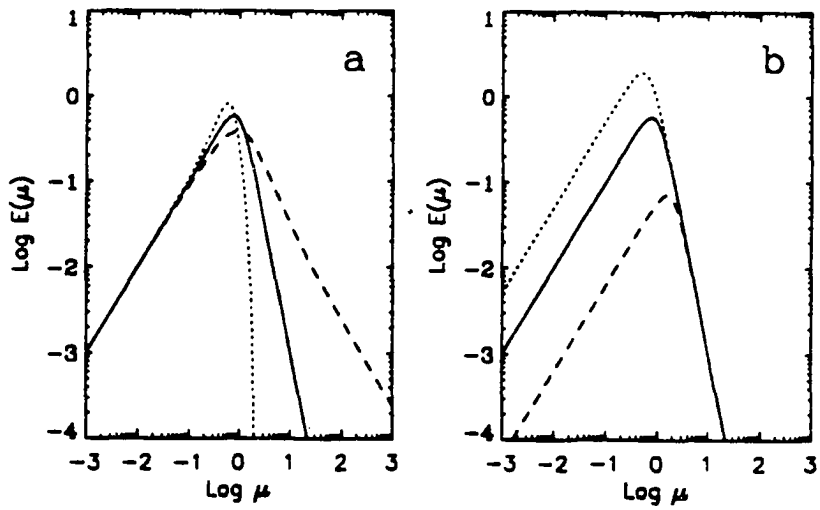

Figure 4.1: Wavenumber spectra evolution with height. Initial (solid), upshifted (long-dashed), and down-shifted (dashed) vertical wave number spectra showing changes by conservative wave propagation (a) and parameterized with a constant shape and a saturated amplitude at large μ (b) for $\beta = \pm 0.5$

in N and ρ, this dependence of m_{*i} with β fully specifies the variation of each component energy with altitude, subject to constraints discussed below.

Consistent with the energy spectrum defined by Fritts and VanZandt (1993) and our discussion of component spectral energies and transfers above, we define a total gravity wave energy as

$$E_0 \simeq \frac{1}{10}\frac{N^2}{m_{*0}^2} = \sum E_j, \tag{4.30}$$

where E_j, the component energies (east, west, south and north), defined previously and given individually by

$$E_j \simeq \frac{1}{40}\frac{N^2}{m_{*j}^2}, \tag{4.31}$$

with

$$m_{*0}^{-2} = \frac{1}{4}\sum m_{*j}^{-2}. \tag{4.32}$$

This insures that equally energetic component spectra share a common characteristic vertical wavenumber $m_{*i} = m_{*0}$ with the total energy spectrum, that each component contributes to the saturated spectral amplitude at large m, and that each component can also be characterized by only one variable.

It then remains only to insure that the component spectral changes implied by mean wind influences on the characteristic vertical wavenumbers are consistent with constraints on wave energy or momentum flux variations with

height. Because wave energy at very small m_i is affected very little by mean wind variations and is not actually described by a scheme that ascribes equal transfers at all wavenumbers based on that inferred at m_{*i}, it is necessary to insure that this approximation does not reduce any spectral component to an artificially small (and irrecoverable) energy. This is accomplished in two ways. First, noting that the total energy is constrained to grow as

$$E_0 \propto N^{1/2} e^{z/H_B}$$

we require that this energy always be equally apportioned between zonal and meridional components, i.e.,

$$E_e + E_w = E_n + E_s = \frac{E_0}{2}$$

and that neither component in either plane may grow more rapidly than allowed by conservative wave propagation, with constant component momentum flux $\rho D E_j$.

This imposes a constraint on those components with $\beta < 0$ given by

$$E_j \leq e^{z/H}. \tag{4.33}$$

This also enables anisotropy to develop and vary among the zonal and meridional spectra in response to variations in the component mean winds in each plane. A second condition is also employed to insure that any single component

spectrum is not reduced to the point where it can no longer have an influence at greater heights. For this purpose, we assume that the characteristic phase speed of any component does not decrease with height and that no less than a fraction α of the zonal or meridional energy may be associated with any one component. Thus, the maximum momentum flux is limited to $(1 - 2\alpha)$ of the total possible if all wave energy in one plane were propagating in the same direction. This results in an equivalent constraint on the anisotropies expressed as

$$(-0.5 + \alpha) \leq b_{x,y} \leq (0.5 - \alpha).$$

given equal zonal and meridional energies.

4.2 Constraints on Energy and Flux Variations with Height

The physical and model constraints on the evolution of the energy spectrum and its fluxes of energy and momentum with height are reviewed here. In the following chapter, these conditions will be used to test our parameterization scheme in several environments representative of the lower and middle atmosphere.

The primary constraint arises as a consequence of gravity wave saturation and the resulting amplitude limits at large vertical wavenumbers. This

implies both an approximately universal vertical wavenumber spectrum and a variation of wave energy density with height and atmospheric stability that may be expressed as

$$E_0 \propto N^{1/2} e^{z/H_E}, \tag{4.34}$$

where $H_E = 2H_u$ and $H_u \geq H$ for a saturated spectrum. In practice, a value $H_E \simeq 2.3H$ appears to describe the variation of energy density (per unit mass) observed in the lower and middle atmosphere (Balsley and Carter, 1982). The variation with N is a consequence of the enhanced saturation that is induced in regions where N increases with altitude (VanZandt and Fritts, 1989).

For simplicity of representation, the total energy is assumed to be composed of four component spectra propagating east, west, north and south, as previously defined by E_e, E_w, E_n and E_s. Each component spectrum has a total energy related to its characteristic vertical wavenumber and intrinsic phase speed as

$$E_j \simeq \frac{1}{40}\frac{N^2}{m_{*j}^2} = \frac{1}{40}c_{*j}^2, \tag{4.35}$$

with m_{*j} as defined before and E_j varying with altitude, apart from variations in the mean wind, as E_0. Thus, only one variable is required to specify each component spectrum. The energies E_j (or alternatively, the characteristic vertical wavenumbers or intrinsic phase speeds, m_{*j} or c_{*j}) are specified in

order to represent the gravity wave energy and anisotropy associated with various wave sources at tropospheric altitudes, as described further in later chapters.

At the new height $z + \Delta z$, the resulting characteristic vertical wavenumber is given by

$$m_* = \frac{m_{*i}}{1 - \beta_i}, \tag{4.36}$$

for $m_{*i} < m_{ci}$, where

$$\beta_i = \frac{\Delta \overline{u}}{c_{*i}} < 1, \tag{4.37}$$

and $\Delta \overline{u}$ is the mean wind change in the height interval Δz , c_{*i} is the characteristic phase speed of the component energy spectrum in that direction (positive east and north).

For $\beta_i > 1$, these expressions fail to describe the spectral change and are replaced by a constraint on the maximum rate of growth of the energy for which $\beta_i < 0$. This is based on eq.(4.35) and the requirement that the wave momentum flux for this component not grow with altitude, giving

$$E_j \propto e^{z/H}, \tag{4.38}$$

with the opposite component constrained to decay as

$$E_{1-j} = \frac{E_0}{2} - E_j, \tag{4.39}$$

and with E_0 varying as previously described.

A final condition is imposed to insure that no component spectrum becomes so small that it cannot achieve significant effects at greater altitudes. This is expressed by

$$\alpha < \frac{2E_j}{E_0} < (1-\alpha), \tag{4.40}$$

where we have taken $\alpha = 0.2$, permitting as much as 80% of the energy in each plane to propagate in one direction, imposing a constraint on the anisotropies (and momentum fluxes) given by

$$-0.5 + \alpha \leq b_{x,y} \leq 0.5 - \alpha. \tag{4.41}$$

Given initial values of the component energies, the above conditions allow computation of the variations of these quantities with altitude, including changes in atmospheric density and stratification, and the local mean wind, i.e,

$$E_j(z+\Delta z) = (\frac{N(z+\Delta z)}{N(z)})^{1/2} e^{\Delta z/H_{\rho}(z)} (1+\beta)^2 E_j(z). \tag{4.42}$$

Applying the above constraints, it is then straightforward to obtain the corresponding energy and momentum fluxes and their vertical divergences from the profiles of E_j. Thus, anticipating spectral energy changes with altitude, the energy and momentum fluxes may be expressed as (refer to Chapter 3)

$$F_E = \sum F_{Ej} = CN \sum \frac{E_j}{m_{*j}}, \tag{4.43}$$

$$F_{Px} = F_{Pe} - F_{Pw} = D(E_e - E_w), \tag{4.44}$$

and

$$F_{Py} = F_{Pn} - F_{Ps} = D(E_n - E_s), \tag{4.45}$$

and the inferred flux divergences are given by

$$\epsilon = -\frac{N}{\rho}\frac{\partial}{\partial z}(\frac{\rho}{N}F_E), \tag{4.46}$$

$$D_{Fx,y} = -\frac{1}{\rho}\frac{\partial}{\partial z}(\rho F_{Px,y}). \tag{4.47}$$

4.3 Specification of Model Parameters

In previous sections, a model parameterization scheme was described in detail based on the gravity wave spectral evolution. In this chapter we will

discuss some model parameters required by the scheme. Observational studies have provided a number of estimates of the magnitude and variability of gravity wave energies and momentum fluxes at various altitudes throughout the lower and middle atmosphere. Our purpose here is to discuss the manner in which these observations may be used to pose representative initial conditions and constraints on the motion field within the framework of our parameterization.

4.3.1 Observations of Velocity Variances

Radar observations near the tropopause have revealed horizontal velocity variances that vary considerably with location and time. Inferred variances are typically $\sim 10 m^2 s^{-2}$ over mountainous terrain under moderate wind conditions (Balsley and Carter, 1982; vanZandt et al., 1990; Nastrom and Fritts, 1992). However, these variances are often enhanced, relative to background levels, due to orographic wave motions (Nastrom et al., 1987; Jasperson et al, 1990; Nastrom and Fritts, 1992), and are likely to be even larger above higher or more rugged terrain. Mean variance estimates over terrain, then, may pose a reasonable upper limit on the mean tropopause velocity variance.

Variances in association with frontal systems, convection, and wind shear are likewise enhanced over background levels and are comparable to or slightly smaller than mean variances over significant terrain, with typical values of $\sim 3 - 8 m^2 s^{-2}$ (Vincent and Eckermann, 1990; Fritts and Nastrom, 1992). In

contrast, variances tend to be much smaller away from obvious wave sources, with representative values $\sim 1m^2s^{-2}$ or less and $\sim$ 6 times less energetic, in general, than the average for identified gravity wave sources (Fritts and Nastrom, 1992).

Velocity variances increase in a nearly uniform manner with height, achieving values of $\sim 400 - 1000m^2s^{-2}$ near the mesopause at $\sim 86km$, based on observations of wind and density fluctuations (Balsey and Carter, 1982; Vincent, 1984; Balsley and Garello, 1985; Meek et al., 1985; Fritts and Yuan, 1989; Rüster and Reid, 1990; Wang and Fritts, 1990). Also noted is a tendency of variances to be somewhat smaller over oceans than over major land masses (Fritts et al., 1989; Vincent and Lesicar, 1991; Fritts and Isler, 1992), suggesting that orographic excitation or enhanced convection over land may contribute to statistically more energetic gravity waves at mesospheric heights. Finally, observations at greater altitudes suggest that gravity waves may propagate to considerable altitudes in the lower thermosphere (Fejer et al., 1985; Gavrilov et al., 1992), but that wave amplitudes apparently cease growth or grow more gradually above $\sim 100km$ (Fritts et al., 1992a).

4.3.2 Observations of Momentum Fluxes

Momentum flux measurements have been made in a variety of ways, including surface pressure analysis, aircraft measurements of mountain wave

structure in the troposphere and lower stratosphere, and radar measurements of anisotropy within the motion field throughout the lower and middle atmosphere. Surface pressure measurements have revealed typical pressure differences across mountainous terrain of $\sim 0.1 - 0.2mb$, with maxima of $\sim 0.5mb$, corresponding to implied momentum fluxes of $\sim 1 - 6Nm^{-2}$ (Smith, 1978; Hoinka, 1984, 1985). Measurements with aircraft, however, reveal substantially smaller maximum values, $\sim 0.3 - 1.5Nm^{-2}$ (Lilly and Kennedy, 1973; Lilly, 1978; Kennedy and Shapiro, 1979; Hoinka, 1984, 1985; Nastrom and Fritts, 1992), suggesting that much of the surface flux is associated with trapped lee wave activity that influences only the lowest levels of the troposphere (Smith, 1978; Palmer et al., 1986).

More typical values are reported to be $\sim 0.1Nm^{-2}$ and are nearly constant throughout the troposphere (Lilly et al., 1982; Hoinka, 1985). Corresponding Reynolds stresses, $\overline{u'w'}$ and $\overline{v'w'}$, are $\sim 0.1 - 0.2m^2s^{-2}$ for typical flows and ~ 10 times larger under more extreme conditions (Lilly and Kennedy, 1973; Lilly and Lester, 1974; Nastrom and Fritts, 1992), providing reasonable bounds on the parameterization of these fluxes.

Momentum flux measurements using a variety of atmospheric radars have provided estimates of the mean values and indications of the degree of variability in several altitude regions. Measurements in the upper troposphere and lower stratosphere using the MU radar have revealed fluxes (per unit mass)

of $\overline{u'w'} \sim -0.1$ to $-1.0 m^2 s^{-2}$, with a mean of $\sim -0.2 m^2 s^{-2}$ (Fritts et al., 1990), in good agreement with inferences from aircraft measurements under typical conditions (Lilly et al., 1982; Nastrom and Fritts, 1992). These measurements also imply a deceleration due to vertical momentum flux divergence of $\sim 1 - 2 ms^{-1} day^{-1}$ above the tropospheric jet core, in reasonable agreement with that required to close the tropospheric jets and balance the Coriolis torques acting on the mean meridional motions at these heights (Palmer et al., 1986; McFarlane, 1987).

Radar measurements in the mesosphere and lower thermosphere likewise suggest significant anisotropy in the motion field and Reynolds stresses, or momentum fluxes per unit mass, ~ 100 times those values obtained near the tropopause. Mean momentum fluxes are as large as $\sim 10 - 20 m^2 s^{-2}$ and generally are anticorrelated with the local mean flow (Vincent and Reid, 1983; Reid and Vincent, 1987; Fritts and Vincent, 1987; Fritts and Yuan, 1989; Tsuda et al., 1990; Wang and Fritts, 1990; Hitchman et al., 1992). In contrast, flux estimates for intervals of $\sim 1 - 8h$ exhibit substantial maxima of $\sim 60 m^2 s^{-2}$ at times of strong modulation by low-frequency motions (Fritts and Vincent, 1987; Reid et al., 1988; Fritts and Yuan, 1989; Rüster and Reid, 1990; Fritts et al., 1992b), while estimates of anisotropy are also large (Ebel et al., 1987; Fritts and Wang, 1991).

4.3.3 Specification of Energies, Anisotropies, and Variability

Spectral parameters may be specified at any altitude that is useful for modeling purposes and representative of the major gravity wave sources. For example, it will likely be useful to specify a wave spectrum due primarily to orography at the mean terrain heights and in terms of the mean wind at that level, where this is possible. Likewise, spectra arising from convection and wind shear will need to be specified, for greatest sensitivity to meteorological conditions, at the heights at which these sources occur for best results at lower levels. At greater altitudes, we anticipate that the character of the wave spectrum will be determined increasingly by filtering influences defined in section 4.1.2. Finally, it may be valuable to distribute the influences of localized sources at lower levels over increasing areas as altitude increases, recognizing the horizontal spread of wave activity due to different propagation directions.

Assuming for our purposes that $E_h = 5m^2s^{-2}$ represents a mean horizontal velocity variance near the tropopause ($\sim 10km$), consistent with the measurements summarized previously, this implies a mean wave energy $E_0 = 4m^2s^{-2}$ and a characteristic phase speed at the surface of $c_* \sim 5ms^{-1}$. Also recognizing that our parameterization will need to accommodate a range in initial source energies to account for smaller background energies and the larger

energies accompanying strong wave forcing, we consider the behavior of our parameterization scheme for initial phase speeds of 3, 5, and 8 ms^{-1}. Consistent with observations, we assume a mean scale height for energy growth (per unit mass) of $H_E \sim 2.3H$ below 85 km and a transition to constant energy above $100km$. It is also recognized that a slowly varying H_E would provide more quantitative agreement with observed energy growth (Balsley and Garello, 1985) and examine the implications of this variability as well. Additionally, it is noted that constant wave energy above $100km$ prevents changing anisotropies at these heights unless the c_{*i} are allowed to decrease with height. Thus, this condition is relaxed above $85km$ in order to insure continued sensitivity to variations in the local mean wind profiles.

Likewise, the test values of initial anisotropy are based on atmospheric observations at lower levels. These suggested maximum values of $b_{x,y} \sim \pm 0.2$ are primarily in association with orography (Fritts et al., 1990; Nastrom and Fritts, 1992). Thus we choose $b_{x,y} = -0.2, 0.0$, and 0.2 to span the range of anisotropies representative of convective, orographic, and shear excitation processes. At greater heights, considerably greater anisotropy is suggested by large momentum fluxes and evidence of strong Doppler shifting in vertical velocity frequency spectra (Vincent and Reid, 1987; Fritts and Vincent, 1987; Reid and Vincent, 1987; Reid et al., 1988; Fritts and Yuan, 1989; Fritts and Wang, 1991). This suggests a higher degree of anisotropy than imposed at

source levels as a consequence of gravity wave filtering and is the motivation for our tolerance of larger anisotropy at greater altitudes. To illustrate this sensitivity, we present results for values of $\alpha = 0.1, 0.2$, and 0.3. As noted in eqs. (4.41 - 4.47), a larger α reduces the maximum possible momentum fluxes, while a smaller value permits greater anisotropy at all heights, larger variations in c_{*j} and E_j at lower levels, and less sensitivity to mean wind variations at greater altitudes where c_{*j} is large.

Chapter 5

Application to CIRA Model Atmosphere

In the previous chapter, a one-dimensional gravity wave parameterization scheme was developed which can be used with different profiles of density, mean wind, and stratification by specifying the characteristic phase speed, $c_{*\pm 0}$, the anisotropy, $b_{x,y}$, of the gravity waves at certain source regions in the troposphere (actually they can be specified at any height of the atmosphere). We also discussed model parameter specifications based on existing observational facts and theoretical knowledge. Now we are in a position to apply the suggested scheme to the real atmosphere. Figure 5.1 presents the canonical winter (solid lines) and summer (dashed lines) mean wind, temperature, and stability profiles obtained from the CIRA 1986 model (January and June at 40^0 latitude in the Northern Hemisphere). For test purposes, these were selected to permit a meaningful comparison of the predicted energy and mo-

mentum fluxes with available observations. Here we assume equal zonal and meridional energy propagation without loss of generalities. Although we only display the zonal energy variations since they respond much more dramatically to mean wind variations, it is easily to extend the scheme to other directions (such as the meridional direction) in GCMs (general circulation model).

The CIRA 1986 zonal mean wind profiles (left panel of Figure 5.1) exhibit a tropospheric jet with eastward maxima of $\sim 30ms^{-1}$ in winter and $\sim 20ms^{-1}$ in summer at altitudes of $\sim 12-13km$, eastward mesospheric jets with maxima of $\sim 60ms^{-1}$ at $\sim 68-70km$, and further reversals of the zonal mean motion above ~ 90 and $86km$ during winter and summer. The temperature profiles exhibit tropopause minima of $\sim 210K$ at $\sim 16-18$ km, stratopause maxima of $\sim 260-270K$ at $\sim 46-48km$, and mesopause minima of $\sim 190K$ and $170K$ at ~ 96 and $92km$, respectively. Corresponding values of N^2 range from $\sim 10^{-4}rad^2s^{-2}$ in the troposphere to $\sim 5\times 10^{-4}$, 3×10^{-4}, and $\geq 6\times 10^{-4}rad^2s^{-2}$ in the stratosphere, mesosphere, and lower thermosphere, while density varies in both seasons with scale heights ranging from $\sim 5-8km$ and a mean value of $\sim 7km$. Despite these height and seasonal variations, density does not vary by more than a factor of 2 from that given approximately by the mean scale height for this altitude interval.

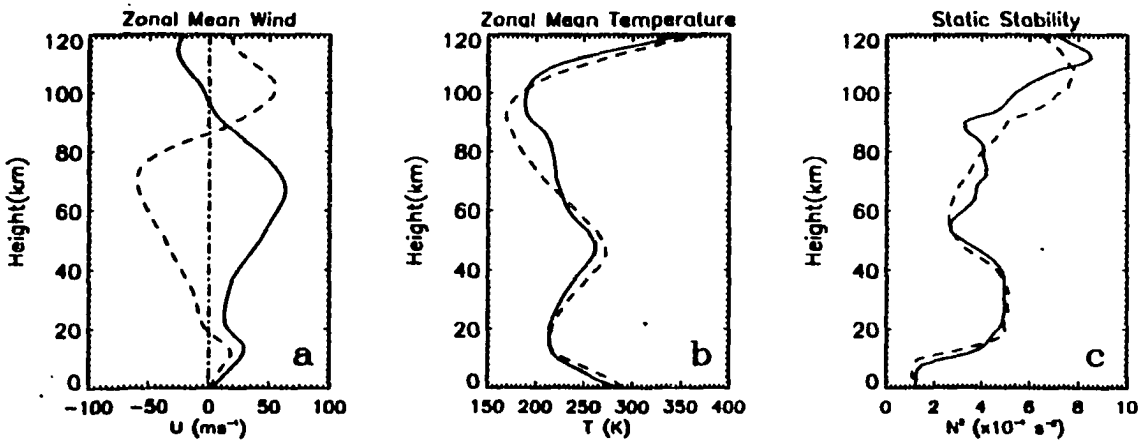

Figure 5.1: CIRA 1986 model atmosphere profiles. Mean zonal wind (a), temperature (b), and N^2 (c) profiles from 0 to 120 km for January (solid) and June (dashed) at $40^0 N$ from the CIRA 1986 model atmosphere.

5.1 Variations of Wave Energies and Fluxes

In this section, the parameterization scheme suggested in the previous chapter will be used together with the above mentioned canonical density, mean wind and stratification profiles. Some gravity wave sources are to be specified on the ground in order to examine the respond of the gravity wave energy and fluxes to the variations of density, wind filtering, and the atmospheric stabilities.

5.1.1 Dependence on Initial Wave Energy

Figure 5.2 shows the zonal phase speed profiles and the eastward, westward, and net zonal momentum fluxes of the canonical winter and summer profiles from 0 to 120 km . Details of these responses at the lower levels are shown below 40 km in Figure 5.3 to enhance sensitivity where phase speeds and fluxes are small. Here we have assumed that the zonal phase speeds, c_{*e}=c_{*w}= $5ms^{-1}$, $b_z = 0.0$, and $\alpha = 0.2$. Both c_{*e} and c_{*w} are related to the zonal energies through eq.(4.35).

As expected from the prescribed growth of wave energies with height, we see a tendency for phase speeds and fluxes to grow and vary in response to variations of the mean zonal wind. Phase speeds increase from their initial value of $5ms^{-1}$ to over $100ms^{-1}$ above $\sim 100km$, the momentum fluxes, initially zero because of our initial choice of $b_z = 0$, increase to maximum

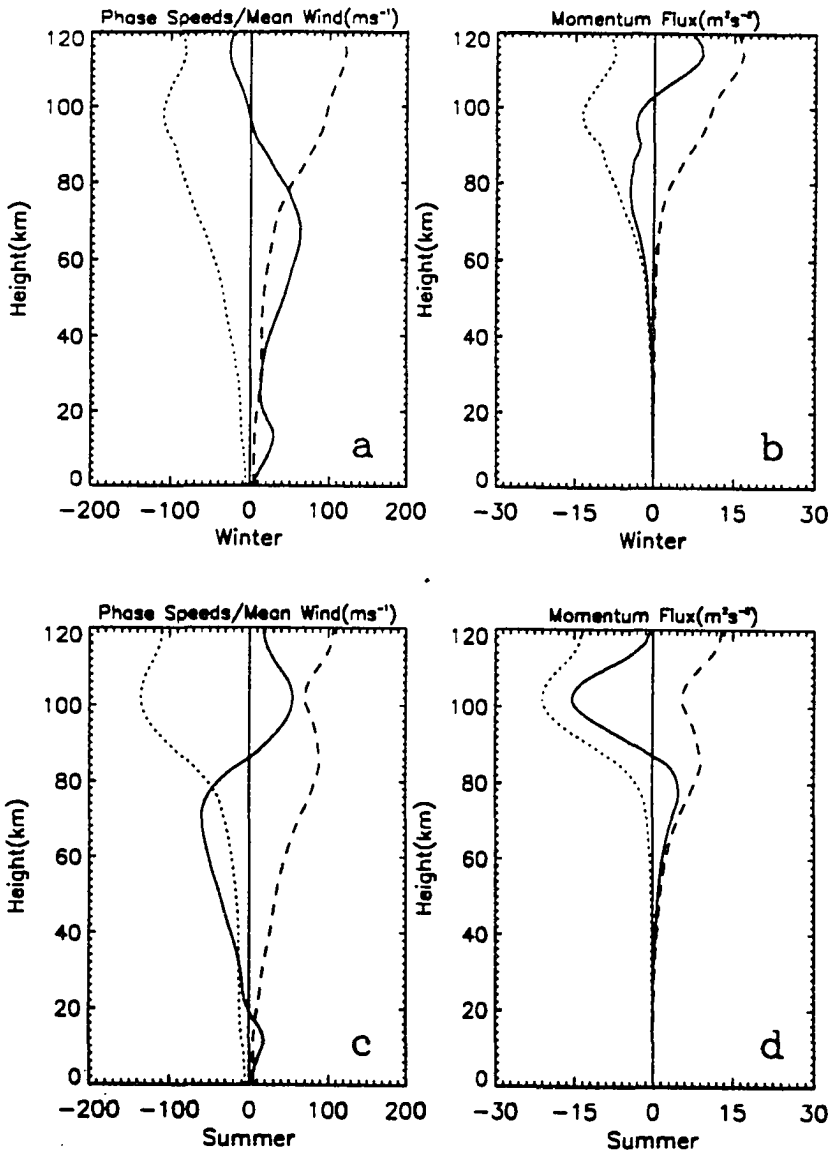

Figure 5.2: Predicted profiles and phase speeds and momentum fluxes. Profiles of mean wind (solid), characteristic phase speeds, c_{*c} (long-dashed) and c_{*w} (dashed) obtained for mean winter (a) and summer (b) profiles and their associated component and total (solid) momentum fluxes (b) and (d) with $c_{*c0} = c_{*w0} = c_{*0} = 5ms^{-1}$, and $b_x = 0.0$, $\alpha = 0.2$.

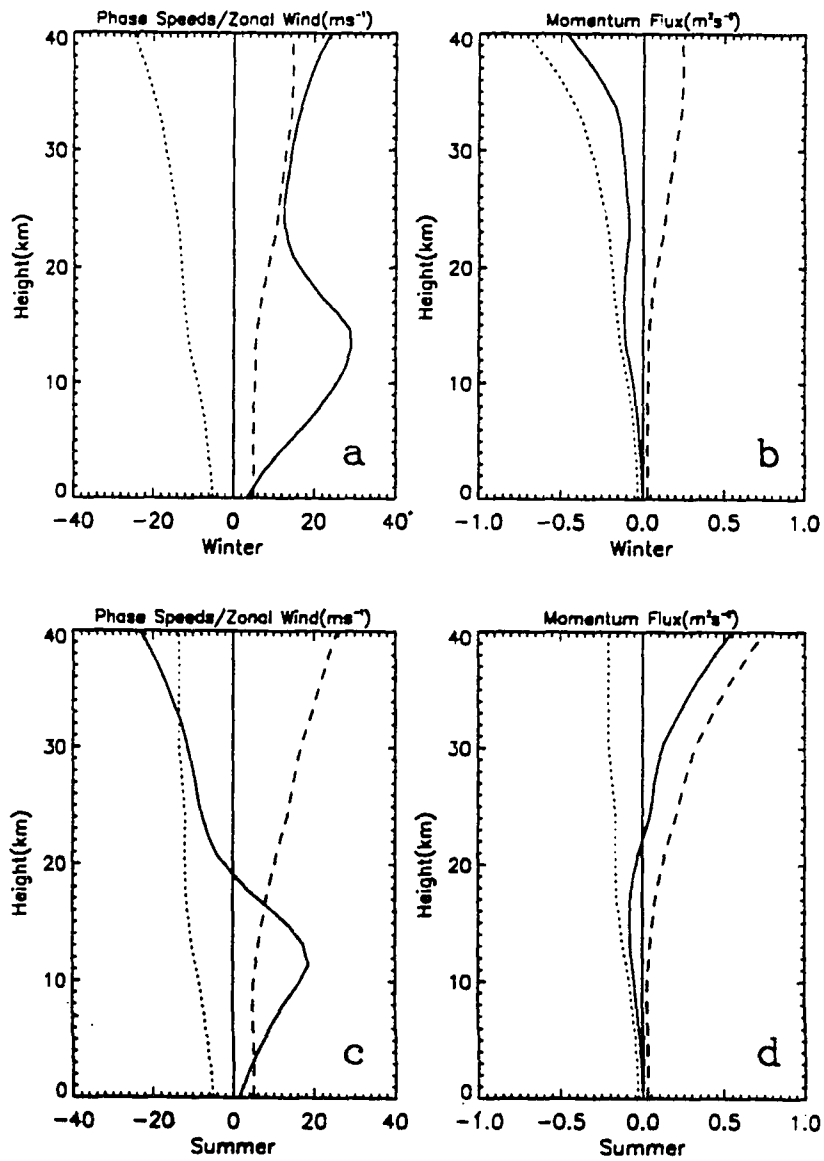

Figure 5.3: Predicted profiles and phase speeds and momentum fluxes. Same as Figure 5.2, but for altitudes $0 - 40km$.

values of $\sim 10 - 20 m^2 s^{-2}$ at altitudes around $60 km$. Throughout the altitude range, intrinsic phase speeds are consistent with those inferred from vertical wavenumber spectra because of our basing of the parameterization scheme on observational data. Phase speeds also exhibit large local variations, especially where propagation is opposite to changes in the mean wind with height, due to the assumed nearly conservative wave propagation of these spectral components.

It is noted that both winter and summer momentum flux profiles display a tendency to be anticorrelated with the mean zonal wind at upper levels and for maximum values to occur near and below reversals in the zonal mean wind, in reasonable agreement with observations. Similar tendencies are noted at lower levels (see Figure 5.3), with momentum fluxes and the zonal mean motion generally anticorrelated and with momentum fluxes in the upper troposphere and lower stratosphere of $\sim -0.2 m^2 s^{-2}$, in good agreement with measurements cited above.

The responses of the parameterization to varying initial phase speeds for both winter and summer zonal mean winds are displayed for upper and lower altitude ranges in Figure 5.4. For this purpose, we assume phase speeds of 3, 5 and 8 ms^{-1} to cover a range of energies from $\sim 2-12 m^2 s^{-2}$ near the tropopause and intended to be representative of weak to very strong wave forcing at lower levels. Smaller initial phase speeds better describing tropopause energies away

from obvious wave sources of $\sim 1 - 2ms^{-1}$ result in very weak responses throughout the altitude range and are not shown.

The momentum flux profiles obtained for different initial phase speeds exhibit an approximately linear response to initial energy at lower levels where phase speeds are strongly influenced by mean wind variations. With few exceptions, especially near the zonal wind minimum in the lower stratosphere, the momentum fluxes reflect the ratio of initial energies below $\sim 80km$. At greater altitudes, however, the fluxes depart from this relationship because the smaller phase speeds are more strongly influenced by mean wind variations than are the larger phase speeds. This accounts for the tendency for momentum fluxes obtained for an initial phase speed of $8ms^{-1}$ to be relatively more negative in winter and more positive in summer than those for an initial phase speed of $5ms^{-1}$ at altitudes above $\sim 80km$. Despite these variations, the general consistency of the flux profiles, whether large or small, with the mean values anticipated from observations lends confidence that variable forcing will nevertheless produce a reasonable mean response.

5.1.2 Dependence on Initial and Maximum Anisotropies

As we mentioned in our previous model spectrum and the scheme description, isotropy and/or anisotropy must be considered in order to give a better representation of observational facts. In this section, we will specify

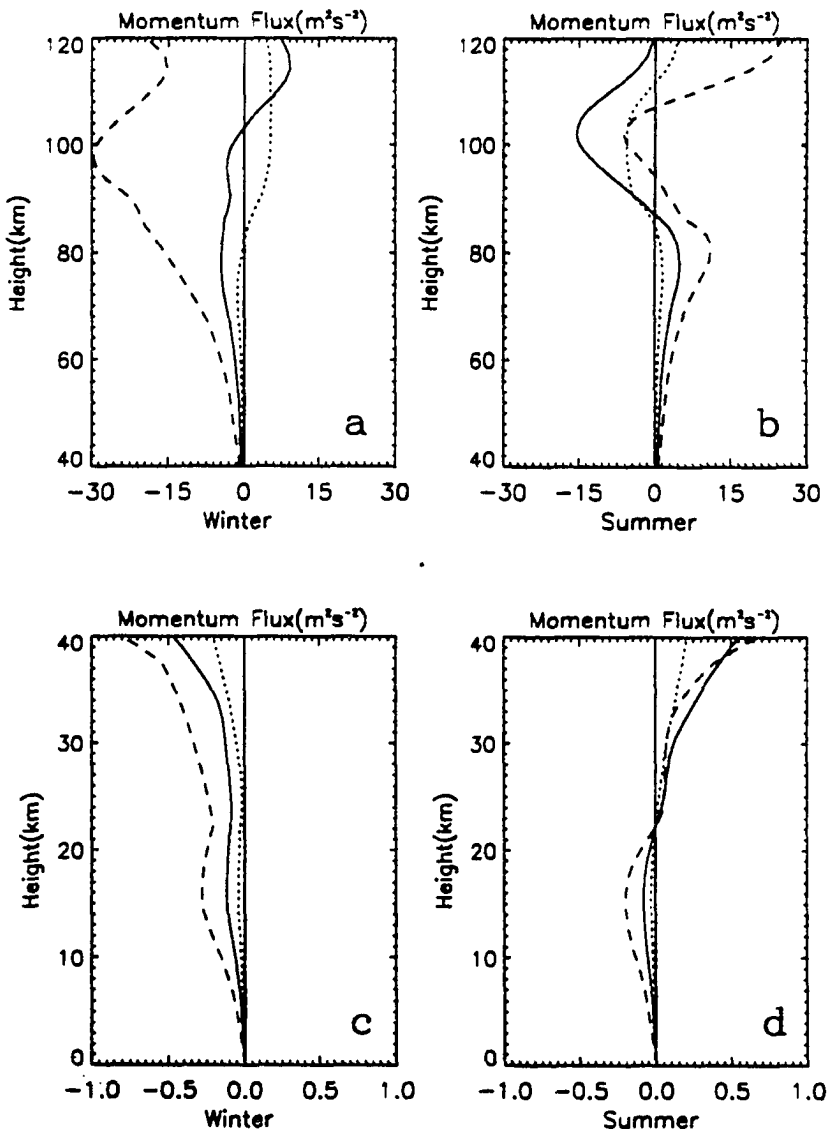

Figure 5.4: Momentum flux profiles for varying phase speeds. Momentum flux profiles obtained with $c_{*0} = 3$ (dashed), 5 (solid), and 8 (long-dashed) ms^{-1}, $b_x = 0.0$, and $\alpha = 0.2$ for canonical winter and summer profiles at $40 - 120km$ (a and b) and $0 - 40km$ (c and d).

different anisotropies represented by b_x in the test of our parameterization scheme.

Figure 5.5 shows the results of momentum flux profiles obtained for winter and summer zonal mean winds with initial anisotropies of $b_x = -0.2, 0.0,$ 0.2 and an initial wave energy corresponding to a mean phase speed $c_{*0} = 5ms^{-1}$. The results of different values of b_x indicate that initial anisotropies have very little influence on the momentum fluxes if they are consistent with the tendency for creation of anisotropy due to mean wind changes with height. Indeed, the profiles displayed in Figure 5.5 for $b_x = -0.2$ and 0.0 are nearly identical at all altitudes, while that for $b_x = 0.2$ results in a more positive momentum flux for both winter and summer wind profiles up to $\sim 50km$ because of a delayed suppression of E_e relative to E_w by lower level shears. Note that momentum flux profiles above $40km$ for all values of b_x are virtually identical at greater heights due to the limits placed on the anisotropy by finite α. Nevertheless, the initial anisotropy may be expected to play a larger role in cases where the mean wind at lower levels in that direction of propagation is not strongly sheared.

Comparing with the negligible influences of b_x at greater altitudes, the maximum allowed anisotropy expressed through α has significant effects at all levels. Momentum flux profiles with $b_x = 0.0$ and $\alpha = 0.1, 0.2,$ and 0.3 are displayed in Figure 5.6. When α decreases, both the maximum fluxes and

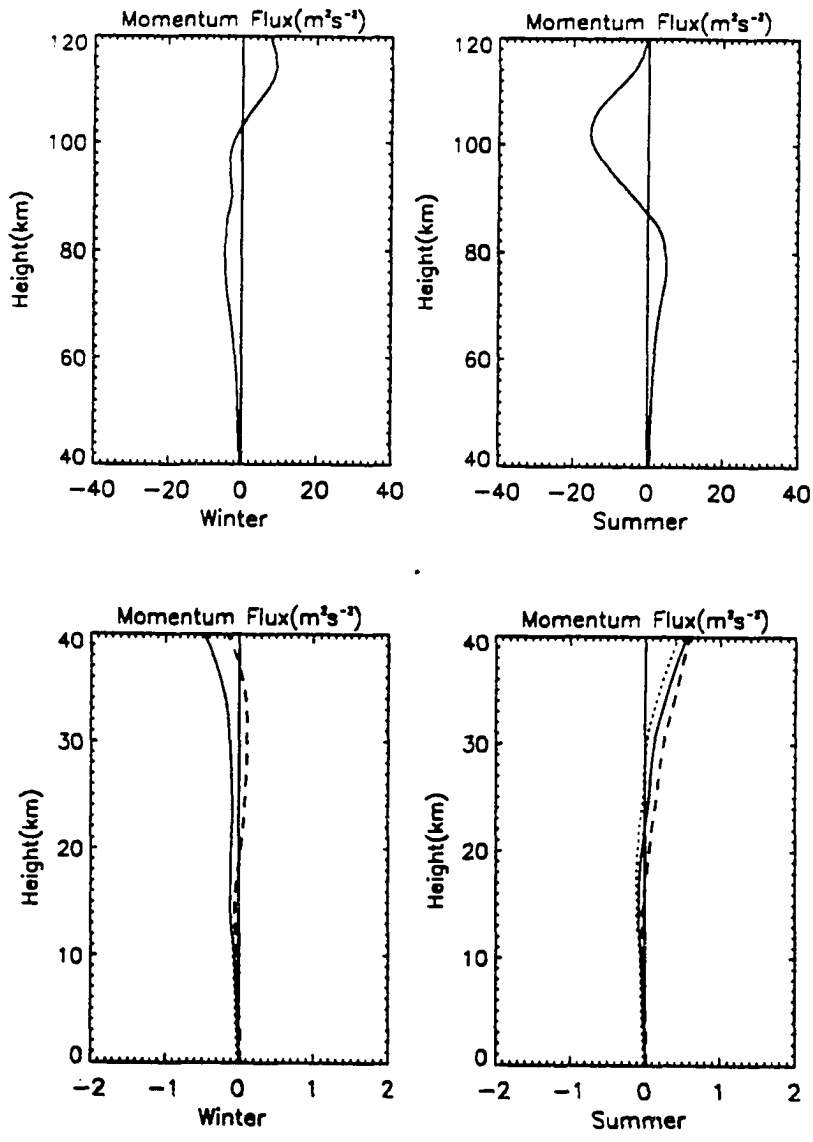

Figure 5.5: Momentum flux profile for different anisotropies. Momentum flux profiles obtained with $b_x = -0.2$ (dashed), 0.0 (solid), and 0.2 (long-dashed), $c_{*0} = 5ms^{-1}$, and $\alpha = 0.2$ below $40km$ for winter (a, and c) and summer (b and d) zonal mean winds. Note that profiles are virtually identical at greater altitudes due to constraints on anisotropy.

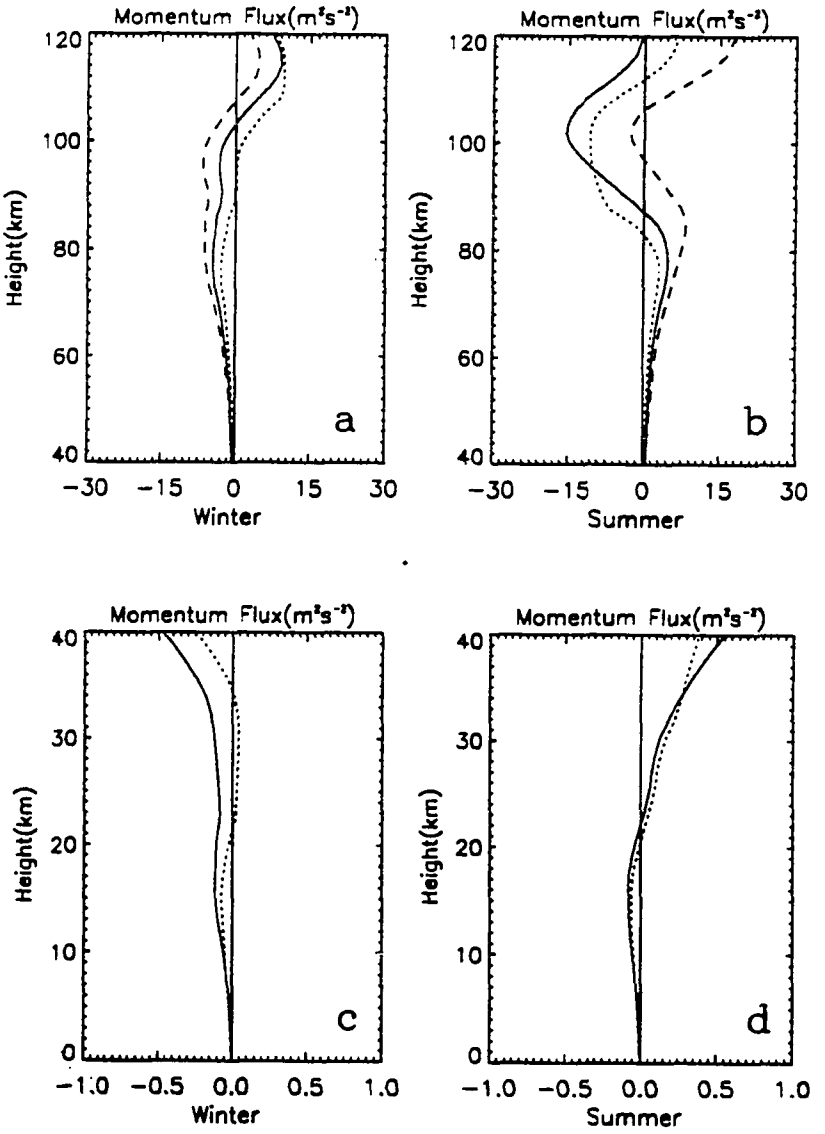

Figure 5.6: Momentum flux profiles for different values of α. Momentum flux profiles obtained with $\alpha = 0.1$ (long-dashed), 0.2(solid), and 0.3 (dashed), $c_{*0} = 5ms^{-1}$, and $b_z = 0.0$ for winter and summer zonal mean winds at $40 - 120km$ (a and b) and $0 - 40km$ (c and d).

the altitudes at which these maxima occur increase. These departures arise because a large allowed anisotropy implies a potentially very small fraction of the total wave energy propagating in one direction and a correspondingly large depth required for that component, even propagating upward in a conservative fashion, to recover a competitive energy and momentum flux.

5.1.3 Implications of Variable H_E

So far all the results we have showed above were based on our assumption of a constant value of $H_E = 2.3H$. As noted by Balsley and Garello (1985) , a slowly varying H_E is in more quantitative agreement with the observed energy growth. Such variations, if large, may impact significantly the distribution of energy and momentum flux divergences and should likely be included in any attempt to incorporate gravity wave forcing in large-scale models. Thus it is very important for us to examine the implications of a variable H_E in our parameterization scheme.

We estimate the degree of variability of the scale height H_E from the observed decrease of energy per unit volume with height and the corresponding scale height for density in the same altitude interval. This yields a range of H_E varying about a mean value of $\sim 2.3H$ by $\sim H$. Thus, to illustrate the effects of this variability, we model the altitude variations as

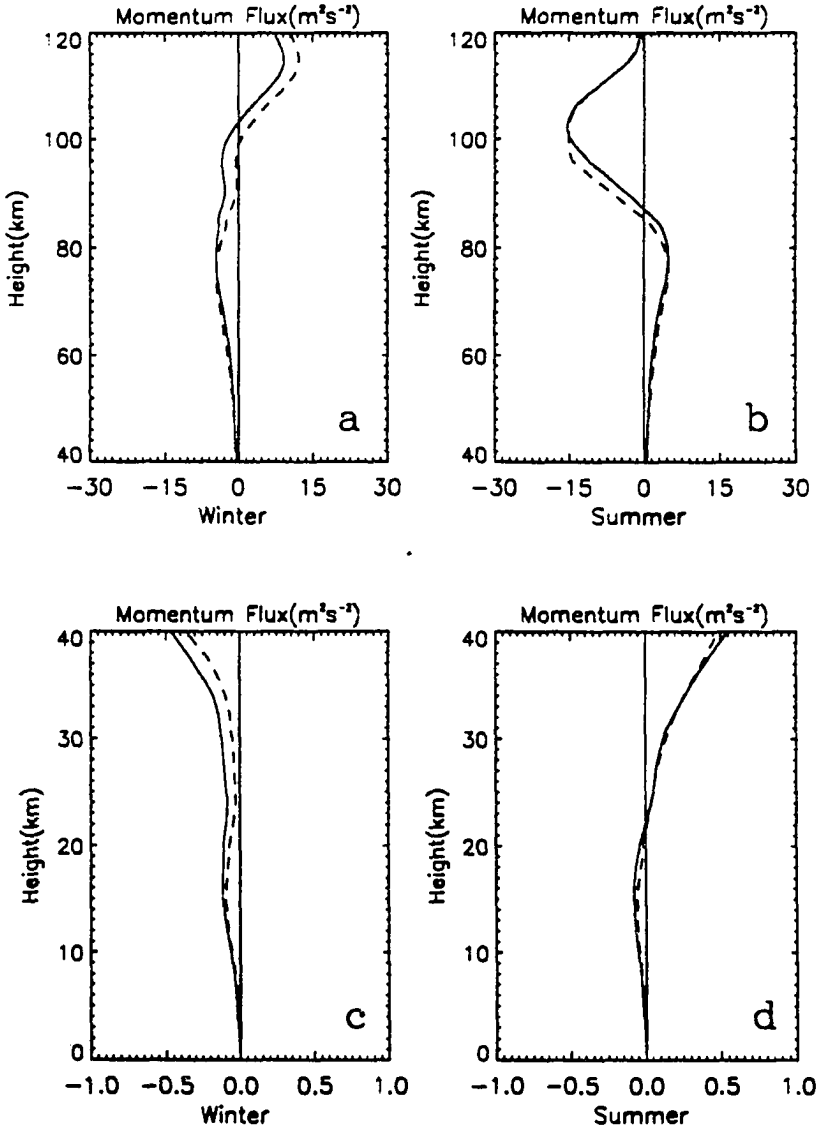

Figure 5.7: Momentum flux profiles for variable H_E. Momentum flux profiles obtained with $c_{*0} = 5ms^{-1}$, $b_z = 0.0$, and $\alpha = 0.2$ for canonical winter and summer profiles at $40 - 120km$(a and b) and $0 - 40km$(c and d) with constant (solid) and variable (dashed) H_E.

$$H_E = 2.3H + \beta H sin(\frac{2\pi z}{60}), \tag{5.1}$$

with z in km. The momentum fluxes obtained for H_E profiles with $\beta = 0$ and 0.8, $c_{*0} = 5ms^{-1}$, $b_z = 0.0$, and $\alpha = 0.2$ are shown in Figure 5.7. These result in similar momentum flux profiles, with a tendency for maxima to occur at slightly lower altitudes and with slightly reduced and enhanced amplitudes at lower and upper altitudes, respectively. The more significant differences between the results for constant and variable H_E obtain from the stronger constraints on wave energies (and fluxes) where H_E is large and are more visible in the vertical flux divergences which are discussed below.

5.1.4 Energy Dissipation Rate and Induced Zonal Acceleration

Now we turn to the vertical profiles of energy dissipation rate and momentum flux divergence implied by the spectral variability and responses to zonal mean wind variations discussed above. Figures 5.8 and 5.9 present the results for the canonical winter and summer profiles for the standard case with $c_{*0} = 5ms^{-1}$, $b_z = 0.0$, $\alpha = 0.2$, and both constant and variable scale height H_E.

Energy dissipation rate ϵ shows a tendency for approximately exponential increases with height for both constant and variable H_E (see Figure 5.8).

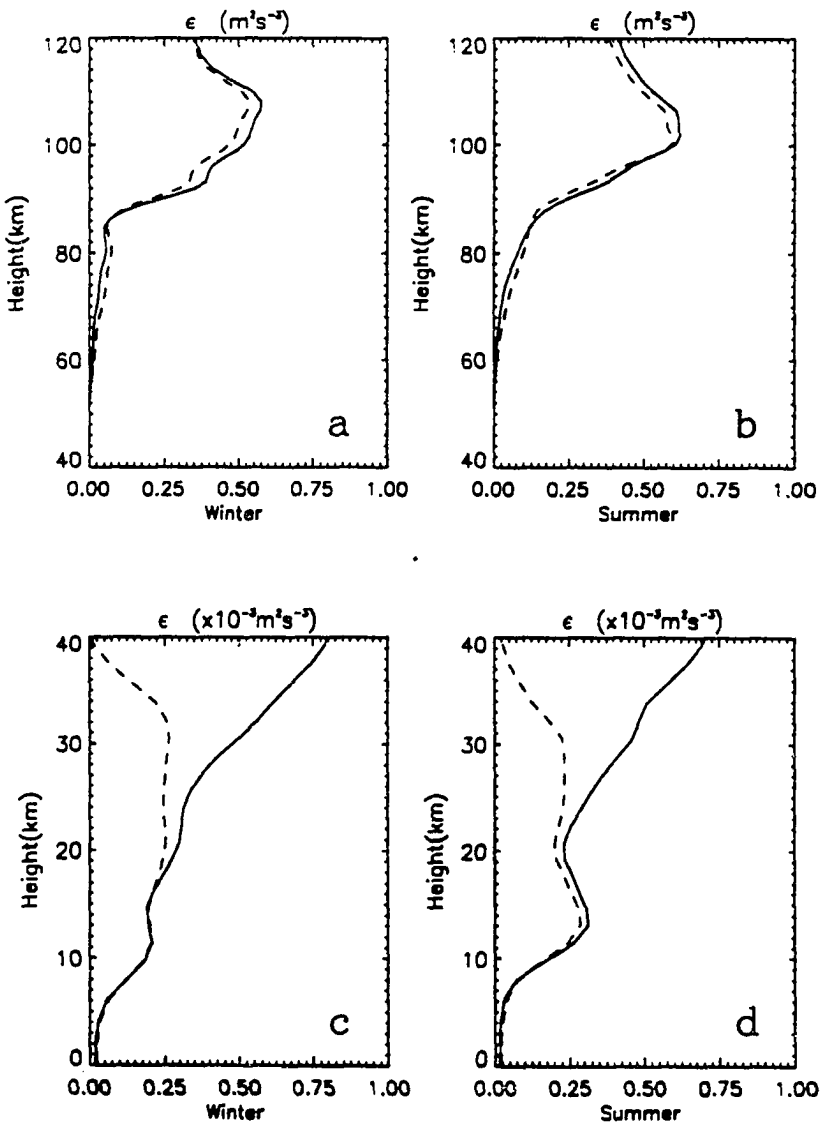

Figure 5.8: Profiles of energy dissipation rate. Profiles of energy dissipation profiles obtained with $c_{*0} = 5ms^{-1}$, $b_x = 0.0$, and $\alpha = 0.2$ for canonical winter and summer profiles at $40 - 120km$ (a and c) and $0 - 40km$ (c and d) with constant (solid) and variable (dashed) H_E.

Departures from exponential growth for constant H_E are due entirely to variations in N and cessation of wave amplitude growth at upper levels. For variable scale height H_E, these departures result additionally from variations in H_E itself. The implications at lower levels are an energy dissipation rate for variable H_E that falls below that for constant H_E because the less rapid growth of wave energy (per unit mass) dominates the increased vertical divergence of wave energy flux where H_E exceeds its mean value. At intermediate levels, the energy dissipation rate for variable H_E increases much faster with increasing height because here H_E is less than its mean value and ε is dominated by increases in the energy fluxes. This preferential growth of ε for variable H_E causes it to exceed the values for constant H_E into the mesopause region and above. The energy dissipation rates reach values of $\sim 0.1 - 0.2\ m^2 s^{-3}$ near the mesopause, in very good agreement with the larger values reported for *in situ* and radar estimates (Hocking, 1985; Blix et al., 1990a, b). Its maximum values are achieved near and above $\sim 100 km$ due to the greater constraints on wave amplitudes at greater altitudes, with somewhat larger values implied during summer with our choices of wind profiles and initial spectral energies.

Zonal acceleration profiles implied by momentum flux divergences (Figure 5.9) indicate values at lower levels for both winter and summer mean zonal winds that vary from $\sim +0.3 ms^{-1} day^{-1}$ below the tropospheric jet to $\sim -2 ms^{-1} day^{-1}$ near $20 km$, in close agreement with observed values and those

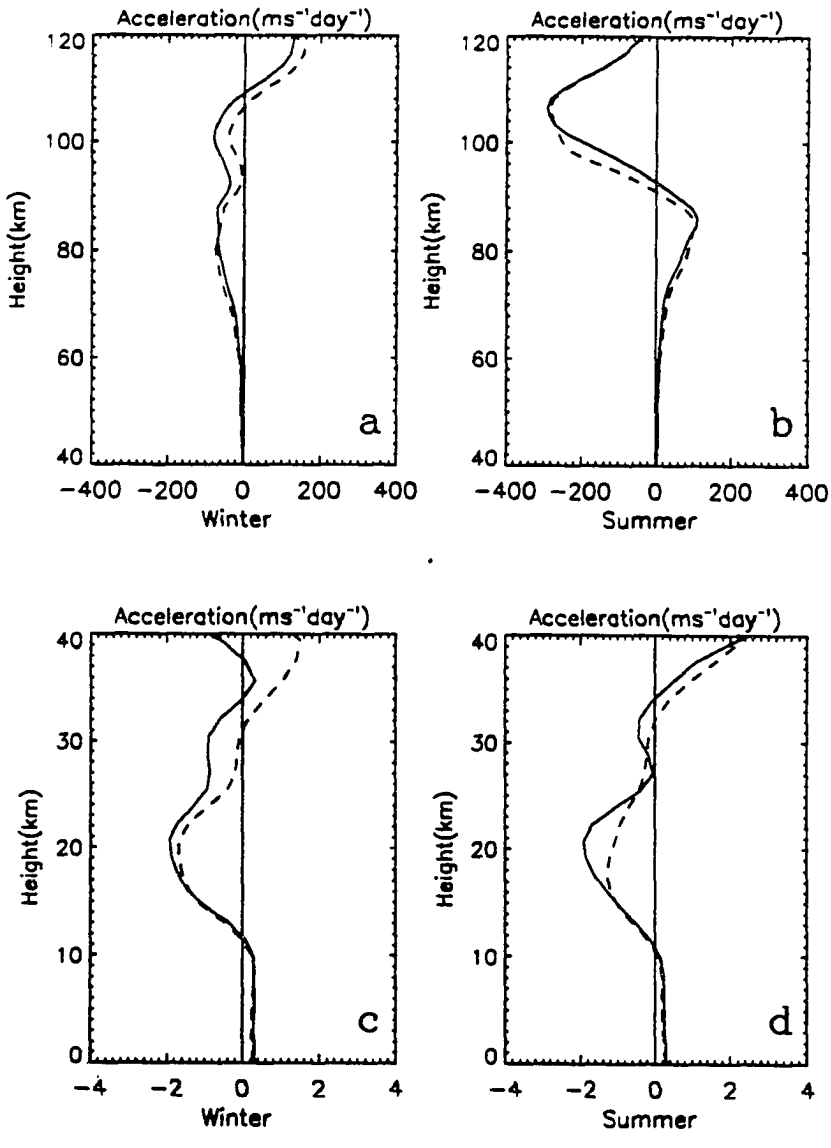

Figure 5.9: Profiles of induced acceleration. Profiles of induced acceleration obtained with $c_{*0} = 5ms^{-1}$, $b_x = 0.0$, and $\alpha = 0.2$ for canonical winter and summer profiles at $40 - 120km$ (a and c) and $0 - 40km$ (c and d) with constant (solid) and variable (dashed) H_E.

needed to provide the requisite decelerations in large-scale models (Fritts et al., 1990; Palmer et al., 1986; McFarlane, 1987). Because of the finite intervals over which divergences were computed, these profiles were smoothed with a 3–point running average. As noted above there is a tendency for those profiles obtained for variable H_E to maximize at lower levels and to have slightly smaller amplitudes due to the slower growth (larger H_E) of wave energies at these heights. Referring to the momentum flux profiles for variable c_{*0} (Figure 5.4), we see that the same general profiles are implied, but with correspondingly smaller or larger accelerations associated with weaker and stronger sources.

At greater heights, there is a tendency for the induced zonal accelerations, like the momentum fluxes themselves, to oppose the mean zonal winds for both winter and summer profiles. The peak accelerations for the $c_{*0} = 5ms^{-1}$ source strength are $\sim \pm 100ms^{-1}day^{-1}$ below the mesopause, while the altitude profiles of momentum flux and its divergence exhibit responses to the variable mean motions that are in good agreement with the limited observations that are available (Vincent and Reid, 1983; Reid and Vincent, 1987; Fritts and Vincent, 1987; Fritts and Yuan, 1989; Wang and Fritts, 1990). At lower altitudes, maxima occur at somewhat lower heights for variable H_E although maximum values tend to be slightly larger. Especially encouraging, perhaps, is that the momentum flux and induced acceleration profiles correspond closely with observations in that region of the atmosphere that is believed to be most

strongly forced by such wave motions. This suggests that the parameterization scheme has accounted, approximately at least, for the spectral energy changes caused by variable mean winds at lower altitudes.

Chapter 6

Gravity Wave-Tidal Interactions

In the previous chapter, the suggested gravity wave parameterization scheme was applied to canonical winter and summer profiles of mean zonal wind, density, and stability. This application results in prediction of systematic variations in the energy and momentum fluxes with altitude due to varying stability and mean zonal wind. The predicted momentum flux profiles are generally consistent both with the mean flux measurements that are available and with the needs of large-scale models.

The above successes suggest that the parameterization scheme may also be useful in describing the interactions of gravity waves with the lower-frequency components of the motion field in the middle atmosphere. This view is reinforced by the mean gravity wave frequencies at which energy and momentum fluxes are communicated based on their spectral forms. These imply character-

istic periods of 1 to 2 h and the potential for significant modulation by motions near tidal periods. Further evidence of the importance of such an interaction is provided by the large variability in hourly momentum flux measurements and observations of anti-correlated fluxes and local mean winds using MF and VHF radars (Fritts and Vincent, 1987; Reid and Vincent, 1987; Reid et al., 1988; Fritts and Yuan, 1989; Wang and Fritts, 1991; Fritts et al., 1992). Such observations have led to the development of several gravity wave-tidal interaction theories. The first, by Walterscheid (1981), attributed gravity wave forcing to wave absorption near critical levels in opposite phases of the tidal motion. More recently, Fritts and Vincent (1987) argued that the maximum effects would occur not near critical levels, where wave amplitudes and fluxes are small, but due to saturation processes where wave amplitudes are large. Indeed, this model was found to be generally consistent with the momentum flux measurements that provided its motivation. It also predicted both tidal amplitude changes and a tidal phase advance in the presence of strong gravity wave modulation. A further study by Forbes et al. (1991) used a discrete wave saturation scheme to simulate this interaction in a global tidal model. They concluded that gravity wave forcing could dramatically reduce tidal amplitudes. Given the potential importance of this problem and the uncertain nature of the interaction and its atmospheric effects at this time, it would seem valuable to consider the implications for such interactions using a grav-

ity wave parameterization that appears to account reasonably for gravity wave momentum fluxes in realistic environments.

Two approaches are taken in the present study. The first uses the canonical winter and summer mean wind and temperature profiles considered in Chapter 5, but with superposed static tidal wind fields, to examine the variation of gravity wave momentum fluxes with altitude for varying tidal phases. These results lead to a simple analytic model of gravity wave influences on apparent tidal amplitudes and phases. The second approach examines the response of a time-dependent tidal motion to the accelerations implied by momentum flux divergence in an interactive manner. Together, the two approaches reveal the potential for momentum flux variability due to modulation by the tidal wind fields and demonstrate the ability of gravity wave momentum flux divergences to dramatically influence tidal amplitudes and phases. Our results suggest (1) that gravity wave-tidal interactions may be an important source of tidal variability in the middle atmosphere and (2) that gravity waves may contribute appreciable temporal variability well into the thermosphere as a consequence of tidal modulation. This application of the gravity wave parameterization scheme has also been described in Lu and Fritts (1993).

6.1 Momentum Flux Profiles for Mean Winds with Static Tides

Given the disparity between tidal periods and the periods characteristic of gravity wave energy and momentum fluxes, it is appropriate ,as a first approximation, to assume that the tidal wind field is constant in time in assessing its filtering of the gravity wave spectrum. Assuming a canonical tidal structure with a vertical wavelength $\lambda = 25km$, and an amplitude that increases as

$$A(z) = .0.65e^{z/3.3H} \tag{6.1}$$

below $\sim 100km$, the tidal amplitude increases exponentially with height and achieves a value of $\sim 50ms^{-1}$ at $100km$. Above $100km$, it is assumed that $A(z)$ has a constant value of $50ms^{-1}$. The gravity wave energy is likewise assumed to vary with height as

$$E_0 \propto N^{1/2}e^{z/H_B} \tag{6.2}$$

up to $\sim 100km$, above which it is assumed to be constant. For consistency with the previous results in the absence of tidal winds, the CIRA 1986 January and June mean wind and temperature fields at 40^0N are used as canonical winter and summer profiles. Again, for simplicity and consistency, we consider only the zonally propagating components of the assumed gravity wave spectrum,

and assume initially isotropic propagation ($b_x = 0$), $\alpha = 0.2$, and characteristic phase speeds of $c_{*0\pm} = 3, 5$, and $8ms^{-1}$.

The tidal wind fields alone and the resulting momentum flux profiles for four phase of the tidal oscillation, the three characteristic phase speeds, $\alpha = 0.2$, and the summer temperature and stability profiles are shown in Figure 6.1. In each case, the maximum momentum fluxes occur at upper levels and are limited by the gravity wave energies and maximum permitted anisotropies. The tidal winds and gravity wave momentum fluxes are seen to be almost exactly out of phase, in excellent agreement with the observations of Fritts and Vincent (1987) and Wang and Fritts (1991).

Figures 6.2a and 6.3a show the canonical winter and summer wind profiles with four phases of superposed tides. The corresponding momentum fluxes are shown for $c_{*0\pm} = 3$, 5, and $8ms^{-1}$ in each case. Consistent with the correlations seen in Figure 6.1, in which mean winds were not present, the tidal winds and computed momentum fluxes for canonical winter and summer profiles are again largely anti-correlated. The momentum flux profiles obtained for the four tidal phases tend to spread about the mean profiles (without tidal winds) below $\sim 80km$. At greater heights, there is a tendency for the means of the tidally varying fluxes to differ increasingly from the means without superposed tides. These mean departures are $\sim 5m^2s^{-2}$ for $c_{*0\pm} = 3ms^{-1}$ above $\sim 80km$ and increase to $\sim 20m^2s^{-2}$ for $c_{*0\pm} = 5$ and $8ms^{-1}$, with individual

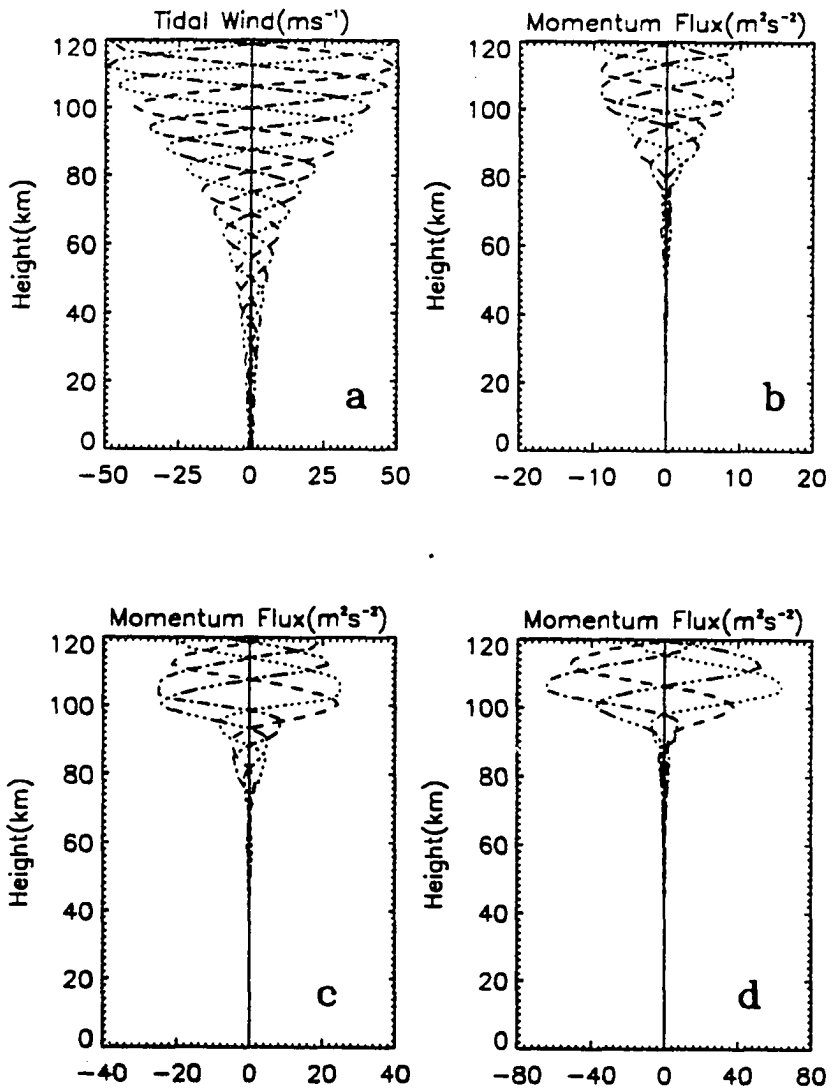

Figure 6.1: Canonical tidal winds and the associated momentum fluxes. Canonical tidal winds at four phases of oscillation (a) and the gravity wave momentum flux profiles due to tidal filtering for $\alpha = 0.2$ and $c_{*0\pm} = 3$ (b), 5(c), and 8(d) ms^{-1}.

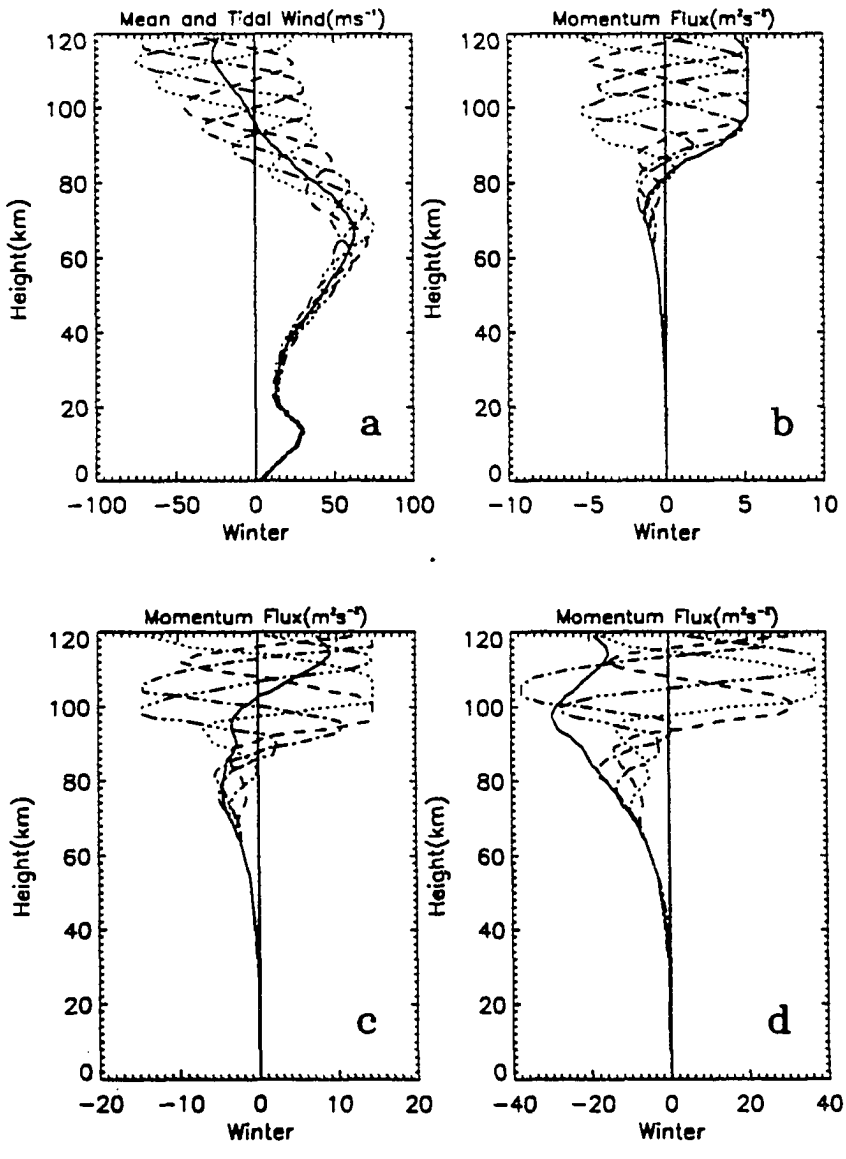

Figure 6.2: Canonical winter mean wind superposed with tidal winds and their associated momentum fluxes. As in Figure 6.1 with the CIRA 1986 winter mean wind profiles. The solid line in each panel shows the mean wind and momentum fluxes in the absence of tidal fluctuations.

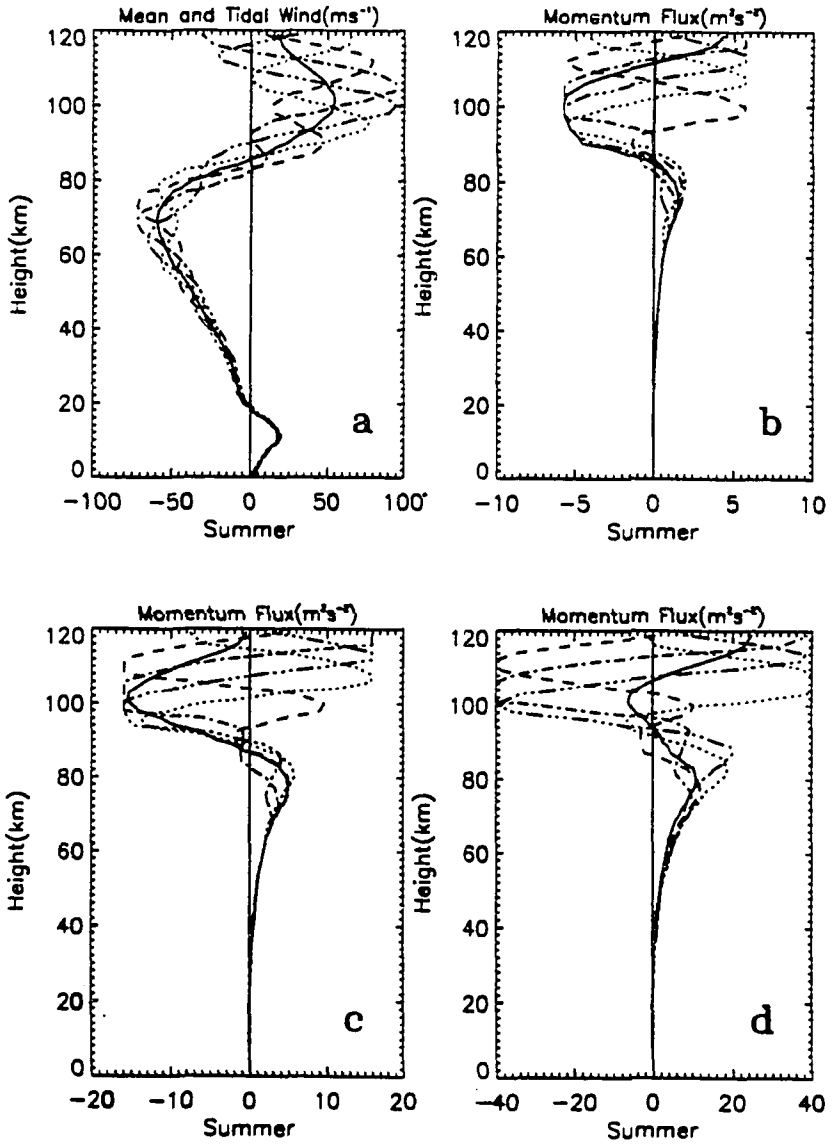

Figure 6.3: Canonical summer mean wind superposed with tidal winds and their associated momentum fluxes. As in Figure 6.2 with the CIRA 1986 summer mean wind profiles.

profiles exhibiting highly variable fluxes and maximum departures as large as $\sim 60\ m^2s^{-2}$. These results suggest that the mean momentum flux profiles due to gravity waves in the presence of a varying tidal wind field may be quite different from those inferred without tidal winds present. It is noted that the magnitudes of the tidally varying momentum fluxes near the mesopause are ~ 5 to $20m^2s^{-2}$, depending on phase speed and altitude, in line with the mean and large-amplitude variations observed by Fritts and Vincent (1987) and Wang and Fritts (1991) at middle and high latitudes.

Given the uncertainty in the maximum degree of anisotropy in the atmospheric gravity wave field, the momentum profiles corresponding to those in Figures 6.2 and 6.3, but with $\alpha = 0.1$, are shown in Figures 6.4 and 6.5. This choice increases the maximum possible momentum flux at any height by 33%. But more significant, perhaps, are the larger recovery depths for $\alpha = 0.1$ resulting in decreased sensitivity to variations in the mean wind at greater altitudes. The major effect is a greater spread in momentum fluxes in opposite phases of the tidal motion. Maximum values are ~ 20 to $50m^2s^{-2}$, in general agreement with mesopause measurements at a number of sites (Fritts and Vincent, 1987; Reid and Vincent, 1987; Reid et al., 1988; Fritts and Yuan, 1989; Wang and Fritts, 1990; Fritts et al., 1992). Indeed, if these gravity wave and tidal amplitudes and gravity wave anisotropies are at all representative of the lower thermosphere, then gravity wave forcing and tidal interactions are

almost certain to be a major source of variability in this region.

In order to examine the magnitude of gravity wave forcing implied by the previous results, the accelerations inferred for the winter and summer superposed mean and tidal winds with $c_{*0\pm} = 5ms^{-1}$ and $\alpha = 0.2$ are shown in Figure 6.6. Below $\sim 80km$ (Figure 6c and d), the canonical tidal winds are small and variations in the inferred accelerations are less than or comparable to mean values. At greater altitudes, however, momentum fluxes are typically larger than mean values due to the large vertical momentum flux gradients implied by tidal filtering of the gravity wave spectrum. The consequences of the anti-correlated tidal winds and gravity wave momentum fluxes and the large momentum flux gradients due to tidal filtering are examined using analytic and numerical techniques in the following sections.

6.2 A Simple Model of Gravity Wave Forcing of Tidal Structures

The principal result of the previous section at greater altitudes is the apparent anti-correlation of the tidal wind field and the momentum flux that arises in response. This suggests a very simple analytic description of the interaction for the purposes of inferring the major potential influences of the gravity wave momentum flux divergences on the tidal structure. The local tidal wind can be expressed as

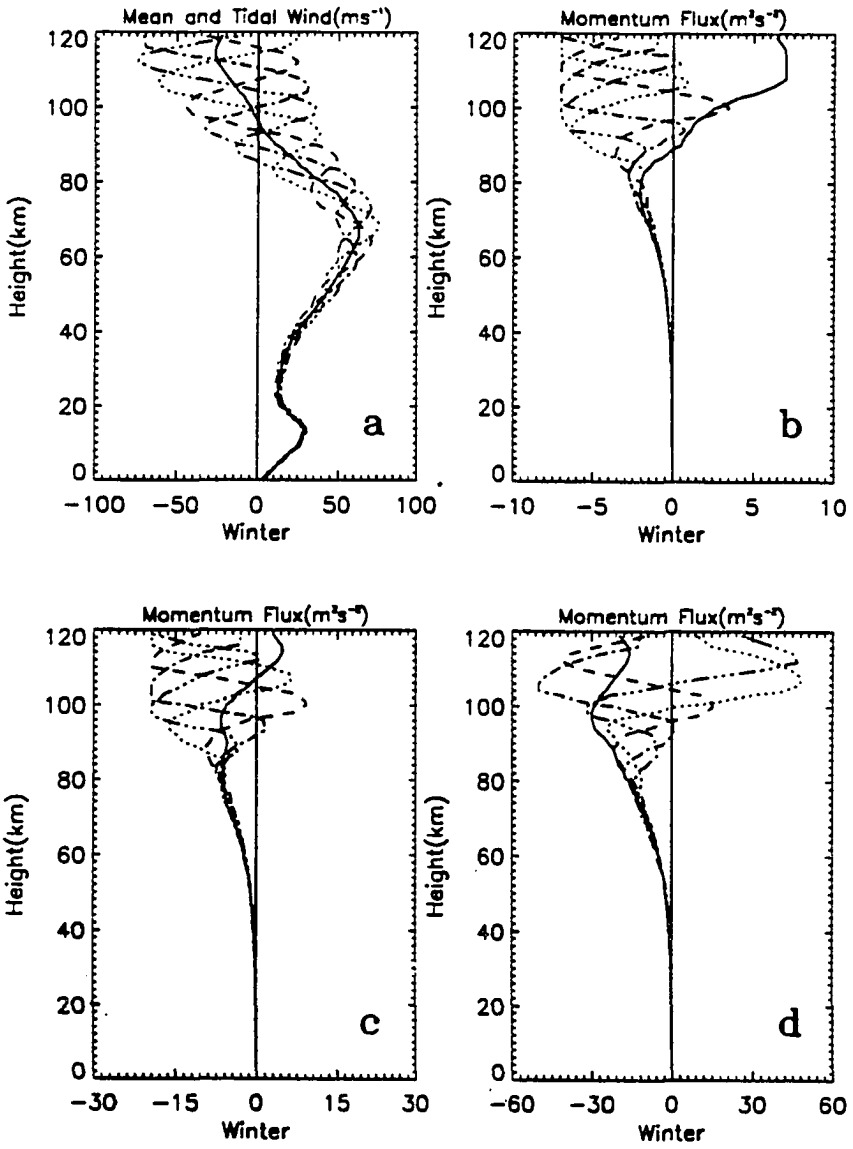

Figure 6.4: As in Figure 6.2 with $\alpha = 0.1$.

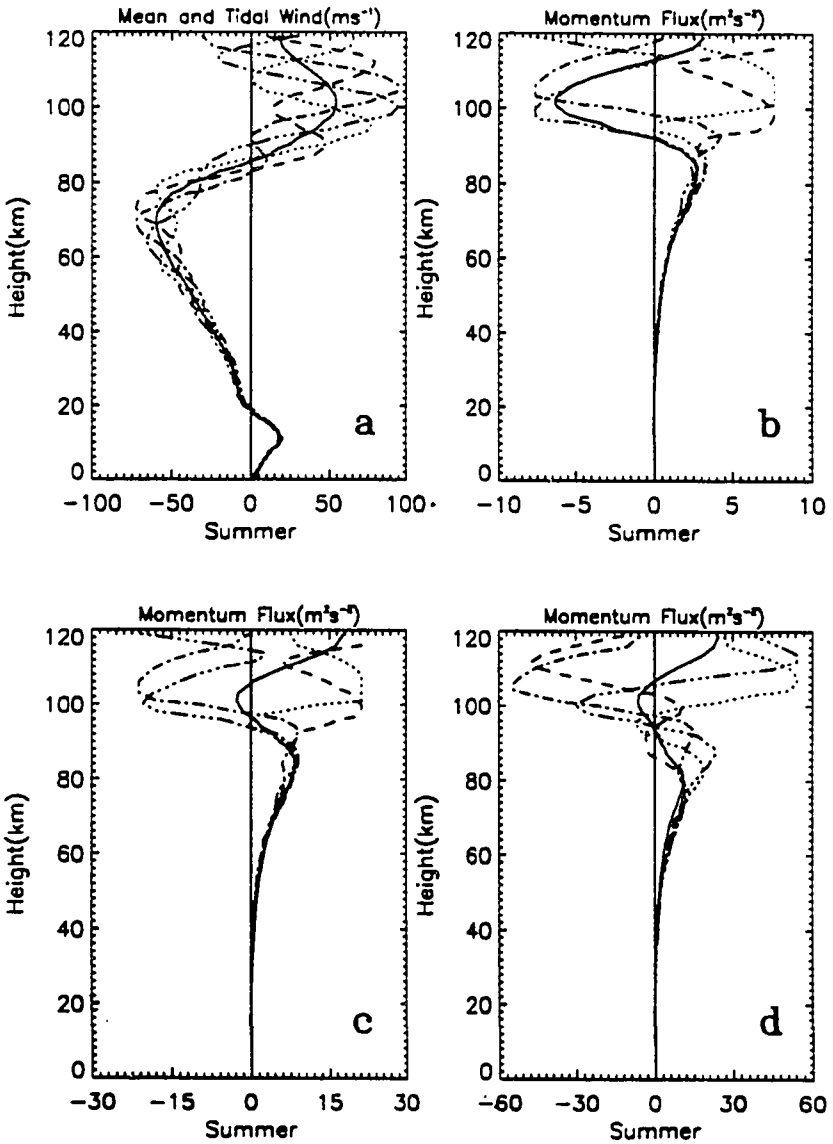

Figure 6.5: As in Figure 6.3 with $\alpha = 0.1$.

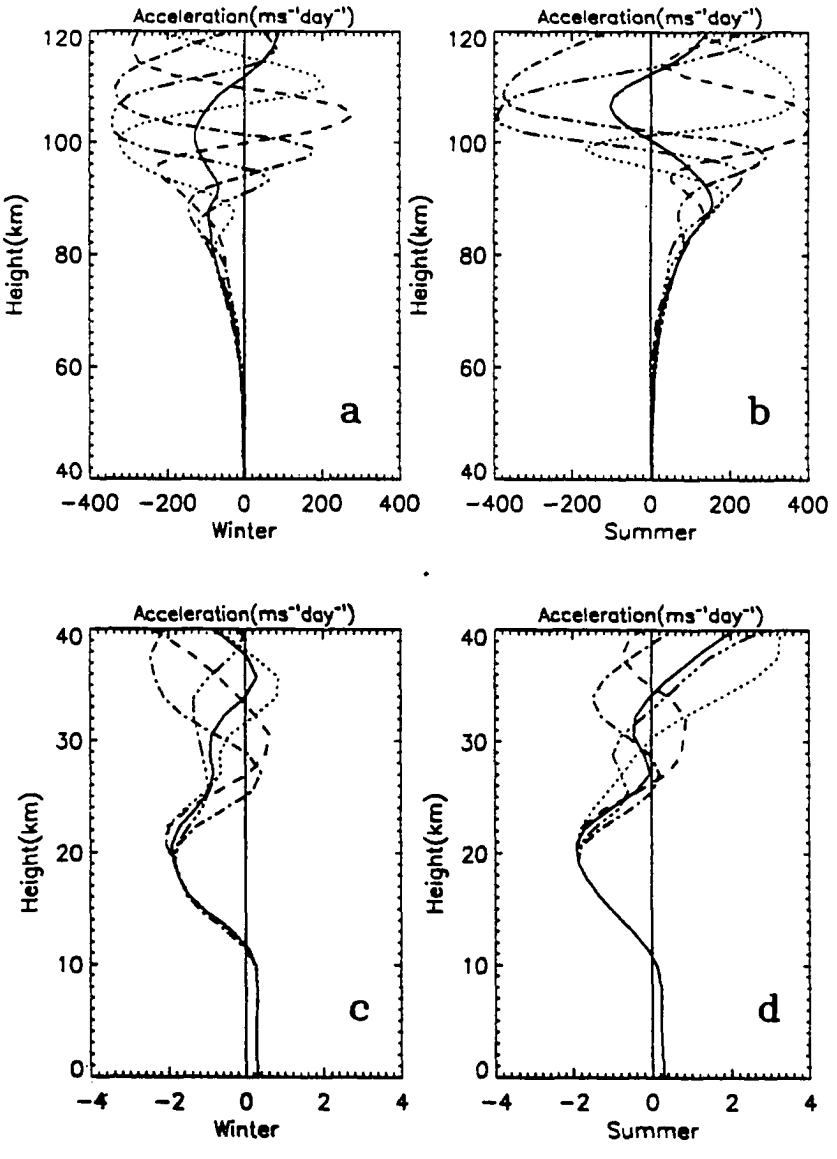

Figure 6.6: Gravity wave induced accelerations for imposed tidal winds. Gravity wave induced accelerations for four phases of the imposed tidal motions with superposed winter (left) and summer (right). The upper (lower) panels display the results above (below) 40 km. Note also the very different magnitudes of the fluxes in the upper and lower panels.

$$\overline{u}_T = u_0 e^{z/H_T} sin(\omega t + mz), \tag{6.3}$$

with ω and m positive and H_T varying slowly with height. Thus the gravity wave momentum flux may be represented as

$$\overline{u'w'} \simeq -a\overline{u}_T, \tag{6.4}$$

where a is a constant, enabling us to obtain analytic expressions for the gravity wave influences.

Computation of the momentum flux divergence then yields gravity wave induced accelerations given by

$$\frac{\partial \overline{u}_G}{\partial t} = -\frac{1}{\overline{\rho}}\frac{\partial \overline{\rho u'w'}}{\partial z} = \frac{a}{\overline{\rho}}\frac{\partial \overline{\rho u}_T}{\partial z}$$

$$= au_0 e^{z/H_T}[-(\frac{1}{H} - \frac{1}{H_T})sin(\omega t + mz) + mcos(\omega t + mz)], \tag{6.5}$$

For comparison, the tidal wind itself experiences an acceleration given by

$$\frac{\partial \overline{u}_T}{\partial t} = \omega u_0 e^{z/H_T} cos(\omega t + mz). \tag{6.6}$$

The gravity wave forcing then provides one term that is in phase with the acceleration within the tidal field and a second term that is in quadrature, with the maximum acceleration displaced downward relative to that of the tide.

The first term thus leads to a larger acceleration and a larger tidal amplitude than would otherwise occur, while the second term biases the net acceleration downward relative to the tide itself. This contributes to an expected phase advance with time, as anticipated by the gravity wave-tidal interaction model of Fritts and Vincent (1987). However, this simple model also predicts an amplitude increase rather than the decrease inferred by those authors.

To assess the importance of these contributions, representative parameters are chosen as $H = 7km$, $\omega = 2\pi/24h^{-1} \simeq 7.27 \times 10^{-5}s^{-1}$, $m = 2\pi/\lambda_z \simeq 2.5 \times 10^{-4}m^{-1}$, $u_0 \simeq 50ms^{-1}$, $\overline{u'w'} \simeq 15m^2s^{-2}$ (corresponding to the results in the previous section with $c_{*0\pm} = 5ms^{-1}$ and $\alpha = 0.2$), $a \simeq 0.3ms^{-1}$, and $H_T \rightarrow \infty$. These result in tidal accelerations of $\sim 3.6 \times 10^{-3}ms^{-2}$ and in-phase and quadrature contributions from gravity wave momentum flux divergences of $\sim 3.75 \times 10^{-3}ms^{-2}$ and $\sim 2.1 \times 10^{-3}\ ms^{-2}$, respectively. Thus the gravity wave-induced accelerations in this case are comparable to that describing the evolution of the tidal structure alone, suggesting that gravity waves with comparable fluxes may well have profound effects on tidal structure, evolution, and variability. Referred to the results of last section with $c_{*0\pm} = 3$ and $8ms^{-1}$, the corresponding coefficients are $a \simeq 0.1$ and 0.6, respectively, suggesting small influences for weak forcing conditions and dramatic effects in response to very energetic forcing.

6.3 An Interactive Model of Gravity Wave-Tidal Interactions

In this section, a simple model of the mutual interactions of a gravity wave spectrum described by the suggested parameterization scheme and a temporally varying tidal wind field having an equilibrium structure given by eq. (6.1) will be discussed. From the correlations noted in section 6.3 and the gravity wave-tidal interaction model posed in section 6.4, however, we anticipate that a strong forcing will substantially alter the imposed tidal structure. Yet the modulation and anticipated amplitude increases can not go on indefinitely because the tidal field is propagated from sources lower in the atmosphere. Nor can a transient forcing forever alter the tidal structure locally. Thus there must be a relaxation of the tidal wind field towards the equilibrium tidal structure in the absence of mean winds. The issue is the time scale on which this relaxation occurs.

Tidal structures vary on many time scales of course. But variations on long time scales are clearly not relevant to this discussion. More important are the time scales of variability of the dominant forcing processes, ozone and water vapor distributions and heating, and the tidal set-up times noted in transient forcing models (Vial et al., 1991). These suggest variability on scales of a few to ten days. As a result, a motion field is considered to be comprised

of two parts,

$$\overline{u} = \overline{u}_T + \overline{u}_G, \tag{6.7}$$

with $\overline{u}_T$ given by eq. (6.3) and $\overline{u}_G$ experiencing an exponential damping with damping times as short as two days. The evolution of the wind field is then described by three terms, with the tidal and gravity wave forcing given by eqs. (6.5) and (6.6) and $\overline{u}_G$ experiencing a decay with time scale τ,

$$\frac{\partial \overline{u}}{\partial t} = \omega u_0 e^{z/H_T} cos(\omega t + mz) - \frac{1}{\rho}\frac{\partial \overline{\rho u' w'}}{\partial z} - \overline{u}_G/\tau. \tag{6.8}$$

The above equation can be solved by using the Leapfrog method. In eq.(6.8), let

$$f(\overline{u}, t) = -(\omega u_0 e^{z/H_T} cos(\omega t + mz) - \frac{1}{\rho}\frac{\partial \overline{\rho u' w'}}{\partial z} - \overline{u}_G/\tau), \tag{6.9}$$

then we have

$$\frac{\partial \overline{u}}{\partial t} + f(\overline{u}, t) = 0, \tag{6.10}$$

Employing the Leapfrog method, $\overline{u}$ at step $n+1$ can then be written as

$$\overline{u}^{n+1} = \overline{u}^{n-1} - f^n 2\Delta t. \tag{6.11}$$

where Δt is the time step. In our computation, $\Delta t = 10s$ has been used. Note here that the Leapfrog scheme is a two step method. Thus, at the first time step, the Euler method has been introduced, in which

$$\overline{u}^1 = \overline{u}^0 - f^0 \Delta t. \tag{6.12}$$

In eq.(6.8), theoretical analysis shows that the Leapfrog solution converges with only the first analytic term on the righthand side. However, together with the second and third terms, there is no way for us to do a theoretical analysis as these two terms are parameterized. In order to insure the convergence of the solutions, several different time steps Δt were chosen to test the results. It was found that for $\Delta t = 5, 8, 10, 15s$, all results were nearly identical. This gives us sufficient confidence in choosing $\Delta t = 10s$.

Solutions for three different cases are presented. First, assuming a constant gravity wave source energy with characteristic phase speed $c_{*0\pm} = 3ms^{-1}$, and $\alpha = 0.2$, and $\tau \to \infty$ (without damping) and by integrating eq. (6.8), the results of the first six-day period are displayed in Figure 6.7 at 6-h intervals. Also shown in Figure 6.7 is the tidal structure in the absence of gravity wave forcing (dashed curves). The solid curves exhibit substantial variability about the imposed tidal structures and general consistency with the model posed in the previous section. Particularly, it is noted that there is a tendency at early times for larger amplitudes and apparent phase advances relative to the pure

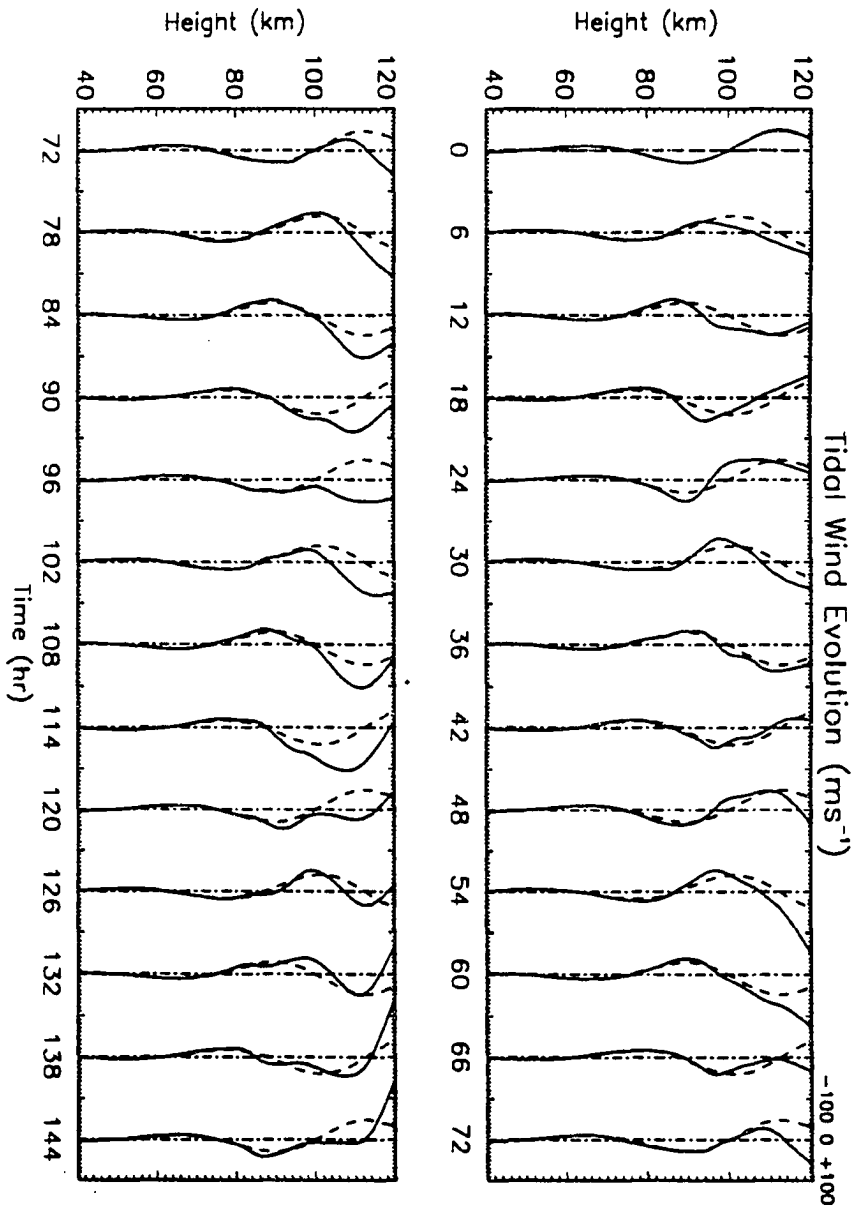

Figure 6.7: Tidal and gravity wave induced mean wind. Tidal and mean winds induced by gravity wave momentum flux gradient due to tidal filtering at 6 - h intervals (solid lines) with $c_{*0\pm} = 3ms^{-1}$ and $\alpha = 0.2$. The gravity wave contributions in this case are undamped. Dashed lines show the pure tidal motions in the absence of gravity wave forcing.

tidal motion in a number of profiles. There are also profiles in which smaller amplitudes and no apparent phase advances occur. These appear to result from the cumulative accelerations due to gravity wave forcing in the opposite tidal phase which act to suppress the subsequent maxima of the opposite sign. The net result is an apparent tidal structure that varies about the pure tide by a factor of ~ 2 and is generally advanced in phase (displaced downward) during intervals with large amplitudes.

Next, considering a time variable gravity wave source with $c_{*0\pm} = 1 + 4sin^2(\pi t/T)$, $T = 3days$, and $\alpha = 0.2$, this results in a maximum forcing that is ~ 3 times stronger than with $c_{*0\pm} = 3ms^{-1}$. The results without damping are shown in Figure 6.8. The strongest forcing intervals are centered at 36 and $108h$ and result in both dramatically larger apparent amplitudes and phase advances and velocity jets that persist through the intervals with weak gravity wave forcing (see the positive maximum between $\sim 80km$ and $90km$ occurring from ~ 48 to $96h$). The maximum amplitudes achieve values ~ 2 to 3 times the imposed tidal structure while the maximum phase advances approach $\pi/2$ (see the profiles at 24 to 36 h and 90 to 96 h). Since the cumulative accelerations due to gravity wave forcing occasionally oppose the local forcing, there are also times at which the vertical structure bears little resemblance to the imposed tide (see the profiles near 60, 84, and 144 h).

Finally, consider a somewhat more realistic situation in which the mean

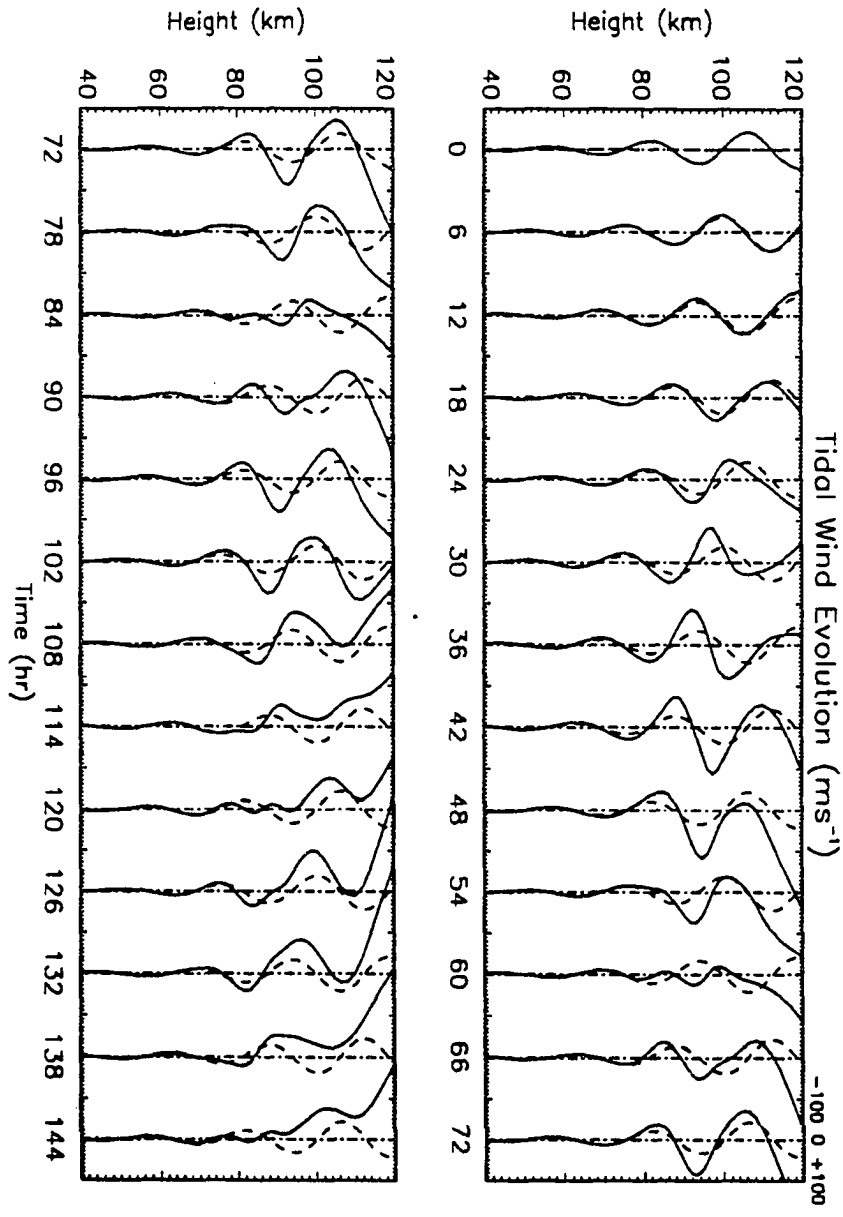

Figure 6.8: Tidal and gravity wave induced mean wind damping. As in Figure 6.7 with $c_{*0\pm} = 1 + 4sin^2(\pi/T)\, ms^{-1}$ with $T = 3days$ and $\alpha = 0.2$.

wind variations induced by the gravity wave spectrum are damped in time, simulating the return of an unforced tidal wind field to its equilibrium structure. In this case, again, the variable gravity wave forcing with $c_{*0\pm} = 1 + 4sin^2(\pi/T)ms^{-1}$ and $\alpha = 0.2$ are used. The wind profiles together with the pure tidal motions obtained with damping times $\tau = 4$ and $2days$ are displayed in Figure 6.9 and 6.10.

As expected, damping of the gravity wave induced departures from the imposed tidal structure results in smaller apparent tidal amplitudes. This kind of reduction is small for a damping time of 4 days but more obvious for the more rapid relaxation rate. The maximum amplitudes in the latter case are now only about twice the imposed tidal amplitudes. Another consequence of the damping of gravity wave induced motions is a greater consistency of the wind structure with the imposed tide. Even when apparent amplitudes are large and phases are advanced, the vertical structure resembles the imposed tide more closely because the damping has now minimized departures due to gravity wave forcing. It is also noted that the maximum amplitudes now coincide more closely with those intervals in which the gravity wave forcing is strong as departures now decay on the time scale of the forcing variability.

Studies of gravity wave-tidal interactions in the presence of the canonical winter and summer mean wind profiles are not presented because the zonal mean wind structures can not be maintained in the presence of large

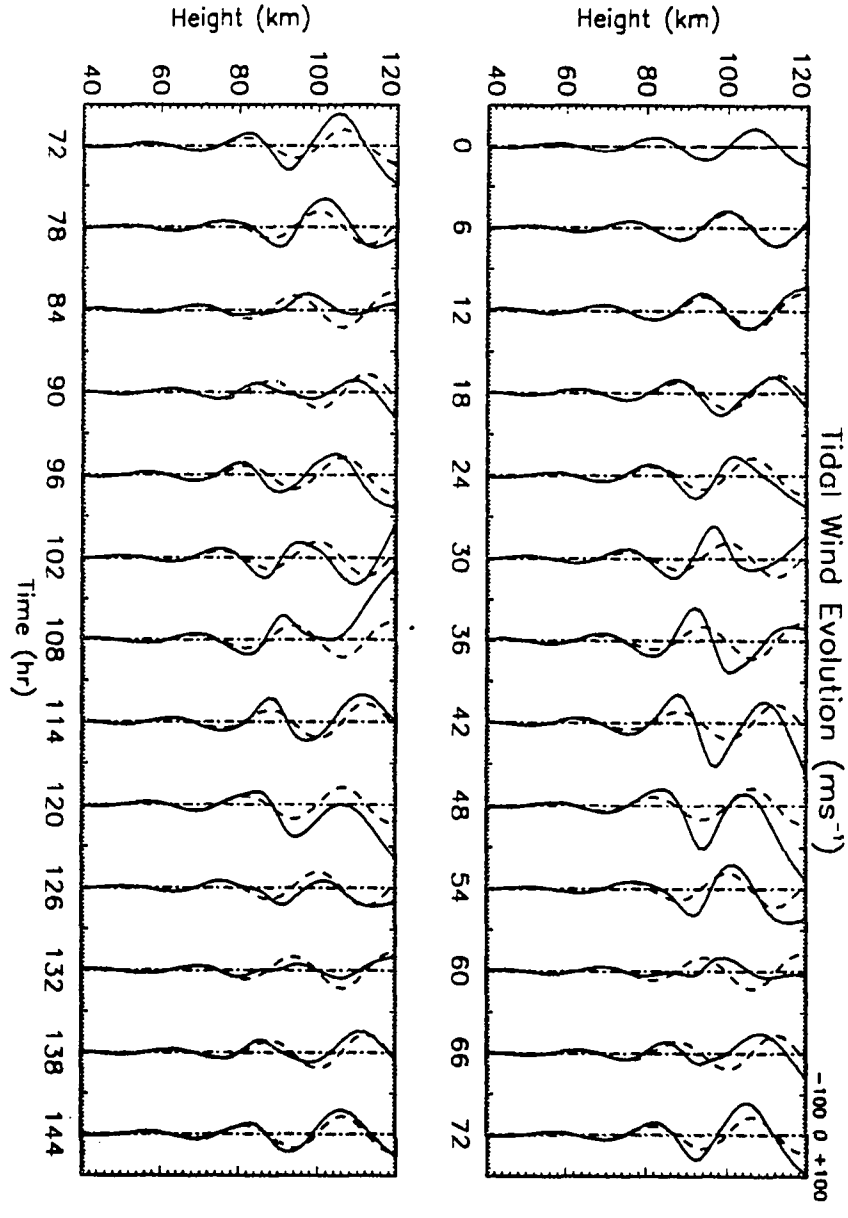

Figure 6.9: Tidal and gravity wave induced mean wind with damping. As in Figure 6.8 with damping of the gravity wave induced winds given by $\tau = 4days$.

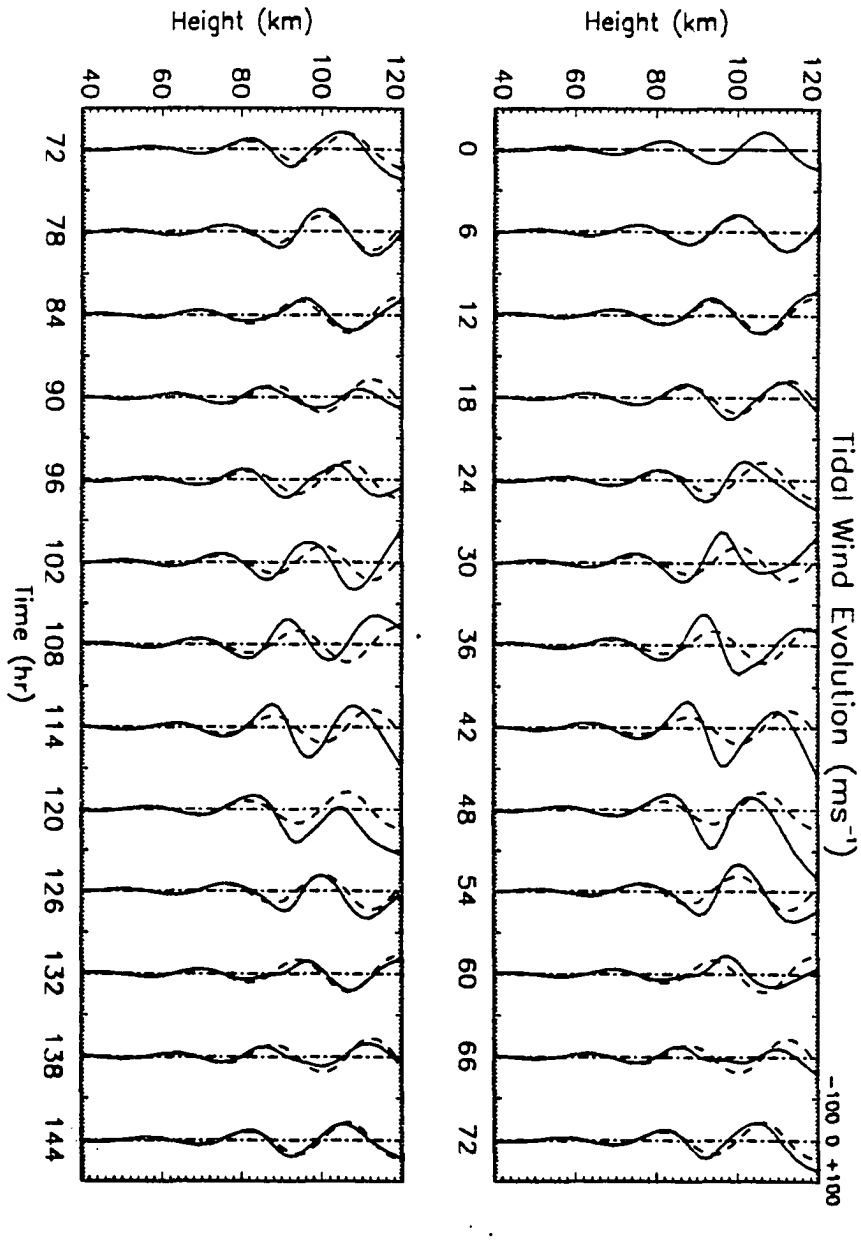

Figure 6.10: Tidal and gravity wave induced mean wind with damping. As in Figure 6.9 with damping of the gravity wave induced winds given by $\tau = 2days$.

mean gravity wave momentum fluxes without compensating torques due to an induced meridional circulation. Nevertheless, it can be inferred that similar consequences due to tidal filtering of the gravity wave spectrum will result because of the similarity of variations in the momentum flux profiles obtained with static tidal structures with and without superposed mean winds. Thus, it is anticipated that the model results presented here may have relevance to apparent tidal variability on time scales of a few days and suggest a substantial role for gravity wave forcing of tidal and mean wind fields in the mesosphere and lower thermosphere.

Chapter 7

Summary and Conclusions

A gravity wave parameterization scheme has been developed by using a spectral model of gravity waves in the atmosphere introduced by Fritts and VanZandt (1993). The gravity wave fluxes of energy and momentum are resulting from variable stability and mean winds. The parameterization scheme is based on a separable and invariant spectral form that is consistent with observations throughout the atmosphere. By choosing representative gravity wave parameters, the scheme yields predictions of mean fluxes of momentum for winter and summer CIRA 1986 profiles that agree well with mean flux observations in the lower and middle atmosphere.

In the troposphere and lower stratosphere, both winter and summer profiles imply a negative zonal mean flux (per unit mass) of $\sim -0.2m^2s^{-2}$, consistent with airborne and radar measurements and the needs of large-scale models. In the mesosphere, mean fluxes tend to oppose the zonal mean wind with

flux maxima above the wind maxima and vertical profiles in general agreement with radar estimates at these heights. Extreme values allowed by the model are likewise in reasonable agreement with the maximum values measured under conditions of strong wave forcing and modulation.

Vertical divergences of energy and momentum fluxes lead to mean energy dissipation rate and zonal acceleration profiles that exhibit structure that agrees well with observations, with $\varepsilon \sim 0.1-0.2\ m^2 s^{-3}$ near the mesopause and accelerations of ~ -2 and $\pm 100 ms^{-1} day^{-1}$ near tropopause and mesopause, respectively.

Energy and momentum flux profiles for varying initial spectral energies and isotropies, intended to permit sensitivity to variable sources and source strengths at lower levels, indicate that the parameterization scheme responds as expected to increases and decreases in the intrinsic phase speeds of the gravity wave spectrum. This is manifested as lesser (greater) sensitivity to varying mean winds for larger (smaller) initial phase speeds. Initial anisotropy was found to be unimportant at greater altitudes because of the strong influences of mean wind shears on the spectral evolution at lower levels where phase speeds are small. In contrast, the maximum allowed anisotropy within the wave field was found to have large effects on the momentum flux profiles, both because it limits the maximum permitted fluxes and because a large anisotropy permits very disparate component energies and potentially large recovery depths for

those components suppressed by strong adverse wind shears.

The effects of a variable scale height H_E for gravity wave energy were examined because of the evidence for such variations in the atmosphere. This was found to suppress fluxes and divergences at lower levels and to increase the magnitudes and lower the altitudes of maximum responses at upper levels.

Furthermore, to assess the importance of gravity wave-tidal interactions, in the middle atmosphere an analysis of the mutual interactions between a canonical gravity wave spectrum and a representative tidal structure was presented based on the parameterization scheme. A diurnal tide was specified to be consistent with observed amplitudes and vertical wavelengths in the mesosphere and lower thermosphere.

The filtering of the gravity wave spectrum by static mean plus tidal wind fields has revealed a strong anti-correlation of the local mean winds and gravity wave momentum fluxes for both winter and summer mean wind profiles. The maximum fluxes occurred at those heights with the maximum gravity wave energies and in response to strong filtering of and anisotropy within the gravity wave field. Diurnally varying momentum fluxes were found to be $\sim$ 5 to $20m^2s^{-2}$ near the mesopause, with larger amplitudes at greater heights and maximum departures of $\sim 60m^2s^{-2}$ from mean values, in line with the limited atmospheric observations to date. A more striking feature of this analysis was the observation of very different mean momentum fluxes above $\sim 80km$ with

and without tidal filtering of the gravity wave spectrum. Also implied by this analysis were large and variable accelerations ($\sim 300 ms^{-1} day^{-1}$), suggesting strong forcing of the mean and tidal wind fields by the gravity wave spectrum in the lower thermosphere.

Based on the observed anti-correlation of tidal winds and gravity wave momentum fluxes in the analysis in section 6.3, a simple analytic model of the gravity wave forcing of the tidal winds was developed. This model was found to predict increases in apparent tidal amplitudes and an advance of the tidal phase at times of strong forcing. These results are likely to be highly sensitive to the details of the filtering process and may also depend on other parameters, such as vertical wavelength, that have not been examined in detail.

An interactive model of gravity wave-tidal interactions was also developed and applied to cases with constant and variable wave source strengths. In the absence of damping of gravity wave induced departures from equilibrium tidal structure, the resulting wind fields were found to be strong and highly variable, but generally consistent with predictions of the analytic model presented in section 6.4. With damping times of 2 and 4 days to represent the relaxation of the equilibrium tidal structure in the absence of continued gravity wave forcing, maximum departures from the mean tidal structures were reduced and the wind fields became much less variable. However, the tendency for amplitude increases and phase advances accompanying strong wave

forcing remained persistent features of this analysis.

The above have shown that gravity wave-tidal interactions are likely to be strong where these wave amplitudes are large. The tidal winds exert a strong control on the anisotropy within the gravity wave field, causing momentum fluxes and their vertical gradients to be large and variable. These momentum fluxes, in turn, provide strong forcing of the mean and tidal wind fields, suggesting apparent tidal structures that may be highly variable in amplitude and phase. Whether this forcing contributes to apparent amplitude decreases, as suggested in the studies by Fritts and Vincent (1987) and Forbes et al., (1991) or to amplitude enhancements as suggested by tidal wind and momentum flux correlations observed is data analysis and model studies by Fritts and Vincent (1987), Wang and Fritts (1991), and this effort, depends on the details of gravity wave filtering by the tidal winds. In either case, if these results are qualitatively applicable to the lower thermosphere, then such wave forcing and interactions will almost surely play a major role in the large- and small-scale variability of this region.

Reference

Andrews, D. G., J. R. Holton, and C. B. Leovy, 1987: Middle Atmosphere Dynamics, Academic Press, Orlando, Florida.

Balsley, S. K., and D. A. Carter, 1982: The spectrum of atmospheric velocity fluctuations at 8 and 86 km, *Geophys. Res. Lett.* **9**, 456-468.

Basley, B. B., W. L. Ecklund, and D. C. Fritts, 1983: VHF echoes from the high-latitude mesosphere and lower thermosphere: Observations and interpretations, *J. Atmos. Sci.* **40**, 2451-2466.

Balsley, B. B., and R. Garello, 1985: The kinetic energy density in the troposphere, stratosphere and mesosphere: A preliminary study using the Poker Flat radar in Alaska, *Radio Sci.*, **20**, 1355-1362.

Blix, T. A., E. V. Thrane, and O. Andreassen, 1990a: In situ measurements of the fine-scale structure and turbulence in the mesosphere and lower thermosphere by means of electrostatic positive ion probes, *J. Geophys. Res.*, **95**, 5533-5548.

Blix, T. A., E. V. Thrane, and D. C. Fritts, U. von Zahn, F.-J. Lübken, W. Hillert, S. P. Blood, J. D. Mitchell, G. A. Kokin, and S. V. Pakhomov, 1990b: Small-scale structure observed in situ during MAC/EPSILON, *J. Atmos. Terres. Phys.*, **52**, 835-854.

Chao, W. C., and M. R. Schoeberl, 1984: A note on the linear approximation of gravity wave saturation in the mesosphere, *J. Atmos. Sci.* **41**, 1893-1898.

Coy, L., and D. C. Fritts, 1988: Gravity wave heat fluxes: A Lagrangian approach, *J. Atmos. Sci.* **45**, 1770-1780.

Desaubies, Y. J. F., 1976: Analytical representation of internal gravity wave spectra, *J. Phys. Oceanogr.* **6**. 976-981.

Dewan, E. M., N. Grossbard, A. F. Quesada, and R. E. Good, 1984: Spectral analysis of 10m resolution scalar velocity profiles in stratosphere, *Geophys. Res. Lett.*, **11**, 80-83, and Correction to "Spectral analysis of ..", *Geophys. Res. Lett.* **11**, 624.

Dewan, E. M., and R. E. Good, 1986: Saturation and the "universal" spectrum for vertical profiles of horizontal scalar winds in the atmosphere, *J. Geophys. Res.* **91**, 2742-2748.

Dong, B., and K. C. Yeh, 1988: Resonant and nonresonant wave-wave interactions in an isothermal atmosphere, *J. Geophys. Res.* **93**, 3729-3744.

Dunkerton, T. J., 1982: Stochastic parameterization of gravity wave stresses, *J. Atmos. Sci.* **39**, 1711-1725.

Dunkerton, T. J., 1983: Laterally-propagating Rossby waves in the easterly acceleration phase of the quasi-biennial oscillation, *Atmos. -Ocean*, **21**, 55-68.

Dunkerton, T. J., 1984: Inertial gravity waves in the stratosphere, *J. Atmos. Sci.* **41**. 3396-3404.

Dunkerton, T. J., 1987: Effects of nonlinear instability on gravity wave momentum transport, *J. Atmos. Sci.* **44**, 3188-3209.

Ebel, A., A. H. Manson, and C. E. Meek, 1987: Short period fluctuations of the horizontal wind measured in the upper middle atmosphere and possible relationships to internal gravity waves, *J. Atmos. Terres. Phys.*, **49**, 385-401.

Ecklund, W. L., K. S. Gage, B. B. Basley, R. G. Strauch, and J. L. Green, 1982: Vertical wind variability observed by VHF radar in the lee of Colorado Rockies, *Mon. Wea. Rev.* **110**, 1451-1457.

Ecklund, W. L., K. S. Gage, G. D. Nastrom, and B. B. Basley, 1986: A preliminary climatology of spectrum of vertical velocity observed by clear-air Doppler radar, *J. Clim. Appl. Meteor.* **25**, 885-892.

Forbes, J.M., J. Gu, and S. Miyahara, 1991: On the interactions between gravity waves and the propagating diurnal tide, *Planet. Space Sci.*, **39**, 1249-1257.

Fritts, D. C., 1984: Gravity wave saturation in the middle atmosphere: A review of theory and observations, *Rev. Geophys. Space Phys.* **22**, 275-308.

Fritts. D. C., 1985: A numerical study of gravity wave saturation: Nonlinear and multiple wave effects, *J. Atmos. Sci.* **42**, 2043-2058.

Fritts, D. C., and H. G. Chou, 1987: An investigation of the vertical wavenumber and frequency spectra of gravity wave motions in the lower stratosphere, *J. Atmos. Sci.* **44**, 3610-3624.

Fritts, D. C., and L. Yuan, 1989: Measurement of momentum fluxes near the summer mesopause at Poker Flat, Alaska, *J. Atmos. Sci.*, **46**, 2569-2579.

Fritts, D. C., and L. Yuan, M. H. hitchman, L. Coy, E. kudeki, and R. F. Wood-

man, 1992: Dynamics of the equatorial mesosphere observed using the Jicamarca MST radar during June and August 1987, *J. Atmos. Sci.*, **49**, in press.

Fritts, D. C., and R. A. Vincent, 1987: Mesospheric momentum flux studies at Adelaide, Australia: Observations and a gravity wave/tidal interaction model, *J. Atmos. Sci.*, **44**, 605-619.

Fritts, D. C., and T. J. Dunkerton, 1985: Fluxes of heat and constituents due to convectively unstable gravity waves, *J. Atmos. Sci.* **42**, 549-556.

Fritts, D. C., and P. K. Rastogi, 1985: Convective and dynamical instabilities due to gravity wave motions in the lower and middle atmosphere: Theory and observations, *Radio Sci.* **20**, 1247-1277.

Fritts, D. C., S. A. Smith, B. B. Basley, and C. R. Philbrick, 1988b: Evidence of gravity wave saturation and local turbulence production in the summer mesosphere and lower thermosphere during the STATE experiment, *J. Geophys. Res.* **93**, 7015-7025.

Fritts, D. C., T. Tsuda, T. Sato, S. Fukao, and S. Kato, 1988a: Observational evidence of a saturated gravity wave spectrum in the troposphere and lower stratosphere, *J. Atmos. Sci.* **45**, 1741-1759.

Fritts, D. C., T. Tsuda, T. E. VanZandt, S. A. Smith, T. Sato, S. Fukao, and S. Kato, 1990b: Studies of velocity fluctuations in the lower atmosphere using the MU radar: II. Momentum fluxes and energy density, *J. Atmos. Sci.* **47**, 51-66.

Fritts, D. C., and T. E. VanZandt, 1987: Effects of Doppler shifting on frequency spectra of atmospheric gravity waves, *J. Geophys. Res.* **92**, 9723-9732.

Fritts, D. C., 1989: A review of gravity wave saturation processes, effects, and variability in the middle atmosphere, *Pure Appl. Geophys.* **130**, 313-371.

Fritts, D. C., U. -P. Hoppe, and B. Inhester, 1990a: A study of the vertical motion field near the high-latitude summer mesopause during MAC/SINE, *J. Atmos. Terres. Phys.* **52**, 927-938.

Fritts, D. C., and J. R. Isler, 1992: First observations of mesospheric dynamics with a partial reflection radar in Hawaii (22^{0}N, 160^{0}W), *Geophys. Res. Lett.* **19**, 409-412.

Fritts, D. C., and T. E. Vanzandt, 1992: Spectral estimates of gravity wave energy and momentum fluxes, I: Energy dissipation, acceleration, and constraints, *J. Atmos. Sci.* **50**.

Fritts, D. C., and R. A. Vincent, 1987: Mesospheric momentum flux studies at Adelaide, Australia: Observations and a gravity wave/tidal interaction model, *J. Atmos. Sci.* **44**, 605-619.

Fritts, D. C., and L. Yuan, 1989: Measurement of momentum fluxes near the summer mesopause at Poker Flat, Alaska, *J. Atmos. Sci.* **46**, 2569-2579.

Fritts, D. C., and D. -Y. Wang, 1991: Doppler-shifting effects on frequency spectra of gravity waves observed near the summer mesopause at high latitude, *J. Atmos. Sci.* **48**, 1535-1544.

Fritts, D. C., D. -Y. Wang, and R. C. Blanchard, 1992a: Gravity wave and tidal structures between 60 and 140 km inferred from space shuttle re-entry data, *J. Atmos. Sci.* **50**.

Fritts, D. C., R. C. Blanchard, and L. Coy, 1989: Gravity wave structure between 60 and 90 km inferred from space shuttle reentry data, *J. Atmos. Sci.*, **46**, 423-434.

Fritts, D. C., and G. D. Nastrom, 1992: Sources of mesoscale variability of gravity waves, II: Frontal, convective, and jet stream excitation, *J. Atmos. Sci.*, **49**, 111-127.

Fritts, D. C., and W. Lu, 1993: Spectral estimates of gravity wave energy and momentum fluxes. Part II: Parameterization of wave forcing and variability. *J. Atmos. Sci.*, **50**.

Garcia, R. R., and S. Solomon, 1985: The effect of breaking gravity waves on the dynamical and chemical composition of the mesosphere and lower thermosphere, *J. Geophys. Res.*, **90**, 3850-3868.

Gage, K. S., 1979: Evidence for $k^{-5/3}$ power law inertial range in mesoscale two-dimensional turbulence, *J. Atmos. Sci.* **36**, 1950-1954.

Gage, K. S., and B. B. Basley, 1984: MST radar studies of wind and turbulence in the middle atmosphere, *J. Atmos. Sci.* **46**, 739-753.

Garrett, C. J. R., and W. H. Munk, 1972: Space-time scales of internal waves, *Geophys. Astrophys. Fluid Dyn.* **3**, 225-235.

Garrett, C. J. R., and W. H. Munk, 1975: Space-time scales of internal waves: A progress report, *J. Geophys. Res.* **80**, 291-297.

Hasselmann, K., 1967: A criterion for nonlinear wave stability, *J. Fluid Mech.* **30**, 737-739.

Hines, C. O., 1960: Internal gravity waves at ionospheric heights, *Can. J. Phys.* **38**, 1441-1481.

Hines, C. O., 1971: Generalizations of the Richardson criterion for the onset of atmospheric turbulence, *Quart. J. Roy. Met. Soc.* **97**, 429-439.

Hines, C. O., 1972: Momentum deposition by atmospheric waves, and its effects on thermospheric circulation, *Space Res.* **12**, 1157.

Hines, C. O., 1988: The generation of turbulence by atmospheric gravity waves, *J. Atmos. Sci.* **45**, 1269-1278.

Hitchman, M. H., K. W. bywaters, D. C. Fritts, L. Coy, and E. Kudeki, 1992: Mean winds and momentum fluxes over Jicamarca, Peru during June and August 1987, *J. Atmos. Sci.*, **49**, in press.

Hoinka, K. P., 1984: Observation of a mountain wave event over the Pyrenees, *Tellus*, **36**, 369-383.

Hoinka, K. P., 1985: Observations of the air flow over Alps during a Foehn event, *Quart. J. Roy. Meteorol. Soc.*, **111**, 199-224.

Hodges, R. R., 1967: Generation of turbulence in the upper atmosphere by internal gravity waves, *J. Geophys. Res.* **72**, 3455-3458.

Holton, J. R., 1982: The role of gravity wave-induced drag and diffusion in the momentum budget of the mesosphere, *J. Atmos. Sci.* **39**, 791-799.

Holton, J. R., 1983: The influence of gravity wave breaking on the general circulation of the middle atmosphere, *J. Atmos. Sci.* **40**, 2497-2507.

Holton, J. R. , 1984: The generation of mesospheric planetary waves by zonally asymmetric gravity wave breaking, *J. Atmos. Sci.* **41**, 3427-3430.

Holton, J. R., and X. Zhu, 1984: A further study of gravity wave induced drag and diffusion in the mesosphere, *J. Atmos. Sci.* **41**, 2653-2662.

Holton, J. R., 1979: An Introduction to Dynamic Meteorology(2nd ed.), *Academic, New York.*

Holton, J. R., 1992: An Introduction to Dynamic Meteorology(3nd ed.), *Academic, New York.*

Holton, J. R., and R. S. Lindzen, 1972: An updated theory of the quasi-biennial cycle of the tropical stratosphere, *J. Atmos. sci.*, **29**, 1076-1080.

Inhester, B., 1987: The effect of inhomogeneities on the resonant parametric interaction of gravity waves in the atmosphere, *Ann. Geophys.* **5**, 209-218.

Jasperson, W. H., G. D. Nastrom, and D. C. Fritts, 1990: Further study of terrain effects on the mesoscale spectrum of atmospheric motions, *J. Atmos. sci.*, **47**, 979-987.

Kennedy, P. J., and M. A. Shapiro, 1979: Further encounters with clear air turbulence in research aircraft, *J. Atmos. Sci.*, **37**, 986-993.

Klostermeyer, J., 1982: On parametric instabilities of finite amplitude internal gravity waves, *J. Fluid Mech.* **119**, 367-377.

Klostermeyer, J., 1984: Observational indicating parametric instabilities in internal gravity waves at thermospheric heights, *Geophy. Astrophys. Fluid Dyn.* **29**, 117-138.

Klostermeyer, J. and R. Ruster, 1984: VHF radar observations of wave instability and turbulence in the mesosphere, *Adv. Space Res.* 4, 79-82.

Lilly, D. K., 1972: Wave momentum flux– A GARP problem, *Bull. Am. Meteor. Soc.* **53**, 17-23.

Lilly, D. K., 1978: A severe downslope wind storm and aircraft turbulence event induced by a mountain wave, *J. Atmos. Sci.* **35**, 59-77.

Lilly, D. K., 1983: Stratified turbulence and the mesoscale variability of the atmosphere, *J. Atmos. Sci.* **40**, 749-761.

Lilly, D. K., and P. J. Kennedy, 1973: Observations of a stationary mountain wave and its associated momentum flux and energy dissipation, *J. Atmos. Sci.* **30**, 1135-1152.

Lilly, D. K., and P. F. Lester, 1974: Waves and turbulence in the stratosphere, *J. Atmos. Sci.*, **31**, 800-812.

Lilly, D. K., J. M. Nicholls, R. M. Chervin, P. J. Kennedy, and J. B. Klemp, 1982: Aircraft measurements of wave momentum flux over the Colorado Rocky Mountains, *Quart. J. Roy. Meteorol. Soc.*, **108** , 625-642.

Lindzen, R. S., 1981: Turbulence and stress owing to gravity wave and tidal breakdown, *J. Geophys. Res.* **86**, 9707-9714.

Lindzen, R. S., 1984: Gravity waves in the mesosphere, in Dynamics of the middle atmosphere(J. R. Holton and T. Matsuno, eds.)(*D. Reidel Publ. Co.*)pp. 3-18.

Lindzen, R. S., 1985: Multiple gravity wave breaking levels, *J. Atmos. Sci.* **42**, 301-305.

Lindzen, R. S., and J. R. Holton, 1968: A theory of the quasi-biennial oscillation, *J. Atmos. Sci.*, **25**, 1095-1107.

Longuet-Higgins, M. S., 1970a: Longshore currents generated by obliquely incident sea waves 1, *J. Geophys. Res.*, **75**, 6778-6789.

Longuet-Higgins, M. S., 1970b: Longshore currents generated by obliquely incident sea waves 2, *J. Geophys. Res.*, **75**, 6790-6801.

Longuest-Higgins, M. S., 1972: Recent progress in the study of longshore currents, *The Waves on Beaches and Resulting Sediment Transport (ed. R. E. Meyer)*, 203-248, Academic.

Lu, D., T. E. VanZandt, and W. L. Clark, 1984: VHF Doppler radar observations of buoyancy waves induced by thunderstorms, *J. Atmos. Sci.*, **41**, 272-282.

Lu, W., and D. C. Fritts, 1993: Spectral estimates of gravity wave energy and momentum fluxes, III: Gravity wave-tidal interactions, *J. Atmos. Sci.*, **50**.

McComas, C. H., and F. P. Bretherton, 1977: Resonant interaction of oceanic internal waves, *J. Geophys. Res.* **82**, 1397-1412.

McFarlane, N. A., 1987: The effect of orographically excited gravity wave drag on the general circulation of the lower stratosphere and troposphere, *J. Atmos. Sci.* **44**, 1775-1800.

Meek, C. E., I. M. Reid, and A. H. Manson, 1985a: Observations of mesospheric wind velocities. II: Cross-sections of power spectral density for 48-8h, 8-1h, 1h-10 min over 60-11-km for 1981, *Radio Sci.* **20**, 1383-1402.

Mied, R. P., 1976: The occurrence of parametric instabilities in the finite amplitude internal gravity waves, *J. Fluid Mech.* **78**, 763-784.

Miyahara, S., Y. Hayashi, and J. D. Mahlman, 1986: Interactions between gravity waves and the planetary scale flow simulated by the GFDL "SKYHI" general circulation model, *J. Atmos. Sci.* **43**, 1844-1861.

Muller, P., G. Holloway, F. henyey, and N. Pomphrey, 1986: Nonlinear interactions among gravity waves, *Rev. Geophys.* **24**, 493-536.

Nastrom, G. D., B. B. Balsley, and D. A. Carter, 1982: Mean meridional winds in the mid- and high-latitude summer mesosphere, *Geophys. Res. Lett.* **9**, 139-142.

Nastrom, G. D., D. C. Fritts, and K. S. Gage, 1987: An investigation of terrain effects on the mesoscale spectrum of atmospheric motions, *J. Atmos. Sci.* **44**, 3087-3096.

Nastrom, G. D., and D. C. Fritts, 1992: Sources of mesoscale variability of gravity waves, I: Topographic excitation, *J. Atmos. Sci.*, **49**, 101-110.

Newton, C. W., 1971: Mountain torques in the global angular momentum balance, *J. Atmos. Sci.* **28**, 623-628.

Palmer, T. N., G. J. Snutts, and R. Swinbank, 1986: Alleviation of a systematic westerly bias in general circulation and numerical weather prediction models through an orographic gravity waves drag parameterization, *Quart. J. Roy. Met. Soc.* **112**, 1001-1040.

Plumb, R. A., and A. D. McEwan, 1978: The instability of a forced standing wave in a viscous stratified fluid: A laboratory analogue of the quasi-biennial oscillation, *J. Atmos. Sci.*, **35**, 1827-1839.

Reid, I. M., and R. A. Vincent, 1987a: Measurements of mesospheric gravity wave momentum fluxes and mean flow accelerations at Adelaide, Australia, *J. Atmos. Terr. Phys.* **49**, 443-460.

Reid, I. M., and R. A. Vincent, 1987b: Measurements of the horizontal scales and phase velocities of short period mesospheric gravity waves at Adelaide, Australia, *J. Atmos. Terr. Phys.* **49**, 1033-1048.

Rind, D., R. Suozzo, N. K. Balachandran, A. Lacis, and G. Russell, 1988: The GISS global climate/middle atmosphere model with parameterized gravity wave drag, *J. Atmos. Sci.* **45**, 371-386.

Reid, I. M., R. Rüster, P. Czechowsky, and G. Schmidt, 1988: VHF radar measurements of momentum flux in the summer polar mesosphere over Andenes (69^0N, 16^0E), Norway, *Geophys. Res. Lett.*, **15**, 1263-1266.

Rüster, R., and I. M. Reid, 1990: VHF radar observations of the dynamics of the summer polar mesopause region, *J. Geophys. Res.*, **95**, 10005-10016.

Sidi, C., and J. Lefrere, F. Dalaudier, and J. Barat, 1988: An improved atmospheric buoyancy wave spectrum model, *J. Geophys. Res.* **93**, 774-790.

Smith, R. B., 1978: A measurement of mountain drag, *J. Atmos. Sci.*, **35**, 1644-1654.

Smith, A. K., and L. V. Lyjak, 1985: An observational estimate of gravity wave drag from the momentum balance in the middle atmosphere, *J. Geophys. Res.* **90**, 2233-2241.

Smith, S. A., D. C. Fritts, and T. E. VanZandt, 1987: Evidence of a saturation spectrum of atmospheric gravity waves, *J. Atmos. Sci.* **44**, 1404-1410.

Schoeberl, M. R., D. F. Strobel, and J. P. Apruzese, 1983: A numerical model of gravity wave breaking and stress in the middle atmosphere, *J. Geophys. Res.* **88**, 5249-5259.

Strobel, D. F., J. P. Apruzese, and M. R. Schoeberl, 1985: Energy balance constrains on gravity wave induced eddy diffusion in the mesosphere and lower thermosphere, *J. Geophys. Res.* **90**, 13067-13072.

Strobel, D. F., M. E. Summers, R. M. Bevilacqua, M. T. DeLand, and M. Allen, 1987: Vertical constituent transport in the mesosphere, *J. Geophys. Res.* **192**, 6691-6698.

Tanaka, H., 1986: A slowly varying model of the lower stratospheric zonal wind

minimum induced by mesoscale mountain wave breakdown, *J. Atmos. Sci.* **43**, 1881-1892.

Thrane, E. V., O. Andreassen, T. A. Blix, B. Grandal, A. Brekke, C. R. Philbrick, F. J. Schmidlin, H.-U. Widdel, U. von Zahn, and F.-J. Lübken , 1985: Neutral air turbulence in the upper atmosphere, *J. Atmos. Terres. Phys.*, **47**, 243-265.

Tsuda, T., K. Hirose, S. Kato, and M. P. Sulzer, 1985: Some findings on correlation between the stratospheric echo power and the wind shear observed by the Arecibo UHF radar, *Radio Sci.* **20**, 1503-1508.

Tsuda, T., Y. Murayama, M. Yamamoto, S. Kato, and S. Fukao, 1990: Seasonal variation of momentum flux in the mesosphere observed with MU radar, *Geophys, Res. Lett.*, **17**, 725-728.

VanZandt, T. E., 1982: A universal spectrum of buoyancy waves in the atmosphere, *Geophys. Res. Lett.* **9**, 575-578.

VanZandt, T. E., 1985: A model for gravity wave spectra observed by Doppler sounding systems, *Radio Sci.* **20**, 1323-1330.

VanZandt, T. E., and D. C. Fritts, 1989: A theory of enhanced saturation of gravity wave spectrum due to increases in atmospheric stability, *Pure Appl. Geophys.* **131(2/3**, 399-420.

VanZandt, T. E., S. A. Smith, T. Tsuda, D. C. Fritts, T. Sato, S. Fukao, and S. Kato, 1990: Studies of velocity fluctuations in the lower atmosphere using the MU radar. Part I: Azimuthal anisotropy, *J. Atmos. Sci.*, *47*, 39-50.

Vincent, R. A., 1984: Gravity wave motions in the mesosphere, *J. Atmos. Terres. Phys.*, **46**, 119-128.

Vincent, R. A., and S. D. Eckermann, 1990: VHF radar observations of mesoscale motions in the troposphere: Evidence of gravity wave Doppler shifting, *Radio Sci.*, *25*, 1019-1037.

Vincent, R. A., and D. C. Fritts, 1987: A morphology of gravity waves in the mesosphere and lower thermosphere over Adelaide, Australia, *J. Atmos. Sci.* **44**, 748-760.

Vincent, R. A., and I. M. Reid, 1983: HF Doppler measurements of mesospheric momentum fluxes, *J. Atmos. Sci.* **40**, 1321-1333.

Wallace, J. M., and J. R. Holton, 1968: A diagnostic numerical model of the quasi-biennial oscillation, *J. Atmos. Sci.*, **25**, 280-292.

Watkins, B. J., C. R. Philbrick, and B. B. Balsley, 1988: Turbulence energy dissipation rates and inner scale sizes from rocket and radar data, *J. Geophys. Res.* **93**, 7009-7014.

Walterscheid, R. L., 1981: Dynamical cooling induced by dissipating internal gravity waves, *Geophys. Res. Lett.* **8**, 1235-1238.

Walterscheid, R. L., 1981: Inertio-gravity wave induced accelerations of mean flow having an imposed periodic component: Implications for tidal observations in the meteor region, *J. Geophys. Res.*, **86**, 9698-9706.

Wang, D. -Y., and D. C. Fritts, 1991: Evidence of gravity wave-tidal interaction

observed near the summer mesopause at Poker Flat, Alaska, *J. Atmos. Sci.*, **48**, 572-583.

Wang, D. -Y., and D. C. Fritts, 1990: Mesospheric momentum fluxes observed by the MST radar at Poker Flat, Alaska, *J. Atmos. Sci.*, **47**, 1511-1521.

Weinstock, J., 1982: Nonlinear theory of gravity waves: Momentum deposition, generalized Rayleigh friction, and diffusion, *J. Atmos. Sci.* **39**, 1698-1710.

Weinstock, J., 1983: Heat flux induced by gravity waves, *Geophys. Res. Lett.* **10**, 165-167.

Weinstock, J., 1985: Theoretical gravity wave spectra in the atmosphere: Strong and weak interactions, *Radio Sci.* **20**, 1295-1300.

Yamamoto, M., T. Tsuda, S. Kato, T. Sato, and S. Fukao, 1987: Interpretation of structure of mesospheric turbulent scattering layers in terms of inertial gravity waves, *Physica Scripa.*

Yeh, K. C., and C. H. Liu, 1981: The instability of atmospheric gravity waves through wave-wave interactions, *J. Geophys. Res.* **86**, 9722-9728.

Yeh, K. C., and C. H. Liu, 1985: Evolution of atmospheric spectrum by processes of wave-wave interaction, *radio Sci.* **20**, 1279-1294.